SMHI
Reports Meteorology and Climatology
No 108, Dec 2005

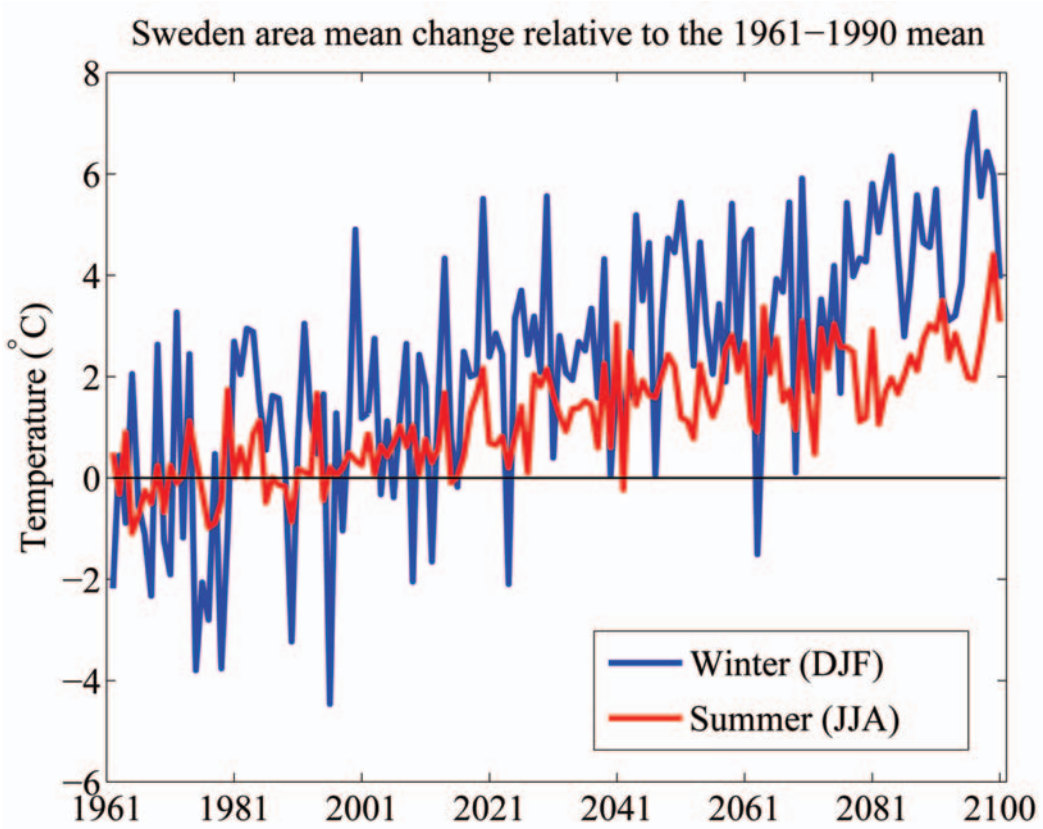

A 140-year simulation of European climate with the new version of the Rossby Centre regional atmospheric climate model (RCA3)

Erik Kjellström, Lars Bärring, Stefan Gollvik, Ulf Hansson, Colin Jones, Patrick Samuelsson, Markku Rummukainen, Anders Ullerstig, Ulrika Willén and Klaus Wyser

Citation:

Kjellström, E., Bärring, L., Gollvik, S., Hansson, U., Jones, C., Samuelsson, P., Rummukainen, M., Ullerstig, A., Willén U. and Wyser, K., 2005. A 140-year simulation of European climate with the new version of the Rossby Centre regional atmospheric climate model (RCA3). SMHI Reports Meteorology and Climatology No. 108, SMHI, SE-60176 Norrköping, Sweden, 54 pp.

Cover illustration:

Evolution of seasonal mean 2m-temperature area averaged over Sweden in the RCA3ECHAM4B2 simulation as compared to the 1961-1990 mean.

RMK
No 108, Dec 2005

A 140-year simulation of European climate with the new version of the Rossby Centre regional atmospheric climate model (RCA3)

Erik Kjellström, Lars Bärring, Stefan Gollvik, Ulf Hansson, Colin Jones, Patrick Samuelsson, Markku Rummukainen, Anders Ullerstig, Ulrika Willén and Klaus Wyser

Report Summary / Rapportsammanfattning

Issuing Agency/Utgivare

Swedish Meteorological and Hydrological Institute
S-601 76 NORRKÖPING
Sweden

Report number/Publikation

RMK No. 108

Report date/Utgivningsdatum

December 2005

Author (s)/Författare

Erik Kjellström, Lars Bärring, Stefan Gollvik, Ulf Hansson, Colin Jones, Patrick Samuelsson, Markku Rummukainen, Anders Ullerstig, Ulrika Willén and Klaus Wyser

Title (and Subtitle/Titel

A 140-year simulation of European climate with the new version of the Rossby Centre regional atmospheric climate model (RCA3).

Abstract/Sammandrag

This report presents the latest version of the Rossby Centre regional atmospheric model, RCA3, with focus on model improvements since the earlier version, RCA2. The main changes in RCA3 relate to the treatment of land surface processes. Apart from the changes in land surface parameterizations several changes in the calculation of radiation, clouds, condensate and precipitation have been made. The new parameterizations hold a more realistic description of the climate system.

Simulated present day climate is evaluated compared to observations. The new model version show equally good, or better, correspondence to observational climatologies as RCA2, when forced by perfect boundary conditions. Seasonal mean temperature errors are generally within $\pm 1^{o}$C except during winter in north-western Russia where a larger positive bias is identified. Both the diurnal temperature range and the annual temperature range are found to be underestimated in the model. Precipitation biases are generally smaller than in the corresponding reanalysis data used as boundary conditions, showing the benefit of a higher horizontal resolution.

The model is used for the regionalization of two transient global climate change projections for the time period 1961-2100. The radiative forcing of the climate system is based on observed concentrations of greenhouse gases until 1990 and on the IPCC SRES B2 and A2 emissions scenarios for the remaining time period. Long-term averages as well as measures of the variability around these averages are presented for a number of variables including precipitation and near-surface temperature. It is shown that the changes in variability sometimes differ from the changes in averages. For instance, in north-eastern Europe, the mean increase in wintertime temperatures is followed by an even stronger reduction in the number of very cold days in winter. This kind of performance of the climate system implies that methods of inferring data from climate change projections to other periods than those actually simulated have to be used with care, at least when it comes to variables that are expected to change in a non-linear way. Further, these new regional climate change projections address the whole 21st century.

Key words/sök-, nyckelord

Land surface modelling, transient change, climate scenario, regional climate modelling, pattern-scaling, Europe, CE, ENSEMBLES

Supplementary notes/Tillägg

This work has been a part of the Nordic Climate and Energy project (CE) and the EU-project ENSEMBLES (GOCE-CT-2003-505539)

Number of pages/Antal sidor

54

Language/Språk

English

ISSN and title/ISSN och title

0347-2116 SMHI Reports Meteorology Climatology

Report available from/Rapporten kan köpas från:

SMHI
S-601 76 NORRKÖPING
Sweden

Contents

1 Introduction 1

2 Method 2

2.1 The regional climate model RCA3 2
2.1.1 Changes in the atmospheric part of the model 2
2.1.2 The land-surface scheme in RCA3 4
2.2 Experiment description 6
2.3 Observational data sets 8

3 The reanalysis-driven experiment (RCA3ERA) 10

3.1 Mean sea level pressure 10
3.2 Surface temperature 11
3.2.1 Time mean temperature 11
3.2.2 Diurnal temperature range 14
3.2.3 Daily maximum and minimum temperatures 16
3.3 Precipitation 20
3.4 Clouds 22
3.5 Wind 24
3.5.1 Mean wind speed 24
3.5.2 Gusty wind speed 25
3.6 Snow 26
3.6.1 Snow water equivalent 26
3.6.2 Duration of snow cover 27

4 The transient climate change experiment 29

4.1 Control climate versus observed climate (RCA3ECHAM) 29
4.2 Transient climate change (1990-2100) 33
4.2.1 Mean sea level pressure 34
4.2.2 Surface air temperature 36
4.2.3 Precipitation 42
4.2.4 Surface winds 44
4.2.5 Snow climate 46

5 Evaluating the method of pattern-scaling in time 48

6 Conclusions 49

Acknowledgements 50

References 51

1 Introduction

The Rossby Centre which is a part of SMHI pursues advanced climate modelling. The efforts include the development, evaluation and application of regional climate modelling in climate and climate change research. This report presents the latest version of the Rossby Centre regional atmospheric model, RCA3. Earlier versions of the RCA model are described by Rummukainen *et al.* (1998, 2001); Räisänen *et al.* (2003, 2004) and Jones *et al.* (2004).

The present report provides an overview of RCA3 with focus on model improvements since the earlier version, RCA2 (Bringfelt *et al.*, 2001; Jones *et al.* 2004). These improvements have been made both to improve identified shortcomings of RCA2 and to increase the usefulness of Rossby Centre regional climate simulations in terms of incorporating additional processes and detail of the regional climate system including a new land surface scheme. The performance of RCA3 is evaluated with so-called "perfect" boundary condition experiments (Sass and Christensen 1995; Christensen *et al.* 1997) in which the model is run using boundary conditions from the ECMWF Reanalysis experiment ERA40 (Uppala *et al.* 2005). ERA40 is probably the most comprehensive account of the state and behaviour of the atmosphere during the last four decades. Consequently, a measure of RCA3 performance is its convergence to both ERA40 and concurrent observations of different kinds. However, ERA40 has some limitations that need to be recognised in this context (*ibid*). Some of these consider its hydrological cycle and snow budget, which are not closed in ERA40. In addition, the resolution of ERA40 is coarse compared to RCA3. The latter can thus generate details that are not present in the ERA40 data. Thus, even if the performance of RCA3 and the impact of model improvements are in part measured in terms of the agreement of RCA3 with ERA40, additional considerations are needed to complete the picture. Appropriate account need to be made to the fact that regional climate models that do not apply data assimilation have some freedom to deviate from the exact large-scale state that corresponds to the boundary conditions. In most instances, a regional climate model is nevertheless expected to have an asymptotic degree of skill in capturing the evolution of weather already contained in the forcing model (see, *e.g.*, Giorgi and Mearns, 1999). However, the interior solution in the regional domain is not always well-constrained, depending on the large-scale circulation state. In such cases, larger discrepancies might arise, although they should not persist. This has been referred to as intermittent divergence in phase space (*cf.* von Storch, 2005). In any case, the use of regional climate models is not in predicting weather as such. Instead, they should provide a consistent and comprehensive tool for understanding the physics and sensitivity of the regional climate system. This implies that an assessment of the value of a regional climate model should also include its performance in representing physical processes (for example, budgets and fluxes) and a wide range of statistics, such as averages, measures of persistence, variability and extremes.

The present report also documents a new type of regional climate change modelling application run with RCA3. Previous regional climate model projections and scenarios have mostly concerned relatively short time periods of 10-30 years, made in so-called

"time-slice" mode. This means running a regional climate model first for the present-day climate and then for one or several future periods of the middle or end of the 21st century. An analysis of the differences between the future and the present-day periods then provides the basis of regional scenarios of climate change. A recent set of four such time slices made at the Rossby Centre are described by Räisänen *et al.* (2003, 2004). These simulations address the periods 1961-1990 and 2071-2100 based on boundary conditions from two global climate models, both run for two different SRES emission scenarios. Here, we use RCA3 in two transient regional climate simulations, each spanning over 140 years from 1961 to 2100. The boundary conditions are taken from one global climate model that in turn is run for two SRES emission scenarios. Compared to regional time-slice simulations, the present long simulations offer several advantages: (i) They address climate change in a continuous fashion over the near, mid and long-term future (*cf.* such impact study applications as forestry and ecosystem modelling, as well as tangible societal adaptation strategies), (ii) offer improved starting points for studying how the forced climate change might emerge from natural climate variability (*cf.* regional detection) and (iii) facilitate the evaluation of pattern-scaling techniques for regional-scale applications (*e.g.* Christensen *et al.* 2001; Rummukainen *et al.* 2003).

The outline of this report is as follows. In section 2 we first describe the modifications to RCA and the set-up of the ERA40 and climate change experiments. In section 3, a description is made of how the regional climate model reproduces the observed climate when forced by the reanalysis data. The transient climate change experiments are discussed in section 4. The matter of using these experiments to evaluate a pattern-scaling method is covered in section 5. Concluding remarks are given in section 6.

2 Method

2.1 The regional climate model RCA3

RCA3 is a regional climate model that includes a description of the atmosphere and its interaction with the land surface. It includes a land surface model and a lake model, PROBE (Ljungemyr *et al*., 1996). RCA3 builds on the previous version RCA2 which is described in Jones *et al*. (2004). Chapter 2.1.1 summarizes the main changes in the atmospheric part of the model as compared to RCA2. In Chapter 2.1.2 an overview of the new land-surface parameterization is given.

2.1.1 Changes in the atmospheric part of the model

There have been changes in the radiation, turbulence and cloud parameterizations in RCA3 compared to earlier versions.

The radiation scheme in RCA2 is a based on the HIRLAM radiation scheme developed originally by Savijärvi (1990) and Sass *et al*. (1994) for NWP purposes. The scheme is computationally fast but highly simplified with only one wavelength band for the longwave (LW) region and one for the shortwave (SW) region. It has been modified to include CO_2 absorption by Räisänen *et al*. (2000). The SW cloud albedo and the LW cloud emissivity in RCA2 are calculated from the cloud condensate amount, with a cloud

mass absorption coefficient depending on height for the emissivity. In RCA3, the cloud emissivity and cloud albedo are now formally linked to cloud water and ice amounts and a diagnosed effective radius (calculated separately for liquid and solid water), see details in Wyser *et al*. (1999). The separation of cloud water into liquid and frozen components has been modified so that water is more rapidly put into the ice phase as a function of decreasing temperature in RCA3 than in RCA2. Therefore the longwave downward radiation from a given (cold) cloud is reduced relative to the RCA2 formulation. The cloud droplet number concentration in the microphysics and in the radiation calculations is allowed to vary depending on the surface type (land, sea, snow-covered land, ice-covered water) and as a linear function of height over land with decreasing pressure from a surface land value to an oceanic value at 0.8 times the surface pressure. In order to reduce an overestimate of clear-sky SW surfaces fluxes found for RCA2, the SW clear-sky absorption and the aerosol effects have been increased. The empirical formula for clear-sky cooling beneath clouds has been modified in RCA3 so only clear-sky flux below the cloud base is considered and not for the whole column as before which leads to an increased downward longwave radiation beneath clouds.

The turbulence scheme in RCA2 is based on prognostic turbulent kinetic energy combined with a diagnostic length scale (Cuxart *et al*. 2000). The scheme is updated in RCA3 to have a smoother transition between stable and unstable conditions and to be more numerically stable (Lenderink and de Rooy 2000, Lenderink and Holtslag 2004). The new scheme has the same basic philosophy but uses a simpler and faster method to calculate turbulent mixing lengths and better matches these to near surface lengths given by similarity theory in the neutral limit. A benefit is also that the calculation of the surface momentum flux is more numerically stable as is the calculation of the prognostic turbulence kinetic energy equation.

Cloud processes in RCA2 and RCA3 are separated into resolved clouds (large or mesoscale) and sub-grid scale (convective) clouds. The large scale clouds are described using the scheme of Rasch and Kristjánsson (1998). Convective clouds are described with an entraining and detraining plume model using the approach of Kain and Fritsch (1993). The treatment of shallow convective clouds, condensate and precipitation has been radically changed in RCA3 compared to RCA2. The main change is that the RCA3 Kain-Fritsch convection scheme assumes that shallow convection is non-precipitating. Shallow convective cloud water produced by Kain-Fritsch convection is then detrained into the environment and a fraction evaporated depending linearly on the local grid box mean relative humidity. The remaining shallow convective cloud water is assumed to reside in a diagnosed shallow cumulus cloud fraction that links the cloud amounts to the liquid and vapour content of the convective plumes and the local relative humidity (Albrecht, 1981). Microphysical conversion for shallow convective cloud water to precipitation is then done by the same scheme as for large scale clouds and condensation. Resulting shallow cumulus clouds and cloud water can then interact with the radiation fields. The main impact of these changes is reduced precipitation from shallow convective clouds, a formal shallow convective cloud fraction (not present in RCA2) and thus shallow convective clouds that contain more water and are more reflective. A more detailed description of the new parameterizations is given in Jones and Sanchez (2002).

In the formulation of large scale precipitation some changes are made to the auto-conversion calculation in RCA3 that acts to reduce the occurrence of weak precipitation, which was too frequent in RCA2. As mentioned above the diagnostic split of total cloud water into liquid and ice is also modified in RCA3.

2.1.2 The land-surface scheme in RCA3

From the atmospheric point of view the land-surface scheme (LSS) in RCA3 has three tiles with respect to temperature: forest, open land, and snow. The open land tile is divided into a vegetated and a bare soil part with respect to latent heat flux (surface resistance). The individual fluxes of heat and momentum from these tiles are weighted to grid-averaged values at the lowest atmospheric model level according to the fractional areas of the tiles. Local surface layer equilibrium is assumed over each tile which means that they have their own aerodynamic resistances. The forest tile is internally divided into three subtiles: forest canopy, forest floor soil, and snow on forest floor. The motivation for this division is that these subtiles are closely related to each other via the temperature and humidity conditions in the canopy air space. All together this gives 3–5 different surface energy balances depending on if snow is present or not. See Figure 1 for a principal sketch of the surface scheme. Samuelsson *et al.* (2006) provides a detailed description of the RCA3 LSS.

The soil is divided into five layers with respect to temperature and consists of 2–4 subtiles depending on if snow is present or not. At the bottom (3.0m depth) a no-flux boundary condition is used.

In total, there are eight prognostic storages of water in the LSS; interception of water on open land vegetation and on forest canopy, snow water equivalent of open land and forest snow, liquid water content in both snow storages and two soil moisture storages.

The soil moisture is assumed to be independent of surface coverage which means that we need only two prognostic soil moisture storages, top and deep soil moisture. The top soil moisture layer has a depth corresponding to the depth of the two top-most soil layers for temperature while the depth of the deep layer is 1.0m in mountainous areas and 2.2m elsewhere. There is no relaxation of soil moisture, thus runoff from the deep layer can be used as input to a routing scheme.

Diagnostic variables of temperature and humidity at 2m and wind at 10m are calculated using Monin-Obukhov similarity theory. These diagnostic variables are calculated individually for each tile and are then area-averaged for larger sub surfaces or for the whole grid square.

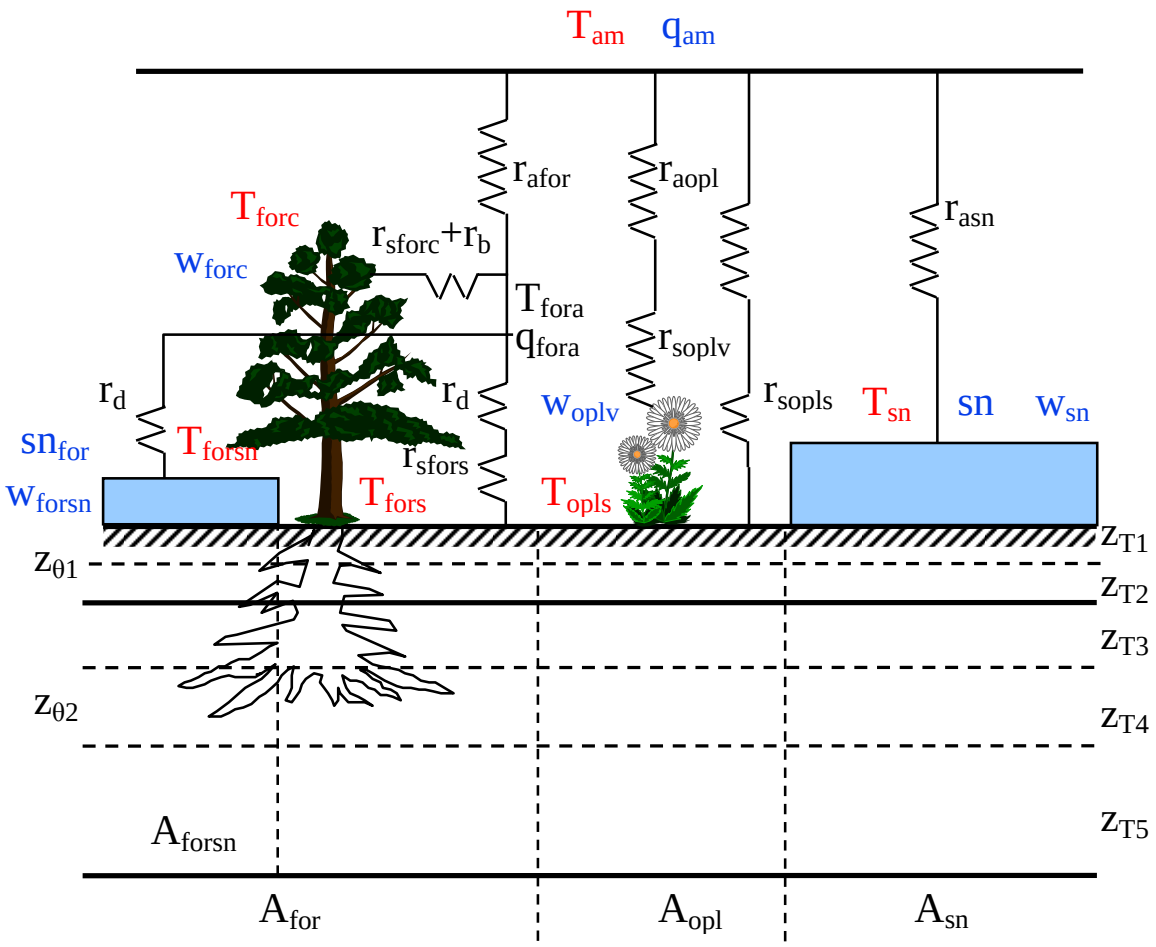

Figure 1. *A principal sketch of the land-surface scheme in RCA3. The LSS is divided into three main tiles: forest (A_{for}), open land (A_{opl}) and snow on open land (A_{sn}). The forest also has a snow subtile (A_{forsn}). Marked in red are prognostic temperatures: atmospheric lowest model level (T_{am}), open land soil surface temperature (T_{opls}), snow surface temperature (T_{sn}), soil temperature below snow (T_{sns}), forest snow surface temperature (T_{forsn}), forest soil surface temperature (T_{fors}), soil temperature below forest snow (T_{forsns}) and forest canopy temperature (T_{forc}). In addition to these temperatures each subbox in the soil (marked by the dashed lines) has its own prognostic temperature. The different soil layers with respect to temperature are denoted by z_{T1}–z_{T5}. The canopy air temperature (T_{fora}) is a diagnostic variable. Marked in blue are the water prognostic variables: specific humidity at the atmospheric lowest model level (q_{am}), open land snow water equivalent (sn), forest snow water equivalent (sn_{for}), intercepted water on low vegetation (w_{oplv}), intercepted water on forest canopy (w_{forc}), snow liquid water (w_{sn}) and forest snow liquid water (w_{forsn}). In addition to these there are two prognostic soil moisture variables corresponding to the layers $z_{\theta 1}$ and $z_{\theta 2}$. The canopy air specific humidity (q_{fora}) is a diagnostic variable. Each individual tile is connected to the lowest atmospheric level via their corresponding aerodynamic resistances (r_a). For evapotranspiration calculations a number of surfaces resistances are used (r_s).*

2.2 Experiment description

Three simulations with RCA3 are described in this report. In the first the present-day climate (1961-2002) is simulated with forcing conditions taken from a reanalysis experiment. The results from this experiment are compared to observations in an effort to evaluate the model behaviour. Secondly, we perform two long transient climate change experiments in which we take lateral boundary conditions from a global climate model for the time period 1961-2100. The control period (1961-1990) in this experiment is first compared to the observed climate and to the reanalysis-driven experiment. Finally, we investigate the regional climate change signal in the transient experiments.

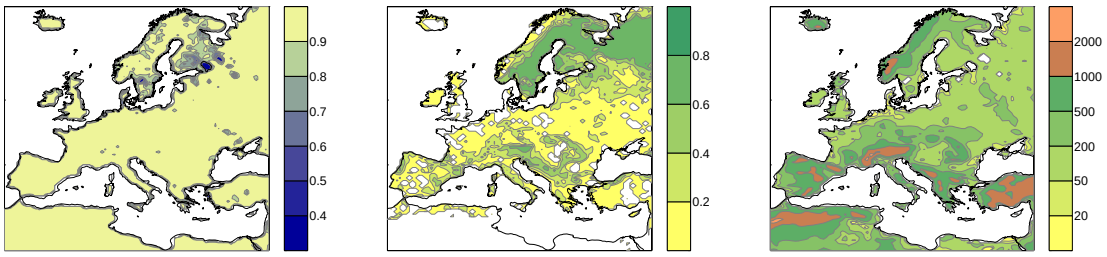

Figure 2. *Land fraction with coastal regions and lakes shown in blue colours (left), forest fraction (middle) and orography in metres (right) in the current model setup.*

The model setup is common for both experiments. RCA3 has been run on a rotated latitude-longitude grid with a resolution of 0.44^{o}, corresponding to 49 km. The land-sea mask, the fractions of lakes and forests, and the orography are shown in Figure 2. The domain covers Europe with 102x111 grid boxes of which the outermost eight on each side are used as boundary relaxation zones. We have used 24 unequally spaced sigma-levels in the vertical. The time step used for the calculations is 30 minutes. In the following results are only shown for the interior model domain (85x95 grid boxes). Each simulation begins four months prior to the starting date of the time period in question. These four months of spinup time are not analyzed or discussed in this report. Also in terms of forcing some parts are identical between the simulations; the land surface is initiated from HIRLAM climatology (Undén *et al.*, 2002), aerosols are kept constant throughout the simulations, and the solar constant is held constant at 1370 Wm^{-2}. Apart from these common forcing agents and the changes in greenhouse gases and sea surface temperatures (SST), as described separately for the different experiments below, we have not included any other types of external forcing.

The reanalysis-driven experiment covers the time period from January 1961 to August 2002 with lateral boundary data and SSTs taken from the European Centre for Medium range Weather Forecasts (ECMWF) ERA40 data set (Uppala *et al.*, 2005) every six hours. The ERA40-data was downloaded on a 2^{o} horizontal resolution and 60 vertical levels of which we used levels 13-60 covering the vertical domain between the surface and 10 hPa. The ERA40-data was interpolated both horizontally and vertically to the RCA grid. In terms of greenhouse gas forcing we have imposed a linear increase with time in carbon dioxide (CO_2) identical to that used for producing the ERA40 dataset (1.5 ppm_v per year). Since RCA3 does not include other greenhouse gases explicitly we do not change their effect with time. This experiment is referred to as RCA3ERA.

In the transient simulations, RCA3 is run for the time period 1961-2100 with lateral boundary conditions and SSTs updated every six hours from a global climate model simulation with ECHAM4/OPYC3 (Roeckner *et al*., 1999) at DKRZ, the Deutsches Klimarechenzentrum GmbH, and the Max-Planck Institute for Meteorology in Hamburg. ECHAM4/OPYC3 is a coupled atmosphere-ocean general circulation model that was run at T42 spectral resolution corresponding to a horizontal grid spacing of 2.8^{o}. Greenhouse gases and the radiative effect of sulfur aerosols is accounted for in terms of equivalent CO_2 concentrations following the A2 and B2 emission scenarios from the Special Report on Emission Scenarios (SRES) by the Intergovernmental Panel on Climate Change (Nakićenović *et al*., 2000), see Table 1 for details. The numbers for each year are interpolated linearly from the decadal values shown in Table 1. These experiments are referred to as RCA3ECHAM4 (for the control period 1961-1990) and RCA3ECHAM4B2 and RCA3ECHAM4A2 for the two scenarios respectively.

Table 1. *The anthropogenic radiative forcing is taken from table II.3.11 in IPCC (2001) and includes the effect of greenhouse gases plus the indirect and direct effects of aerosols under the SRES B2 and A2 emissions scenarios. The equivalent CO_2 concentration for a certain time is calculated using the radiative forcing (ΔF) by $\Delta F=5.35\ln(CO_2/CO_{2ref})$ where CO_{2ref} is the concentration in 1990 (expression taken from Table 6.2 in IPCC, 2001). Note that other greenhouse gases at their present levels are indirectly accounted for in the RCA3 radiation scheme, it is only the CO_2 concentrations that are changed. This means that the equivalent CO_2 concentrations in the Table are lower than the ones inferred from the greenhouse gas concentrations in the atmosphere.*

Year	**Radiative forcing (W/m^2)**	**Equivalent CO_2 concentration (ppm_v)**	
		SRES B2	SRES A2
1960	0.39	313	313
1970	0.41	314	314
1980	0.68	331	331
1990	1.03	353	353
2000	1.33	373	373
2010	1.82	409	403
2020	2.36	453	426
2030	2.81	492	470
2040	3.26	536	532
2050	3.70	581	602
2060	4.11	628	702
2070	4.52	678	823
2080	4.92	730	963
2090	5.32	787	1123
2100	5.71	847	1316

In addition to the ERA40-driven simulation with RCA3 an identical simulation in terms of boundary conditions, forcing, time periods and model grid is undertaken with the previous model version RCA2 (Jones *et al*., 2004). This is referred to as RCA2ERA40 in the following. By comparing these two simulations we explore to what degree changes in the model have led to an improved agreement with the observed climate.

The results of the model experiments are mostly shown as maps of seasonal averages. In both the reanalysis driven experiment and the control period of the transient climate change experiments we compare model results to observations for the time period 1961-1990 unless otherwise noted. Monthly means for a few areas are used to illustrate the seasonal cycles. The regions used are shown in Figure 3. Also the simulated interannual variability of monthly means is investigated both in terms of its magnitude and how well it correlates to the observed climatology.

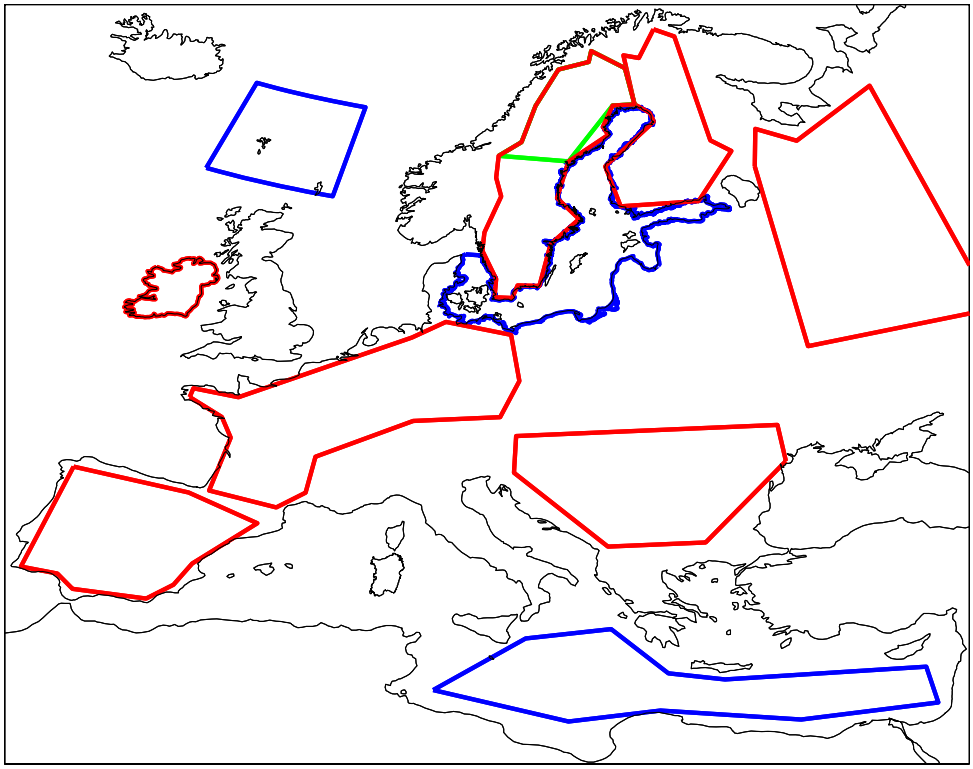

Figure 3. *Land (red) and ocean (blue) areas that are used in this report. These are referred to as Sweden, Northern Sweden (green), Finland, North-Western Russia, Ireland, Western Europe, South-Eastern Europe, Iberian Peninsula, North Atlantic, Baltic Sea and Southern Mediterranean.*

2.3 Observational data sets

Evaluation of the model performance in today's climate has been done by the aid of several data sets. These include both gridded climatologies and data from climatological stations. A compilation of all used data sets can be found in Table 2.

Table 2. *Data sets that have been used for model evaluation in this report. *) As a first order correction these climatologies have been adjusted for differences in elevation compared to the RCA grid by using a lapse rate of -0.0065 K* m^{-1}.

Dataset	Variables	Resolution		Reference
		Temporal	Horizontal	
CRU TS 2.1	T_{2m} *), precipitation, cloud cover	Monthly	0.5°	Mitchell *et al*. (2005)
Willmott 3.02	T_{2m}, precipitation	Monthly	0.5°	Willmott and Matsura (1995)
ERA40	T_{2m} *), precipitation, MSLP, wind speed	Monthly	1.0°	Uppala *et al.* (2005)
GPCP 2	Precipitation	Monthly	2.5°	Adler *et al*. (2003)
ECA	T_{2max} *) and T_{2min} *)	Daily	Station data	Klein Tank *et al*. (2002). See also <http://eca.knmi.nl>.
ISCCP D2	Cloud cover	Monthly	2.5°	Rossow and Schiffer (1999)
Snow	Snow water equivalents	Annual	Station data	Raab and Vedin (1995)
Snow season duration	Snow cover	Daily or higher	Station data	SYNOP
Lake data	Temperature	Monthly	Station data	See Figure 3.2.3
MESAN	Wind gusts	Hourly	22 km	Häggmark *et al*. (2000)

3 The reanalysis-driven experiment (RCA3ERA)

In this section the 40-year experiment with ERA40 as the driving model is analyzed. We compare RCA3-results both to the ERA40-data itself and to different sets of observations. It is to be expected that the RCA3 results should not be too different from the ERA40-data since it is forced by those data on the lateral boundaries. But, at the same time, in the inner parts of the model domain RCA3 is running in free climate mode, while the ERA40-data are based on analyses or 6-hr forecasts. Also, several of the parameterizations differ between RCA3 and the ECMWF-model underlying the ERA40-data. We also make comparisons to the previous model version, RCA2 (Jones *et al.*, 2004), which has been extensively used at the Rossby Centre during the last couple of years (*e.g.* Rummukainen *et al.*, 2004; Räisänen *et al.*, 2003; 2004; Kjellström, 2004).

3.1 Mean sea level pressure

As expected, the differences in climatological mean sea level pressure (MSLP) between RCA3 and the forcing ERA40 reanalysis are rather small indicating that RCA3 reproduces the large-scale circulation in the driving reanalysis (Figure 4). There are, however, some notable differences. In the Mediterranean region the MSLP is higher in RCA3 than in ERA40 in all seasons, particularly in fall and winter. This is a feature also noted by Jones *et al.* (2004) for the earlier model version RCA2. They speculated that RCA2 does not represent lee cyclogenesis downstream of the Alpine and Pyrenean mountain chains properly. In winter there is also a negative bias in Eastern Europe of more than 1 hPa indicating a stronger cyclonic activity over this part of Europe than in the ERA40 data. Both these biases are basically not changed in RCA3 as compared to RCA2. It can also be noted that the effect of the lateral boundary conditions is seen also at the outermost 1-2 gridpoints in the interior model domain for most locations and seasons as differences between RCA3 and ERA40 are smaller there than in gridpoints further inwards in the RCA3 model domain. Large differences in high altitude regions are due to differences in the orography in the two different model grids, with the ERA40 orography being much smoother than in RCA3.

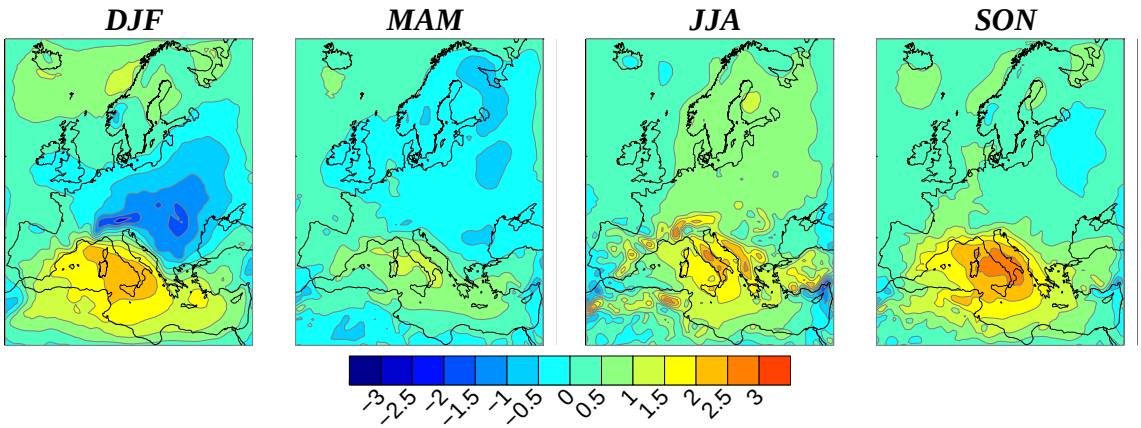

Figure 4. *Difference in MSLP between RCA3 and ERA40. Units are hPa.*

The simulated interannual variability is close to that in the ERA40 data set. Figure 5 shows the correlation between the time series of monthly anomalies (i.e. the monthly mean value for a particular month minus the climatological average for that particular month) in ERA40 and RCA3. The correlations in Sweden are high (higher than 0.9) in all seasons which is the case also for most other European regions except in south-east Europe where the degree of correlation is lower in the summer half of the year. It is a general tendency in all regions that the agreement is best during winter and worst during summer. This relates to the fact that the lateral boundary conditions have its highest impact on the interior parts of the model domain in winter while the summer climate is more locally determined. In both areas shown in Figure 5 (as in the other studied areas) the RCA3 simulation show an improved agreement with the observed interannual variability compared to RCA2.

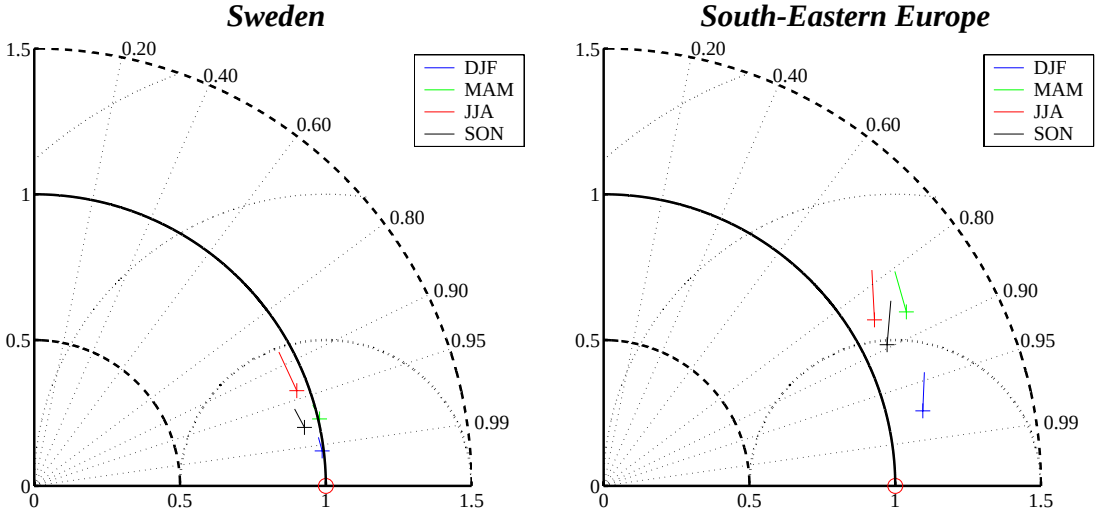

Figure 5. *Taylor diagrams (Taylor, 2001) showing the standard deviation of the simulated monthly mean anomalies in MSLP normalized by the standard deviation of the monthly mean anomalies from ERA40 (radial distance to the origin). The diagram also shows the correlation coefficient between the time series of RCA3 and ERA40 (the angle from the abscissa as indicated on the outermost circle). ERA40 is indicated with (○) and RCA3 results for the different seasons with (+). The radial distance between the observations (ERA40) and the RCA3 results is the RMS error. The starting point of the lines that ends in the (+) represents the RCA2 simulation. Ideally a model improvement should lead to an arrow pointing towards the (○).*

3.2 Surface temperature

3.2.1 Time mean temperature

In general RCA3 simulates temperatures within ±1^{o}C in most regions and seasons with two major exceptions, both during fall and winter (Figure 6). These exceptions are; a warm bias in the north-eastern part of the model domain and, a cold bias in the Mediterranean region. In these areas local biases of 3-4^{o}C can be seen. The biases in the north-eastern part of the domain are particularly strong compared to CRU during winter.

The wintertime bias in northern Scandinavia may partly be an artefact since many stations are located in valleys that tend to be colder than their surroundings in winter (Räisänen *et al.*, 2003). The bias in Sweden is much smaller compared to ERA40 and the Willmott dataset which lends some confidence into this statement, Figure 7. But, RCA3 is too warm also in the north-eastern part of the domain, particularly in North-Western Russia, which can not be explained by an artefact in the CRU data. In that area RCA3 simulates higher temperatures than RCA2 for two reasons: i) the downward longwave radiation below clouds is higher than in RCA2 and ii) there is less snow in RCA3 (see Ch 3.6). The warm bias in summer in south-eastern Europe as noted for several RCMs (Christensen *et al.*, 1997) including RCA2 (see Jones *et al.*, 2004) is largely reduced in RCA3 (Figure 7) due to the decrease in clear-sky downward shortwave radiation. Further south, in the Mediterranean region, this reduction in downward shortwave radiation in RCA3 leads to a negative temperature bias during fall and winter.

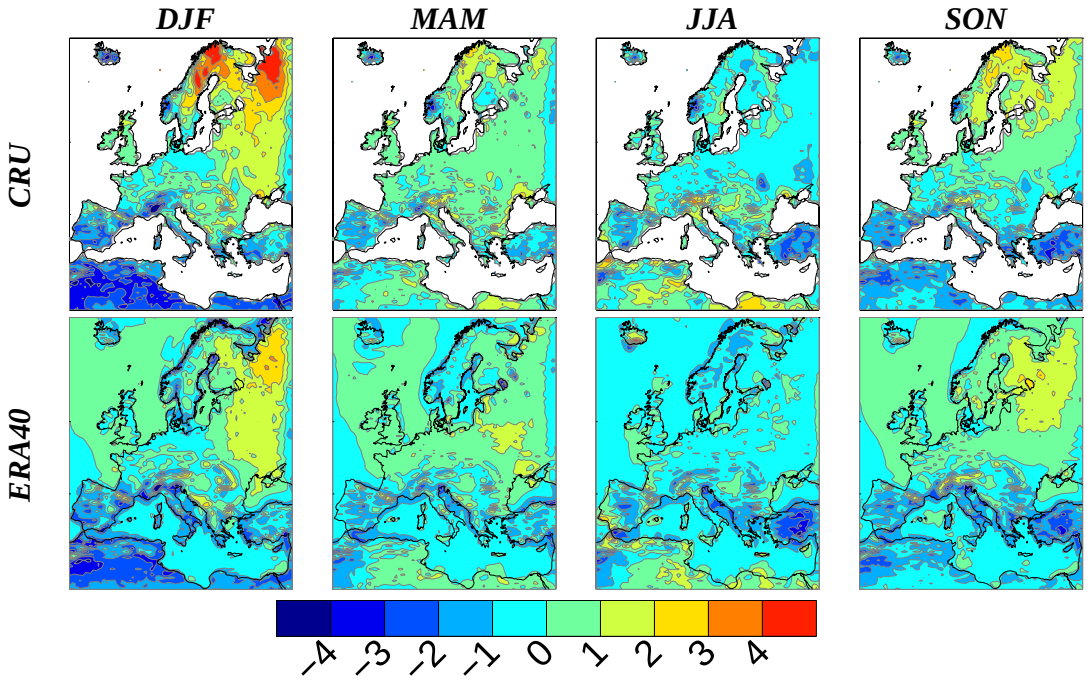

Figure 6. *Seasonal mean difference in T_{2m} between RCA3ERA40 and observations as indicated to the left. The differences are based on grid box T_{2m} in RCA3. Units are ^{o}C.*

The big lakes in northern Europe (Lake Ladoga and Lake Onega in Russia and Lake Vänern in Sweden) also stand out in the lowermost panels of Figure 6, being warmer (colder) in RCA3 in fall and winter (spring and summer) than in ERA40 which does not include a description of lakes. The thermal inertia of the lakes in RCA3 leads to a lag in the seasonal cycle which is more in line with the observed seasonal cycle of the temperature climate of these lakes (Figure 8), indicating the benefit of having a lake model coupled to the atmospheric model.

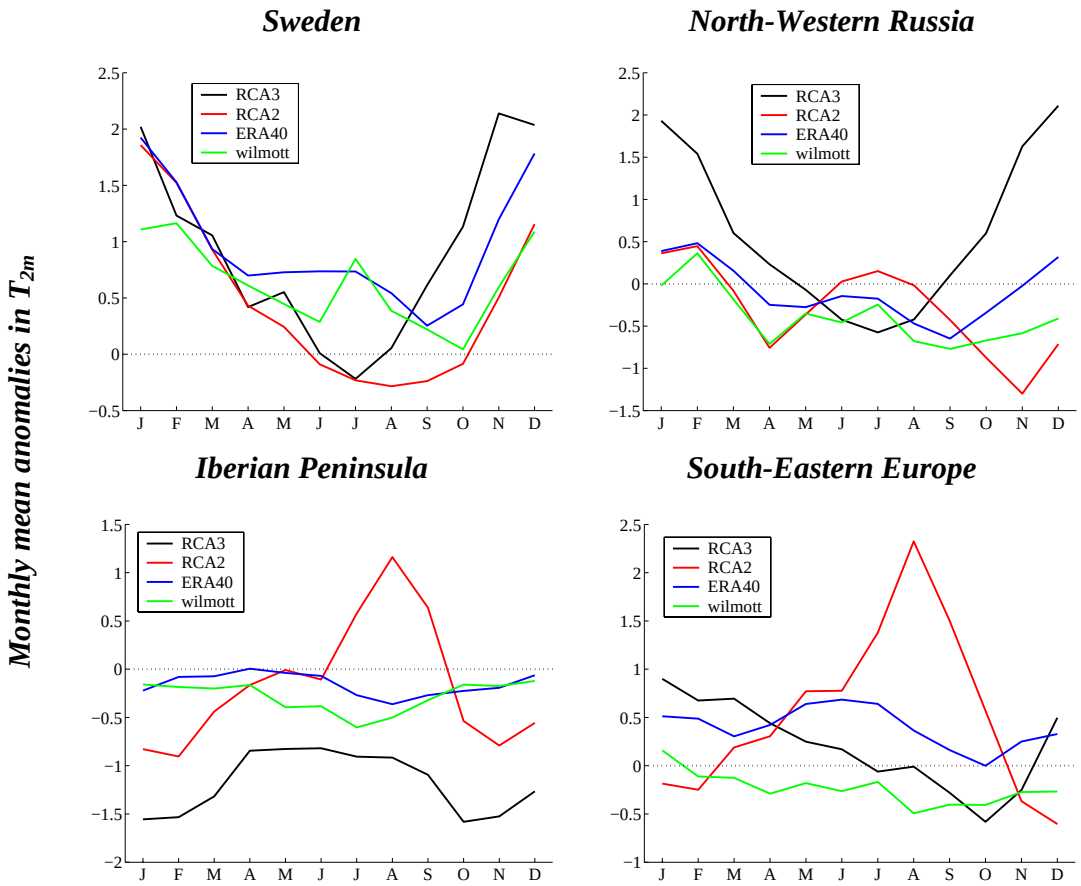

Figure 7. *Monthly mean anomalies in T_{2m} for RCA3, RCA2, ERA40 and Wilmott as compared to CRU. Units are ^{o}C.*

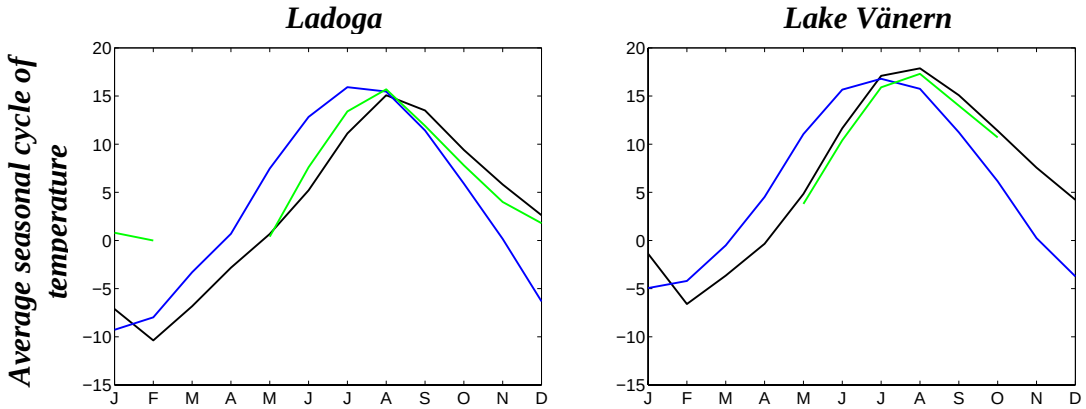

Figure 8. *Average seasonal cycle of surface temperature in Ladoga and Vänern. RCA3 (black) and ERA40 (blue) are averages over the time period 1961-1990. Observations (green) from Ladoga are at 0.1 m depth in the northern part of the lake for the time period 1958-1988 (Long Standing Data of Conditions and Resources of Inland Surface Waters, 1 (5)(1986) Publ. House Hydrometeoizdat, Leningrad, 688 pp. (In Russian). The observations from Vänern are surface temperatures at Mergrundet for the time period 1981-1985 (Statistiska Centralbyrån, Naturmiljön i siffror, 1987). Units are ^{o}C.*

In most areas the interannual variability is captured better in ERA40 than in RCA3 (Figure 9). This is a result of the data assimilation that lies behind the ERA40 data. Still, the correspondence between RCA3 and CRU is quite good with correlation coefficients of about or more than 0.9 for most areas and seasons and an interannual variability that lies within ±20% of the observed one. The interannual variability is in general smaller in RCA3 than in RCA2 in continental areas which leads to an improvement particularly in southern and central Europe during summer, Figure 9.

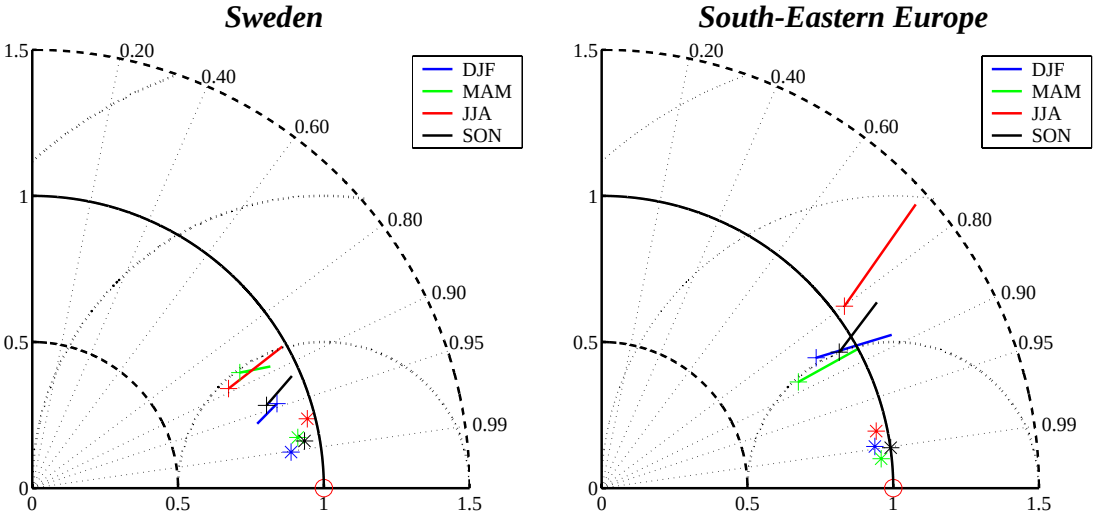

Figure 9. *As Figure 5 but for T_{2m} instead of MSLP. The reference data set is from CRU (○), model simulations from RCA2 and RCA3 (line and +) and ERA40 (*).*

3.2.2 Diurnal temperature range

The diurnal temperature ranges for the observations and models are shown in Figure 10. For CRU, RCA3 and RCA2 the annual mean diurnal temperature range is defined as the average difference between the daily maximum and minimum temperature while for ERA40 it is calculated as the average of daily maximum difference between six hourly instantaneous temperature values. Thereby the ERA40 should give smaller diurnal range than the other three. Also differences in gridcell size may contribute. In general CRU gives a larger diurnal range than the models. One contribution to this difference is that CRU data is based on open land observations while the model results are given as grid averaged temperature including water and forest. From land-surface perspective RCA3 should give larger diurnal range than RCA2 since the land surface scheme in RCA3 is more responsive to changes in energy fluxes than the land surface scheme in RCA2. However, this effect is only seen in the southernmost part of the domain while in other areas the results show the opposite situation.

The generally reduced diurnal range in RCA3 compared to RCA2 is mainly explained by more cloud water which tends to increase downward long-wave radiation, making the temperature drop less during night time, and to decreased clear-sky downward short-wave radiation, making the daily maximum temperature lower. The increase of cloud water is most pronounced in the northern half of the domain during the spring, summer and fall. Compared to ERA40 there is a larger fraction of low clouds and more cloud

water in RCA3 during summer which leads to a smaller diurnal temperature range in RCA3 compared to ERA40. The larger diurnal temperature range in the south in RCA3 compared to ERA40 is in better agreement with CRU and is explained by a corresponding smaller amount of clouds in that part of the model domain.

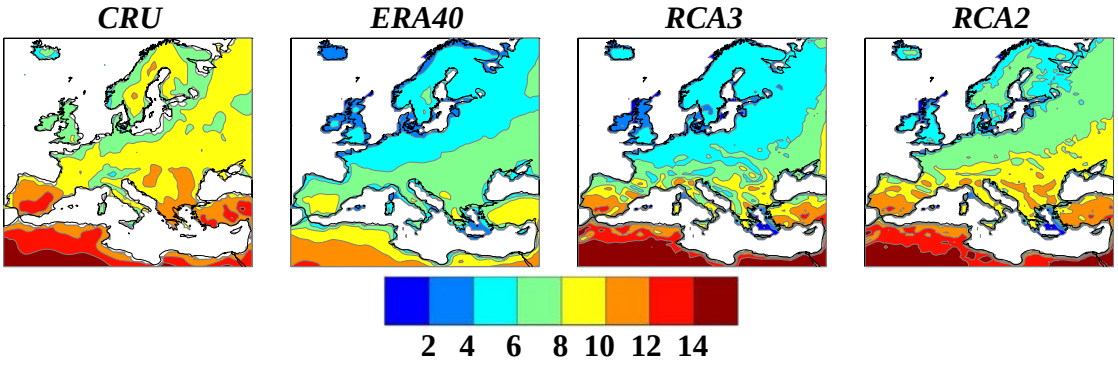

Figure 10. *30-year annual mean diurnal temperature range in CRU, ERA40, RCA3 and RCA2. Units are ^{o}C.*

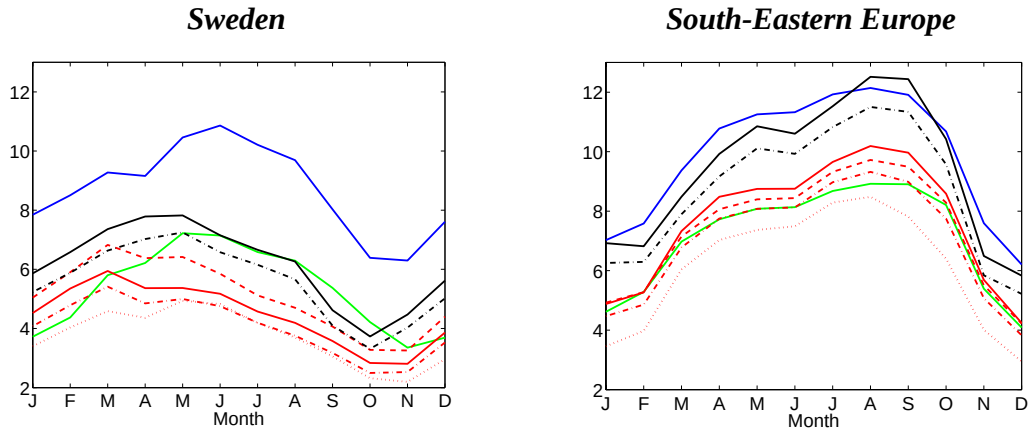

Figure 11. *The area averaged seasonal cycles of the diurnal temperature range in Sweden and South-East Europe. The line colours represent CRU (blue), ERA40 (green), RCA3 (red) and RCA2 (black), respectively. The line types represent daily max – daily min (full), except for ERA40 which is based on 6 hourly output (for RCA and ERA40 grid-averaged temperatures are used), diurnal range based on 3 hourly model output of grid-averaged temperature (dash-dotted), diurnal range based on 3 hourly model output of open-land temperature (dashed) and diurnal range based on 3 hourly model output of forest temperature (dotted), respectively. Units are ^{o}C.*

From the seasonal cycles of the diurnal temperature range as shown in Figure 11 it is clear that a diurnal cycle based on the difference between maximum and minimum daily temperatures generally is larger than a cycle based on less frequent output. For RCA3 it is also seen that the open-land diurnal range is larger than the forest diurnal range. Note that in a forest dominated landscape, as in Sweden, the 3 hourly open-land temperatures give larger diurnal range than the difference between maximum and minimum daily grid-averaged temperatures.

3.2.3 Daily maximum and minimum temperatures

This section focuses on the seasonal variation of two selected extreme percentiles of daily minimum and maximum temperature. These are the 5th and the 95th percentiles computed for each season. In essence, these percentiles can be interpreted as the values that will be exceeded on average four to five times each three-month season. For the 5th percentile the exceedance is in negative direction, i.e. towards colder temperatures and for the 95th percentile the exceedance is towards warmer temperatures.

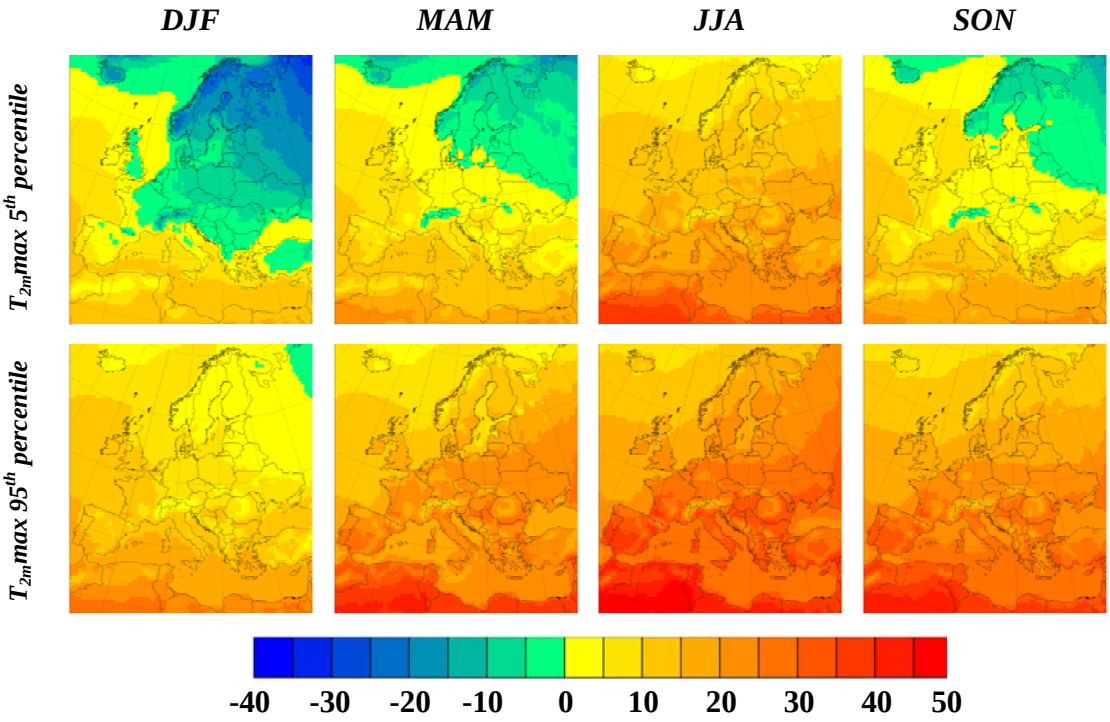

Figure 12. *Seasonal variation of gridcell average T_{2max}. The upper row shows the 5th percentile (extremely low), and the bottom row shows the 95th percentile (extremely high). Units are °C.*

Figure 12 shows the seasonal cycle of daily T_{2max} in RCA3. The annual amplitude in the 5th percentile is about 40°C (-30 to +10) in northern Scandinavia and 25°C (-5 to +20) in the European Mediterranean region. For the 95th percentile the annual cycle has an amplitude of about 20°C (0 to +20) in the north and 25°C (+10 to +35) in the European Mediterranean region. In Figure 13 the corresponding maps for gridcell average daily minimum are shown. The annual cycle in the 5th percentile is about 45°C (-40 to +5) in northern Scandinavia and about 20°C (0 to +20) in the European Mediterranean region. For the 95th percentile the annual cycle has an amplitude of about 20°C (-25 to 0) in the north and about 10°C (+5 to +15) in the European Mediterranean region.

Evaluation of how well these results are capable to reproduce the observed climate requires datasets of maximum and minimum temperatures with daily resolution. Presently, no gridded time-series datasets of comparable temporal resolution are

available. We therefore use the ECA dataset (see Table 2) that comprises quality controlled station observation time-series. We use the 'blended dataset' in which data from closely located stations occasionally have been merged to form one long time-series. Only station series with less than 300 missing observations were accepted. In total 126 stations were used, of which 91 series were complete and 9 series had more than 31 observations (one month) observations missing. The verification of the simulated gridcell average is done with respect to observations at a specific location within the gridcell.

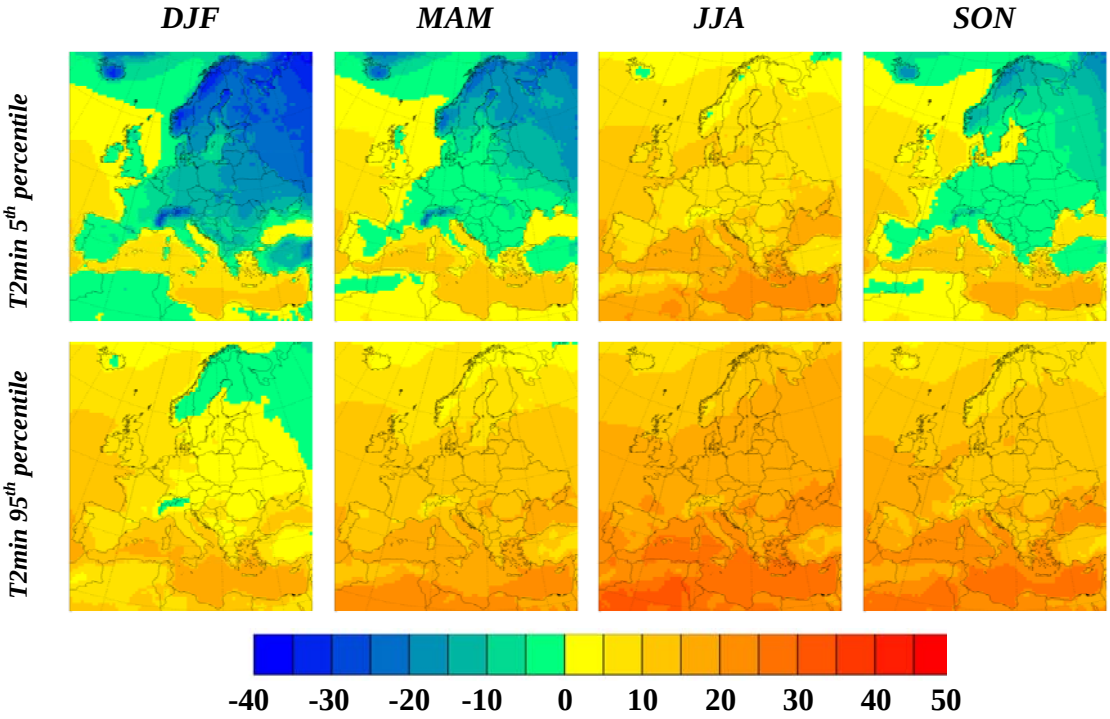

Figure 13. *Same as Figure 12 but for daily T_{2min}. Units are °C.*

RCA3 simulation underestimates the 95th percentile T_{2max} (hot conditions) by some 0 to 6°C, with the exception of the Mediterranean region where instead the 95th percentile is overestimated by 0 to 6°C at many stations during spring, summer and fall (Figure 14). During spring and summer the 95th percentile is overestimated at three coastal stations in Scandinavia probably because of local conditions near the coast. Similarly, during winter the warm conditions are slightly (0 to 2°C) overestimated at six inland stations in the northeast. The general underestimation of the 95th percentile T_{2max} during the summer half year is mainly related to an overestimation in the cloud water content and the excessive downward longwave radiation in north and central Europe (cf. section 3.4 and 3.2.2). Now turning to the 5th percentile, the picture is more complex. The broad picture is that the model overestimates daily T_{2max} during the coldest days in all seasons but the summer. The overestimate is most pronounced in the northeast during autumn and winter. Exception to the general overestimate is southern Scandinavia, Germany, and the British Isles during winter and spring. Typically, the error is within ±6°C, but for a few scattered stations the error can be larger, especially during the autumn and winter.

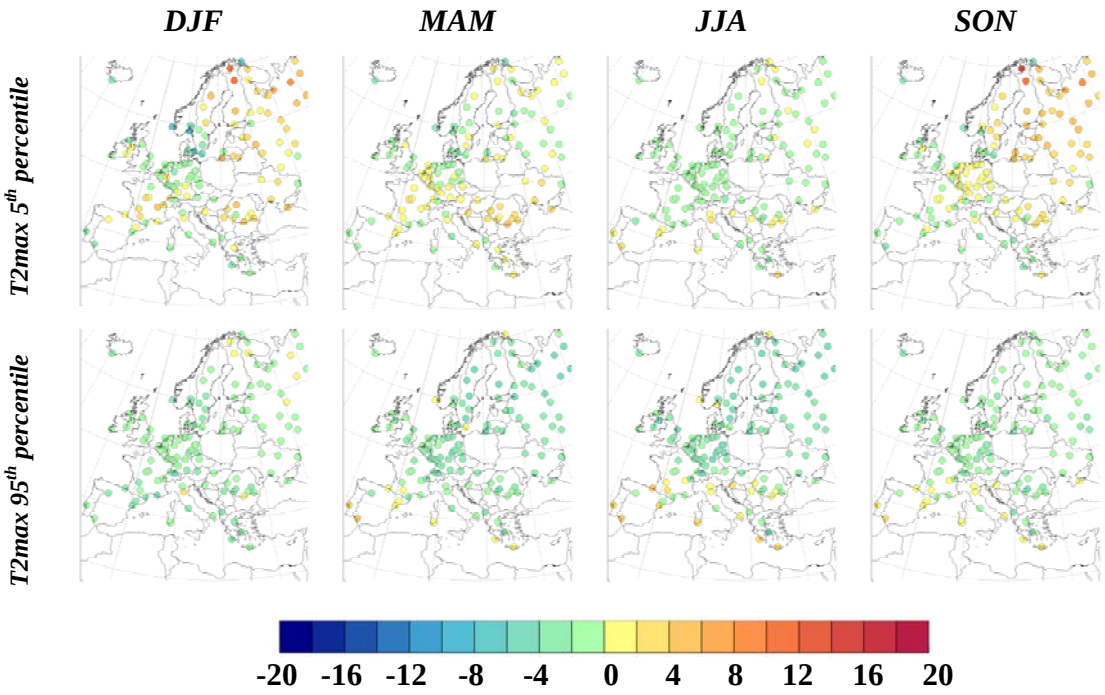

Figure 14. *Verification of gridcell average daily maximum 2 metre temperature in the reanalysis run (cf. Figure 12) versus station observations. The maps show the difference RCA3 minus observations selected ECA stations. The top row shows the seasonal 5th percentile based on the period 1961-1990, and the bottom row shows the corresponding 95th percentile. Units are °C.*

The extreme percentiles of T_{2min} shows an almost opposite pattern (Figure 15) in the 95th percentile (warm conditions) compared to that of T_{2max}. Here the model overestimates the temperature except for in the Mediterranean and south-eastern European region. The errors are typically modest, in the range -2 to +4 °C, with slightly larger negative values for a cluster of stations in SE Europe. And, again, the pattern is more complex and the errors are larger in the 5th percentile. In the north-eastern part of the region the model consistently overestimates the very low temperatures, more so during autumn and winter. Again, these errors are reflecting the errors in cloud water and downward longwave radiation (*cf*. section 3.4).

By combining the low 5th percentile of daily minimum temperature with the 95th percentile of daily maximum temperature we define for the purpose of this report an annual temperature span as a measure of continentality. As it is the annual difference between very warm daily maximum and very cold daily minimum conditions this temperature interval will be exceeded (in positive or negative direction) only during about 10 days per years. According to the RCA3 simulation, this annual span (Figure 16) is about 35 to 45°C in the north-eastern regions, and even larger along the eastern boundary, and in southern Europe it is about 20 to 25°C. Over the oceans this span is substantially lower due to the thermal inertia of the oceans, 5 to 15°C in the NE Atlantic region and 10 to 20°C over the North Sea and over the Mediterranean. Over some

oceanic regions, north of Iceland, the Gulf of Bothnia and the White Sea where there may be a seasonal sea-ice cover, the annual span approaches that of the adjacent land areas. While the overall pattern of the simulated continentality index closely resembles that of the observations, the point observations generally show an annual span that is about 5°C wider.

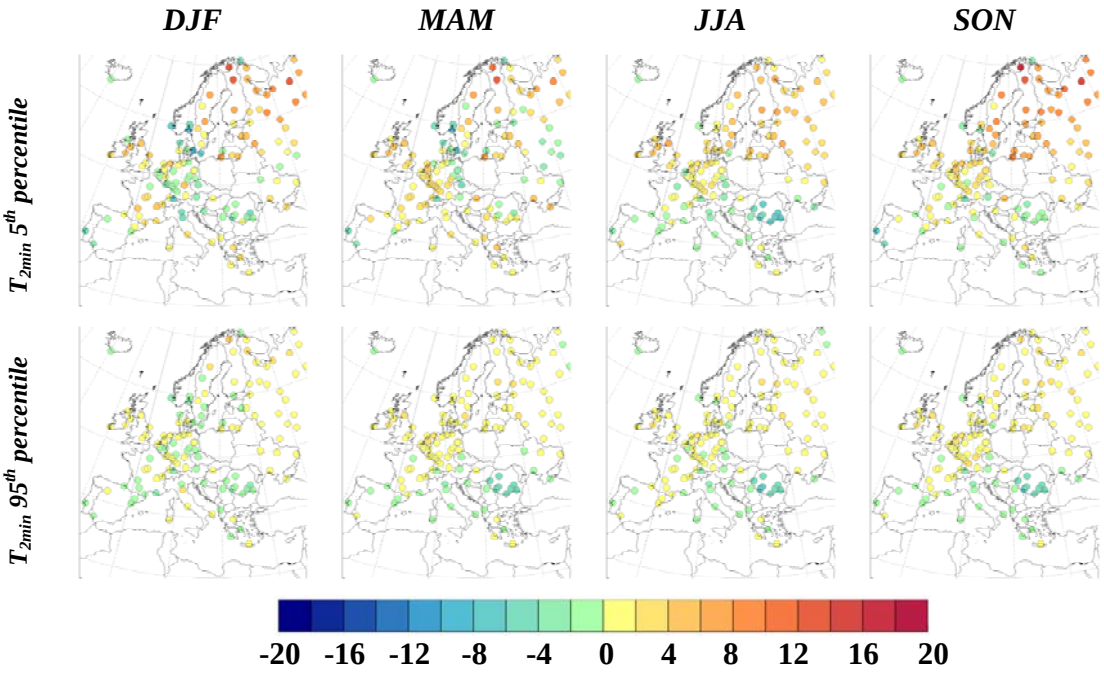

Figure 15. *Same as Figure 14 but for T_{2min} in the reanalysis run (cf. Figure 13) versus station observations. Units are °C.*

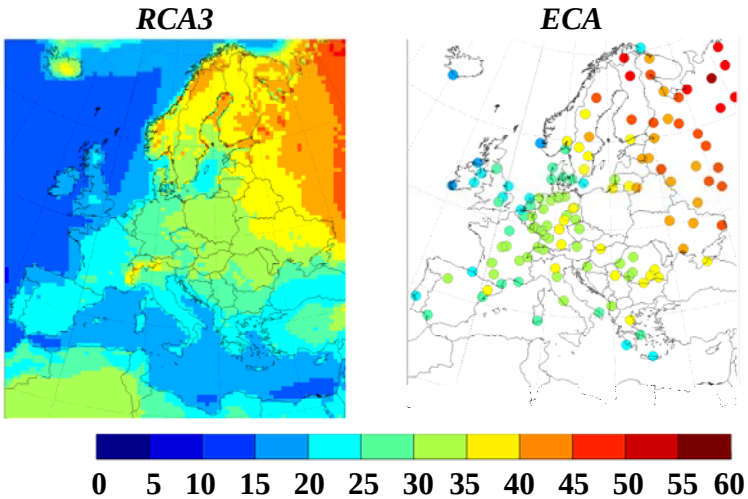

Figure 16. *The continentality index is for the purpose of this report defined to be the difference between the summer-time (JJA) 95th percentile of T_{2max} and winter-time (DJF) 5th percentile of T_{2min}. Units are °C.*

3.3 Precipitation

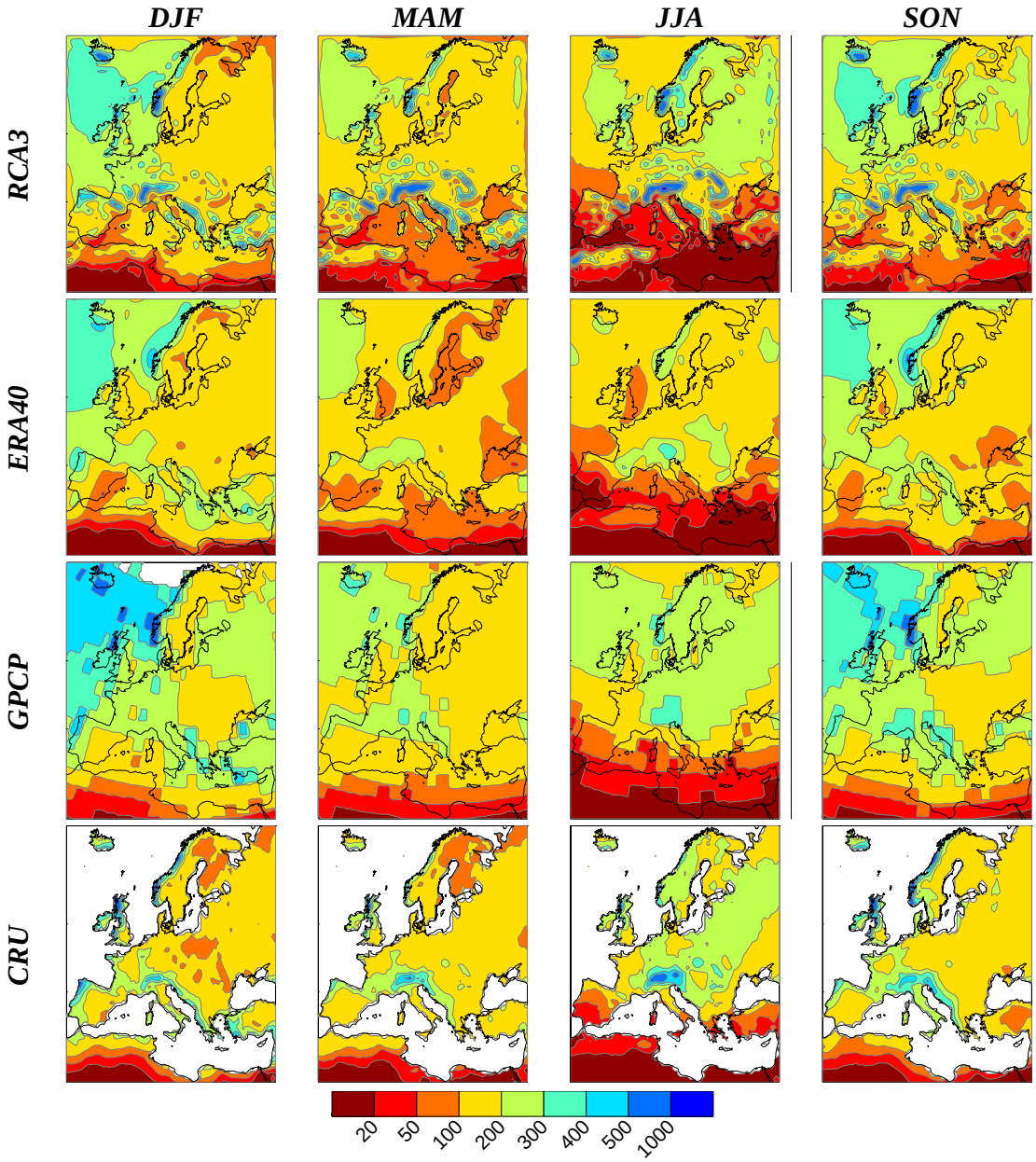

Figure 17. *Seasonal mean precipitation in RCA3, ERA40, GPCP and CRU. Units are mm per 3 months.*

The geographical distribution of precipitation and its seasonal cycle is simulated in a realistic way in RCA3 (Figures 17 and 18). The higher resolution in RCA3 as compared to the ECMWF model used for producing the ERA40 data is clearly seen in some areas like the Atlantic coast of Norway where RCA3 shows more precipitation over land than ERA40 which, due to its smoother orography has more precipitation to the west over the sea. Also, the geographical distribution of precipitation over the British Isles is much better captured in RCA3 compared to ERA40 in all seasons. In all high-altitude areas

RCA3 simulates more precipitation than in ERA40 and CRU. The fact that CRU is lower may partly be explained by the well-known problem of undercatch in precipitation observations, see for instance Rubel and Hantel (2001).

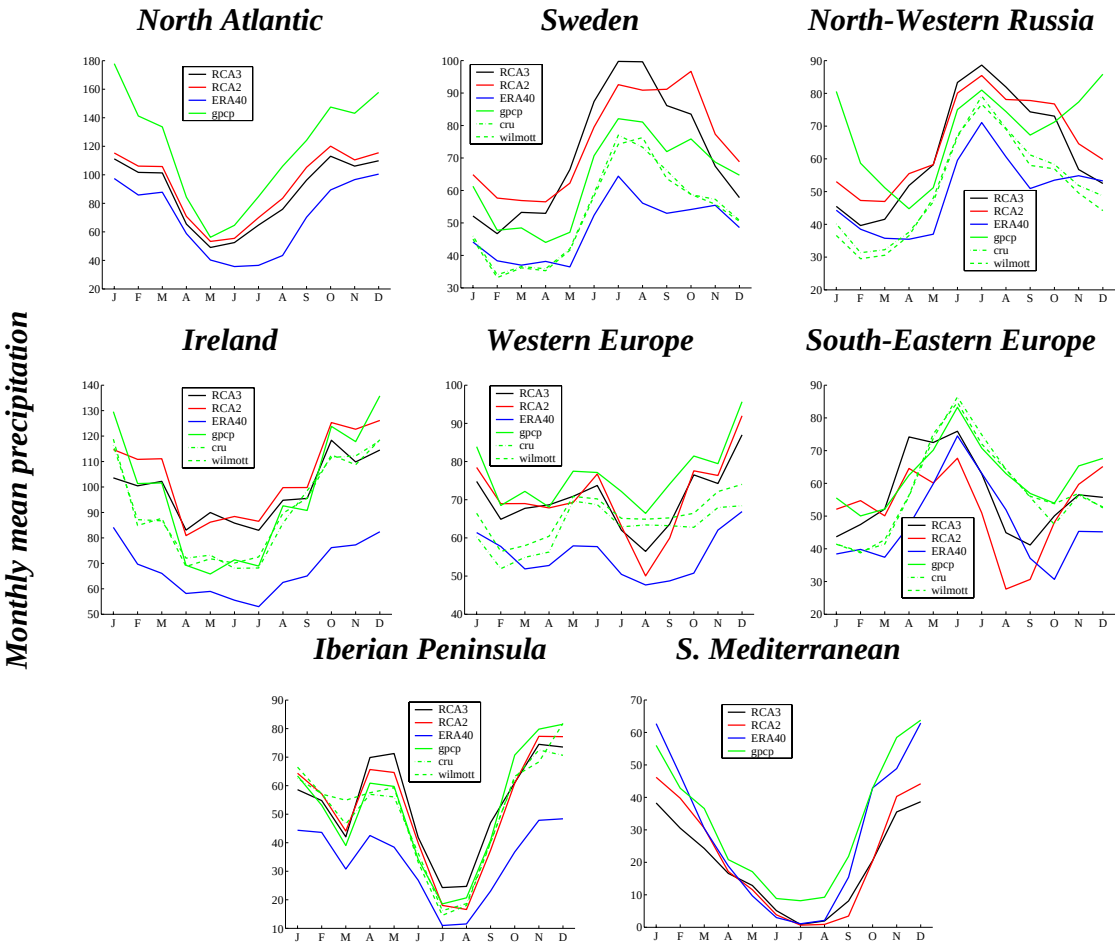

Figure 18. *Seasonal cycle of precipitation in eight regions. Units are mm / month.*

The seasonal cycles in Figure 18 clearly reveal that ERA40 underestimates precipitation over large parts of Europe. This underestimation has been attributed to too little precipitation in connection to extratropical cyclonic systems (Hagemann *et al.*, 2005) and the problem is much smaller in the southern Mediterranean. RCA3 tends to overestimate precipitation in northern Europe during summer and underestimate it in the south-east. It should be noted that RCA3 shows a better agreement to the observations in South-Eastern Europe during summer than RCA2. This improvement is probably contributing to the smaller temperature bias in this region in RCA3 (*cf.* section 3.2). This is the only notable differences between the two model versions in terms of total precipitation. Over the Southern Mediterranean RCA3 underestimates precipitation compared both to ERA40 and the GPCP climatology. Part of this difference may be attributed to the bias in mean sea level pressure discussed in section 3.1 although the largest differences in precipitation over the Mediterranean Sea are not in the same regions or seasons as the largest differences in MSLP.

The interannual variability in RCA3 is similar to that in ERA40 indicating that the data assimilation can not alone outweigh the better agreement of RCA due to the higher resolution (Figure 19). The changes in going from RCA2 to RCA3 are mostly pointing in the right direction but they are small and no systematic improvement is seen between the regions and seasons.

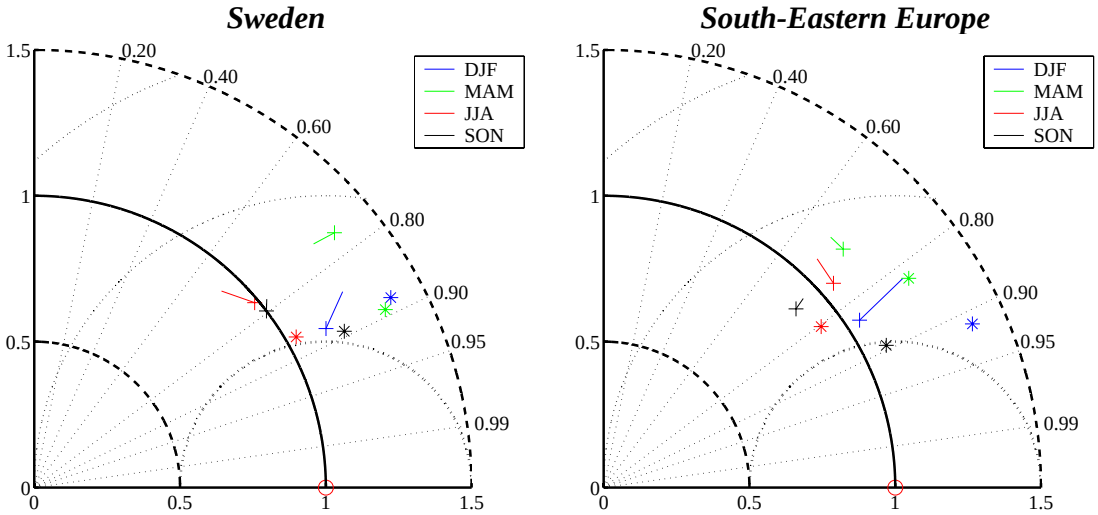

Figure 19. *As figure 5 but for precipitation instead of MSLP. The reference data set is from CRU (○), model simulations from RCA2 and RCA3 (line and +) and ERA40 (*).*

3.4 Clouds

Observed and simulated cloud cover is shown in Figures 20 and 21. In general, there is a north-south gradient in total cloud cover with, on annual basis, more than 70% cloud coverage in parts of northern Europe down to 30-40% south of the Mediterranean region. Another prominent feature is the seasonal cycle with a minimum during summer in most parts of the area except for the North Atlantic where the minimum occurs during spring. RCA3 captures these main features of the observed regional cloud cover. Notable biases are; i) an overestimation of the cloud cover in large parts of northern Europe during summer and, ii) an underestimate in north-western Russia and Finland, and over the British Isles when compared to ERA40 and CRU. In large parts of northern Europe RCA3 shows better agreement with CRU and ERA40 compared to ISCCP which shows a weaker seasonal cycle. Despite of the biases, deviations between RCA3 and the observations within single regions are in general less than 10% (absolute difference) for all months.

Generally, RCA3 simulates more clouds in high altitude regions by more than 20% compared to ERA40 and the observational data sets. The fact that there are more clouds in high altitude locations in RCA3 than in ERA40 can partly be explained by the higher elevation of the surface in RCA3 due to the higher resolution. This leads to a stronger adiabatic cooling of air that is lifted in mountainous regions and thereby more condensation. We also note that there is a large negative bias in the outermost 3-4 gridboxes compared to all other datasets. This is a result of how the relaxation to the

lateral boundary conditions is done in RCA3. As there is no relaxation of cloud water or cloud ice towards the boundaries (these are set to zero there) the model has too little moisture in the boundary zone.

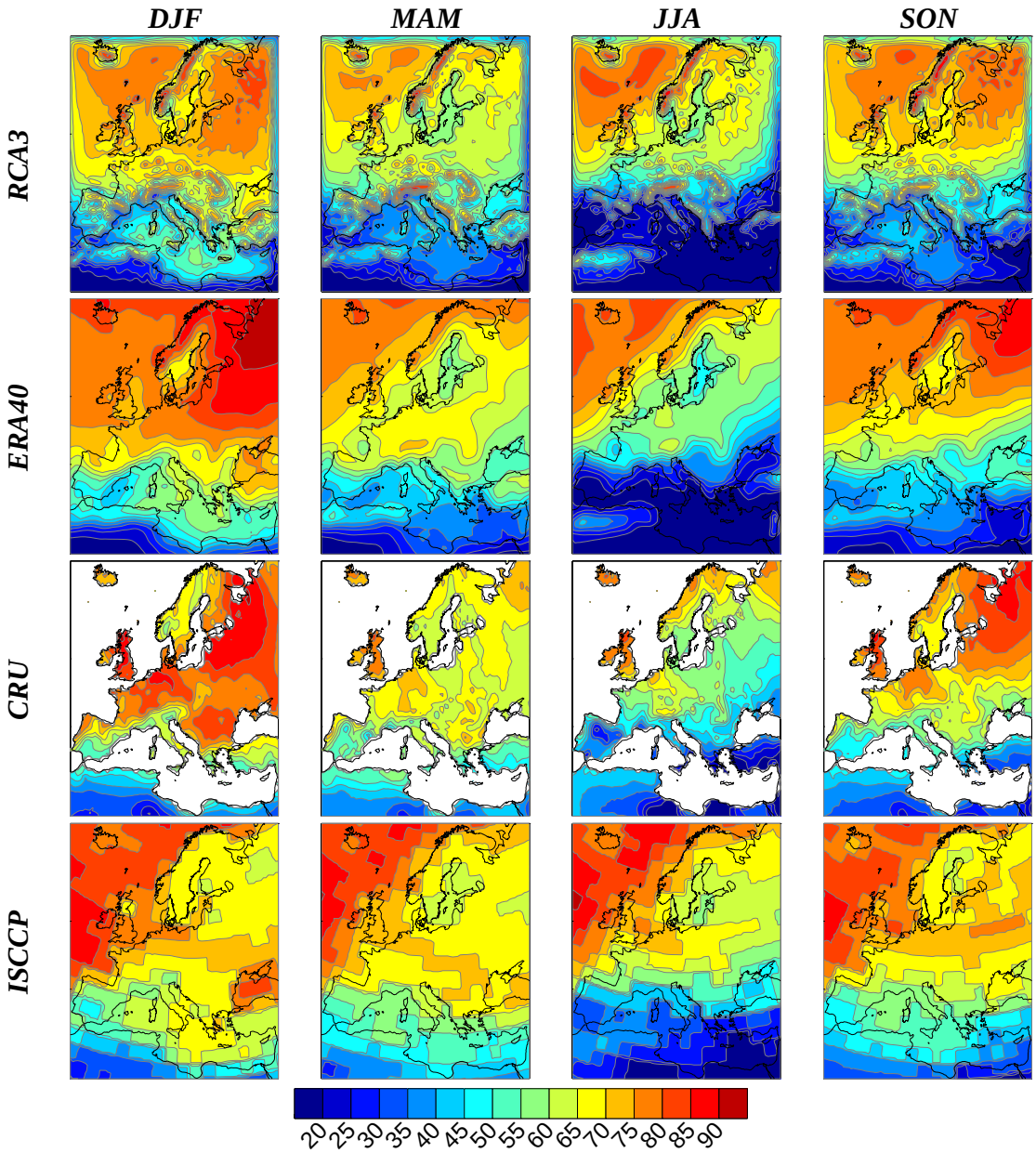

Figure 20. *Seasonal mean total cloud cover from RCA3ERA40, ERA40, CRU and ISCCP. Units are %.*

Owing to the changes in parameterizations (Section 2.1.1) the total cloud cover is substantially reduced in RCA3 compared to RCA2 in northern Europe. This reduction leads to a better agreement with both ERA40 and CRU as illustrated for Sweden and the Baltic Sea region in (Figure 21). Despite of the smaller total cloud fraction the clouds in RCA3 contain more cloud water than the clouds in RCA2 during the summer half of the

year (not shown). The cloud water has increased in RCA3 due to reduced amount of excessive drizzle. This has strong implications for near-surface temperatures (see Section 3.2).

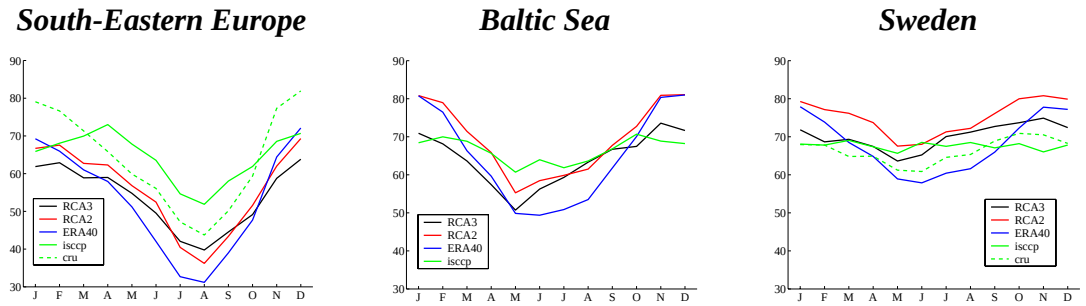

Figure 21. *Seasonal cycle of total cloud cover. Units are %.*

The differences between the two model versions in southern Europe are small and RCA3 captures the pronounced seasonal cycle with maximum in winter and minimum in summer. In most of the model domain the differences between RCA3 and ERA40 are smaller than the differences between RCA3 and the two observational data sets. Further it can be noted that the two observational data sets do not fully agree with each other. The most prominent difference between them is in the north-eastern part of the model domain where the bias in RCA3 differs in sign depending on which observational data set that is used.

3.5 Wind

3.5.1 Mean wind speed

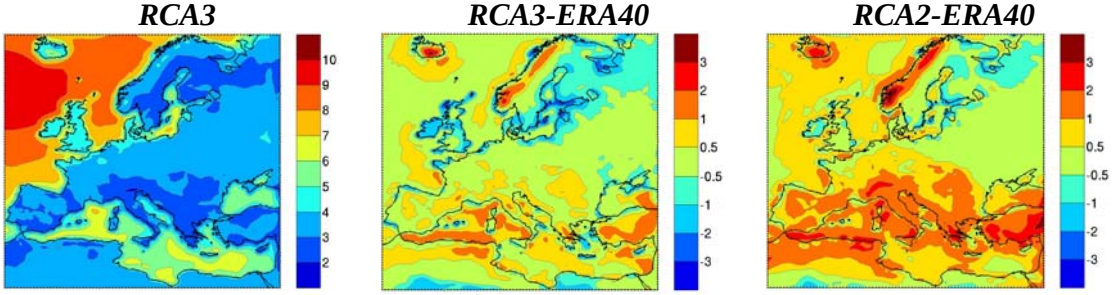

Figure 22. *The annual mean 10 m level wind speed according to RCA3 and the corresponding differences between RCA3/RCA2 and ERA40. Units are m* s^{-1}.

The contrast in wind speed between land and sea is obvious from the simulated wind speed shown in the RCA3 simulations in Figure 22. The agreement between RCA3 and ERA40 analysed wind speed is generally quite good. However, a couple of regions show significant differences. RCA3 gives higher wind speed over the Scandinavian mountain range than ERA40. One reason for such differences in mountainous areas is that wind observations are sparse and that their representativness is questionable since observations are mostly taken in valleys. Also, in ERA40, to induce enough drag, which is needed to get the large scale flow correctly simulated, quite a large orographic roughness is used

over mountains (P. Kållberg, personal communication). The high roughness makes low level wind speeds too low which shows up as a positive bias in the RCA3-ERA40 difference plot. In coastal areas, especially around the Baltic, RCA3 seems to underestimate the wind speed compared to ERA40. The reason for this is not clear but it is probably connected to how the prognostic roughness length over sea in RCA3 depends on *e.g*. stability. As RCA3, RCA2 shows higher wind speed over mountainous areas than ERA40. The wind speeds in RCA3 are generally lower compared to RCA2 in all areas and all seasons. ERA40 and RCA3 there is a tendency for overestimation of the wind speed in the Mediterranean area in RCA2.

3.5.2 Gusty wind speed

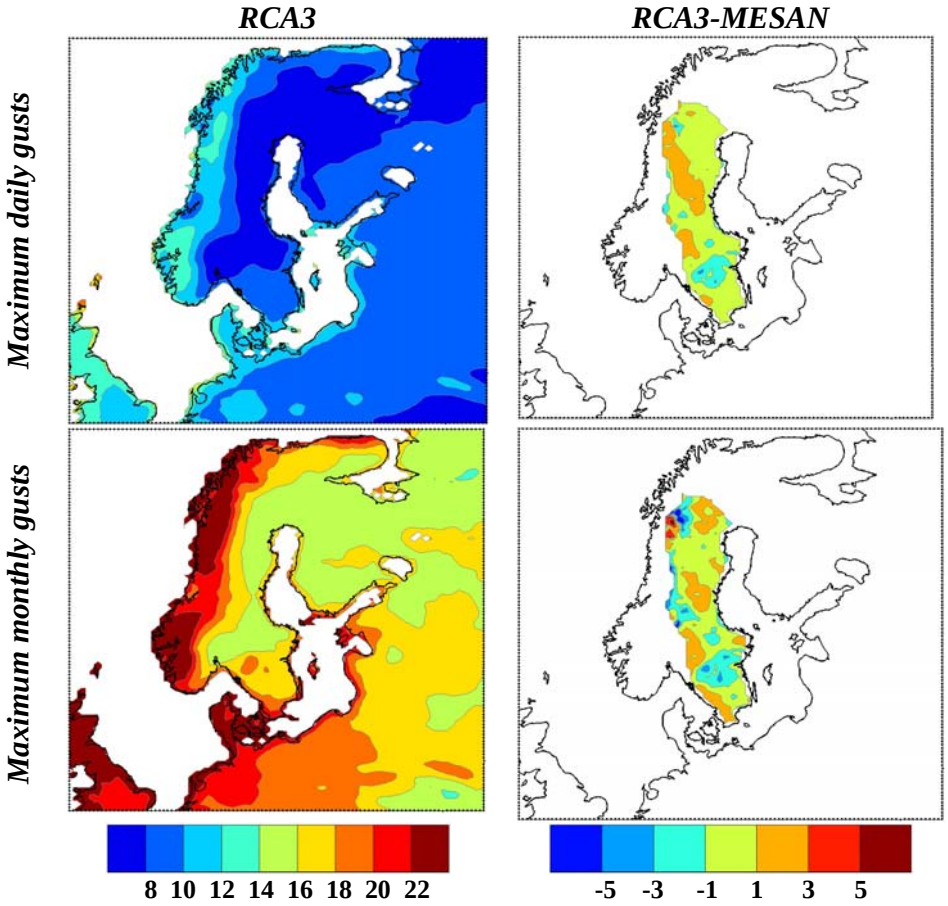

Figure 23. *The winter (DJF) maximum daily gusts (top) and maximum monthly gusts (bottom) (m s^{-1}) as mean values over the period 1999-2004 according to RCA3 and the difference between RCA3 and MESAN. Units are m s^{-1}.*

From a risk and infrastructure perspective it is really the extreme wind speeds that are of most importance. Although those are occurring for very short periods of time, the damage they cause can be severe. The reason for their high damage potential is that the energy in the wind increases with the power three of the wind speed. A parameterisation of these gusty wind speeds has been implemented in RCA3 by Nordström (2005). The parameterisation is based on the wind gust estimate (WGE) method by Brasseur (2001).

The WGE method calculates which model level that contributes to gusty wind speed close to the surface based on the relationship between the turbulent kinetic energy and the static stability in the boundary layer. In Figure 23 the estimated gusty wind speed from RCA3 is compared to observed gusty wind speed from the operational mesoscale analysis system MESAN, developed at SMHI (Häggmark *et al*., 2000). We only had access to observations of gusty wind speeds over Sweden why the rest of the domain has been excluded in the comparison between RCA3 and MESAN as shown in the right column of the figure. Note that RCA3 results have been interpolated to the MESAN grid, which has twice as high horizontal resolution as RCA3. Thus, small scale patterns show up in the difference plots which RCA3 cannot resolve. The agreement between RCA3 and observations is quite satisfactory for both the maximum daily gusts and for the maximum monthly gusts although there is a tendency for underestimated gusty wind speeds around the big lakes in Southern Sweden.

3.6 Snow

3.6.1 Snow water equivalent

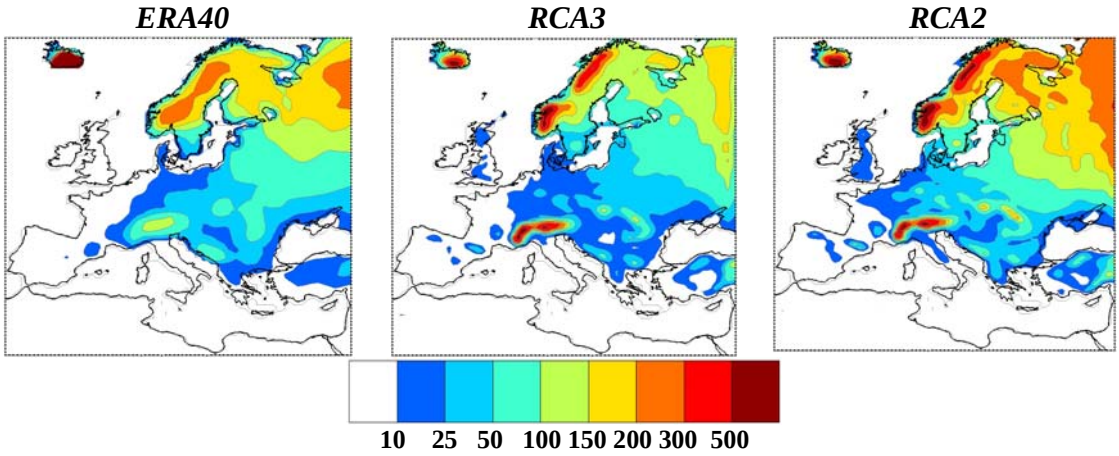

Figure 24. *The average yearly maximum water content of the snow pack according to ERA40, RCA3 and RCA2 respectively. Units are mm.*

The relatively coarse horizontal resolution of ERA40, and consequently a quite smooth orography, acts to distribute the snow more evenly than the higher resolved models RCA2 and RCA3 (Figure 24). This effect is most obvious in the west-east gradient of the water content of the snow, the snow-water equivalent (SWE), in northern Scandinavia. RCA3 and RCA2 give much more snow in the mountainous terrain than east of the mountains. RCA3 tends to give less snow in Finland and in Northwest Russia compared to ERA40 and RCA2. The reason for the difference with ERA40 and RCA2 is mainly the warm bias in RCA3 in that area. The warm winter bias makes the snow fall fraction of the total precipitation smaller in RCA3 and leads to a more rapid melting of snow on the ground. Also the total amount of precipitation is slightly smaller in RCA3 compare to RCA2 during winter (*cf.* Figure 18). Direct observations of SWE at a number of SYNOP stations in Sweden generally correspond well with the simulated values in RCA3 and RCA2, especially for south and mid Sweden for RCA3, as seen from Figure 25. Close to

the Scandinavian mountain range the snow accumulation becomes very sensitive to local conditions with respect to the orography which means that good agreements between observations and simulated values cannot be expected due to the horizontal resolution of the models.

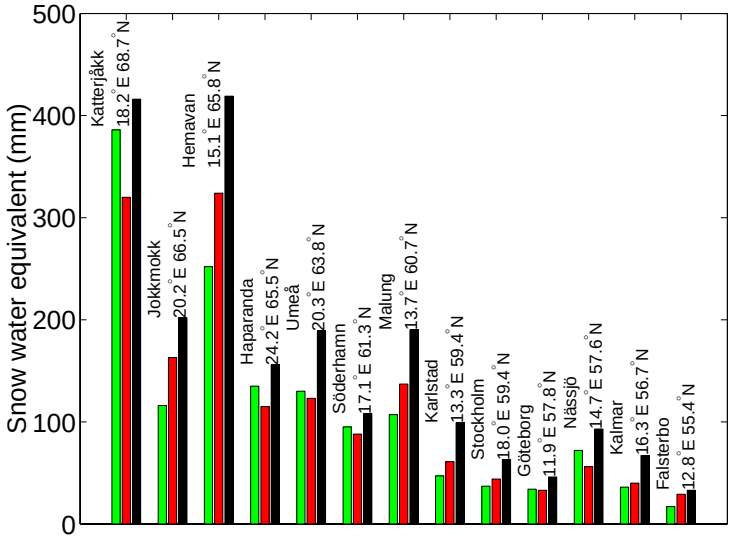

Figure 25. *Average annual maximum snow water equivalent at selected Swedish locations in RCA3 (red), RCA2 (black), and from observations (green) (Raab and Vedin 1995, p 96). All data represent the period 1968-1993.*

3.6.2 Duration of snow cover

Observed duration of snow as shown on the left hand side of Figure 26 is based on SYNOP observations. An observer reports snow as long as half of the observed area is covered with snow. The duration of snow cover, as estimated from the model results, is based on the simulated snow cover fraction. At the start of the snow season very thin layers of snow, covering large areas, often exist. For numerical reasons such thin snow layers cannot be allowed in a model simulation. Thus, the simulated snow cover initially increases slower in the model than in the reality. Therefore, when calculating the duration of snow cover based on simulated snow cover fraction this has to be accounted for, but exactly how this should be done is far from obvious. Here, the definition used for the total number of days with snow cover is the sum of snow cover during the first and last half of the year summed together. The number of days during the first half of the year is counted as the number of days with simulated snow cover exceeding 50%. The number of days during the second half of the year is counted as the number of days with simulated snow cover exceeding 10%. The resulting simulated length of the snow season is shown on the right hand side of Figure 26. For northern Sweden the agreement with the observed snow season is acceptable for both model versions although with a slight overestimation of the length in RCA2. For southern Sweden RCA2 clearly overestimates the length of the snow season while RCA3 tends to underestimate it.

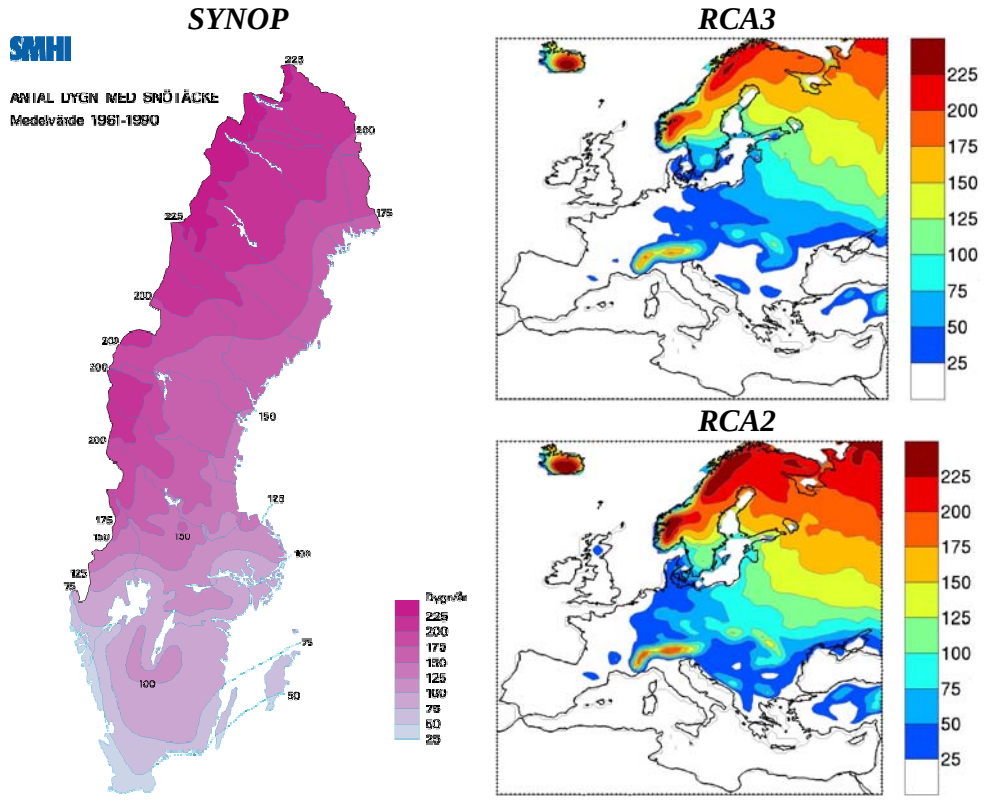

Figure 26. *The average annual duration of the snow season according to SYNOP observations and as estimated from simulated snow fraction in RCA3 and RCA2. Units are days.*

4 The transient climate change experiment

4.1 Control climate versus observed climate (RCA3ECHAM4)

The quality of the lateral boundary conditions is crucial to the regional climate model. In the case of downscaling results from ECHAM4/OPYC3 over Europe, Räisänen *et al*. (2003) investigated its impacts on the control climate as simulated in RCAO which builds on the previous atmospheric model version RCA2 (Jones *et al*., 2004). They found that many aspects of the climate were captured in those simulations indicating that the global model did perform well in the region. Nevertheless, some biases were reported. For instance, biases in the sea-level pressure during much of the year indicated too cyclonic time-mean conditions in the middle of the domain. This is illustrated here in Figure 27 showing the average seasonal cycle of the north-south pressure gradient between Portugal and Iceland and the east-west pressure gradient between the Faeroe Islands and Åland in the Baltic Sea. It is clearly seen that in the winter months (here November to February) the north-south pressure gradient is stronger in RCA3ECHAM4 as compared to RCA3ERA indicating a too strong zonality in ECHAM4. During the period January to April the east-west gradient is too weak indicating a too weak meridional circulation in the Scandinavian region. Räisänen *et al*. (2003) also found that RCAO simulated, in general, too cloudy and rainy conditions in northern Europe while the climate in southernmost Europe was too cold. In this section, we look into some more aspects of the control climate in ECHAM4 and investigate if the new model version RCA3 offers any improvements over RCAO given the same boundary conditions.

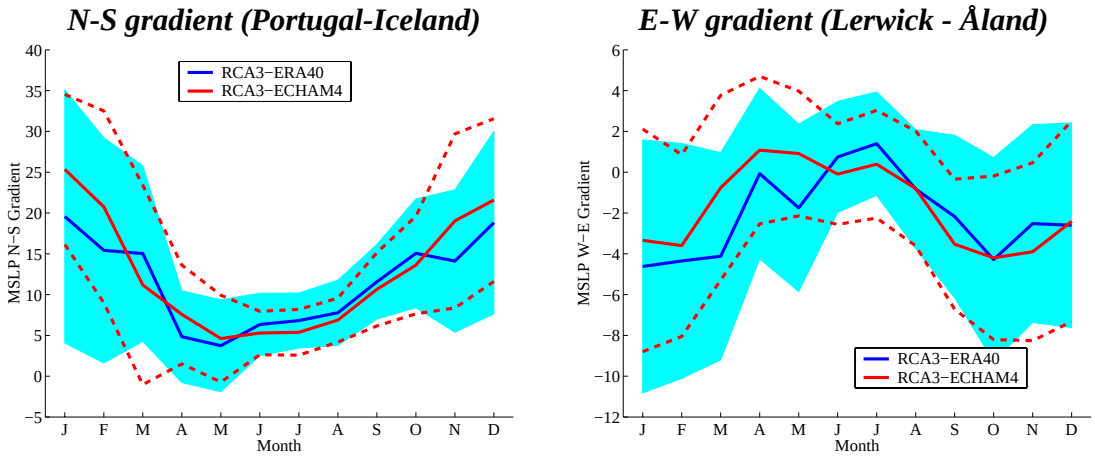

Figure 27. *30-year (1961-1990) monthly mean pressure gradients (full lines). The interannual variability is indicated as plus/minus one standard deviation by the shaded blue area for RCA3ERA and by the dashed lines for RCA3ECHAM4. Units are hPa.*

The sea surface temperatures (SSTs) from the driving global model have a too small seasonal cycle in large parts of the model domain used in this work influencing the European area. The SSTs are too high during winter and too low during summer, particularly in the North Sea area and in the Black Sea (Figure 28). In the far north, north of Scandinavia the opposite is true with an overestimation of the seasonal cycle in SSTs. The figure also reveals that the SSTs are too low both during winter and summer in the Baltic Sea. Since we run RCA3 standalone without the coupled regional ocean model RCO in the Baltic Sea, as in the previously documented experiments with RCAO (Räisänen *et al*., 2003) we may therefore expect some differences in the near-surface climate in the Baltic Sea area.

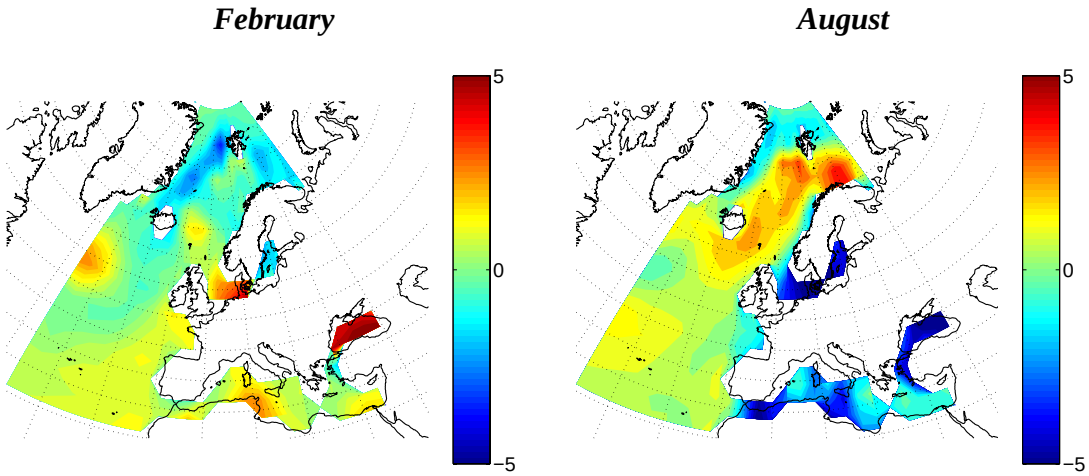

Figure 28. *Monthly mean bias in the ECHAM4/OPYC3 sea surface temperature during the control period 1961-1990 compared to the gridded climatology by Smith and Reynolds (2004). Units are* ^{o}C.

The temperature bias in RCA3ECHAM4 compared to CRU is shown in Figure 29. A general feature of the temperature biases are that they are larger when RCA3 is forced by ECHAM4 than when it is forced by ERA40 (cf. section 3.2), a result from biases in the global model. The too zonal conditions during winter (cf. Figure 27) are reflected in a warm bias in most of central, eastern and northern Europe. Also, the warm bias in south-eastern Europe during summer is more pronounced here than in the RCA3ERA40 simulations indicating the importance of the lateral boundary conditions also during summer. Some of the above mentioned errors in SSTs are reflected in the simulated air temperature. Local maxima in air temperature bias are found close to the coasts surrounding the North Sea both in summer and winter.

Also for precipitation the biases compared to observations are larger in RCA3ECHAM4 when compared to RCA3ERA for all seasons. This is true both for the positive bias in the north and the negative bias in the south, Figure 30. As for the RCA3ERA simulation the relative biases are very large over North Africa due to the small rainfall amounts.

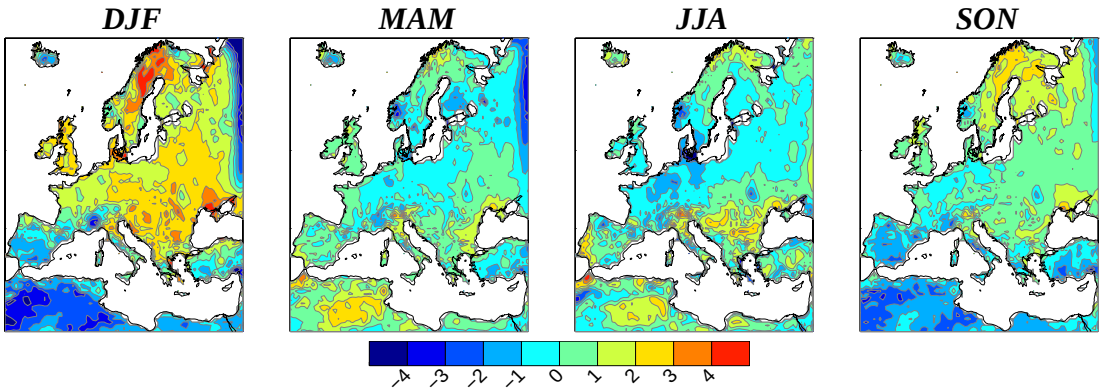

Figure 29. *Seasonal average bias in T_{2m} (grid box average) in RCA3ECHAM4 compared to CRU. Units are ^{o}C.*

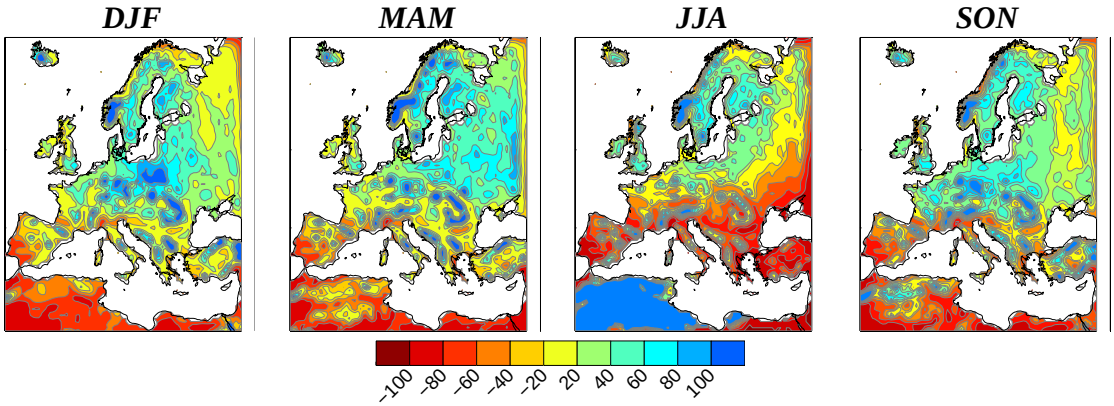

Figure 30. *Seasonal average bias in precipitation in RCA3ECHAM4 compared to CRU. Differences are given in %.*

The seasonal bias with respect to both the reanalysis run and the selected ECA stations of extremely warm daily maximum (minimum) temperatures during summer (winter) are shown in Figure 31. In the difference maps RCA3ECHAM4 minus RCA3ERA the anomalous impact of the too weak seasonal cycle in the SST is clearly evident, particularly over the Baltic, in southern Scandinavia and over the Black Sea. The apparent strong anomaly in the coastal regions of the Mediterranean in T_{2max} MAM and JJA is an effect of the coarser grid resolution of the land-sea mask in the forcing SST fields. The extreme daily maximum temperatures are mainly overestimated in south-eastern Europe during the summer and autumn. During winter, the extremely cold daily minimum temperatures are generally warmer by up to 6°C in the control climate of the transient run compared to the ERA40 run, with the exception of the north-eastern corner, where there is a negative bias. This negative bias remains for all seasons except the summer. For other land regions the bias is small. Compared with the ECA station data the biases in the control climate (RCA3ECHAM4) are typically larger than for the biases in RCA3ERA (*cf*. Figures 14 and 15).

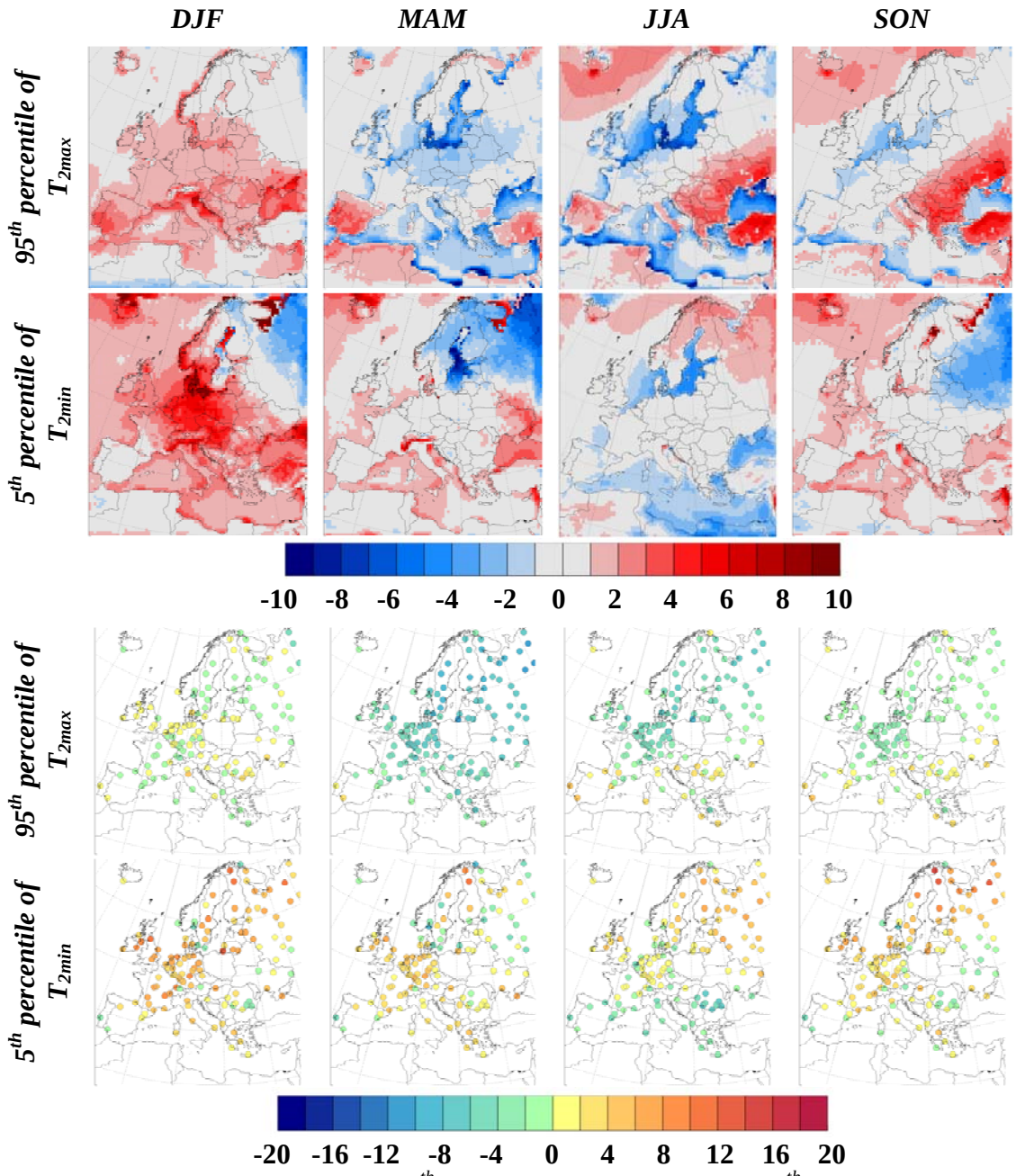

Figure 31. *Seasonal biases in the 95th percentile of T_{2max} and in the 5th percentile of T_{2min}. The upper rows show the seasonal differences due to lateral boundary conditions, RCA3ECHAM4 minus RCA3ERA. The lower rows show the seasonal biases with respect to the ECA station observations (RCA3ECHAM4 minus ECA stations data). Units are °C.*

4.2 Transient climate change (1990-2100)

In this section the simulated climate change signals, defined as differences in climate between 30-year periods and the control period (1961-1990) are described. We present results in the form of climate change maps for four 30-year periods covering the period 1981-2100. The first of these periods is partly overlapping the control period. In addition to showing climate change in the form of maps we show time series of area average changes for certain regions. These time series are compared to the control climate and in particular we address the question as to whether the difference between periods is statistically significant. Prior to presenting the results we first describe the method used for determining statistical significance.

The climate shows a high degree of natural variability. This makes it difficult to detect climate change since the signal needs to exceed the noise level caused by the natural variability. To do this we apply the method described by Räisänen *et al*. (2003) on annual or seasonal mean differences between a certain time period and the control period. In short this means that we use a *t*-test, in which the error variance of the simulated change has been adjusted for serial correlation as outlined below. The test is used to determine if the null hypothesis "there is no difference between the means of the two periods" can be rejected or not. The *t* statistics can be calculated as

$$t = \frac{\Delta X}{\sqrt{V(\Delta X)}} \tag{1}$$

In which ΔX is the simulated mean change in variable X between the control period and a period in the scenario simulation. $V(\Delta X)$ is the pooled variance of the the two periods.

$$V(\Delta X)_0 = \frac{1}{n}(V_{x,1} + V_{x,2}) \tag{2}$$

Here $V_{x,1}$ and $V_{x,2}$ are the interannual variances of X within the two time periods and n is equal to 30 (i.e. the number of years in each of the periods). The error variance is adjusted for autocorrelation following Zwiers and von Storch (1995) by replacing (2) with

$$V(\Delta X) = \frac{1 + r_1}{1 - r_1} V(\Delta X)_0 \tag{3}$$

Where r_1 is the pooled lag-1 autocorrelation estimated from the simulations. As discussed in Räisänen *et al*. (2003) the estimate is kept conservative by setting r_1 to zero where the number derived directly from the data is negative. This means that the *t* statistics will be smaller than what it would have been for negative numbers of r_1. For the samples used here (n=30), the *t* statistics are almost normally distributed. This means that there is a probability of about 5% to get $|t| > 2$ by pure chance. We can therefore reject the null hypothesis at the 95% significance level if *t* is larger than 2.

4.2.1 Mean sea level pressure

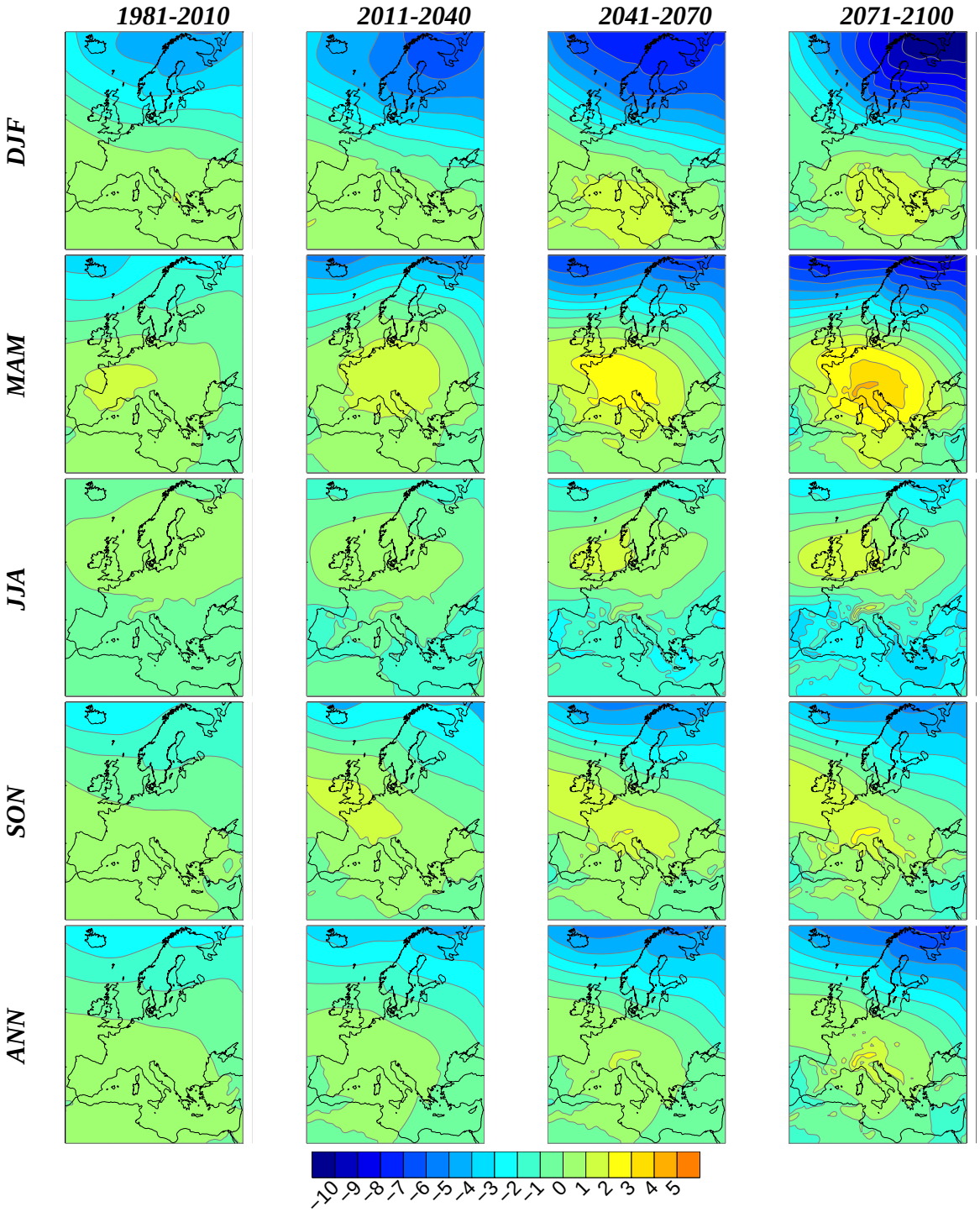

Figure 32. *Changes in seasonal and annual mean sea level pressure (differences from the control period 1961-1990) in RCA3ECHAM4A2. Units are hPa.*

The sea level pressure in the regional climate model is in essence determined by the lateral boundary conditions given from the driving global model. In the ECHAM4/OPYC3 simulations used here there is a strong decrease with time in pressure in the northern half of the domain and an increase in the south as discussed in Räisänen *et al*. (2004). These changes lead to an increase in the north-south pressure gradient in northern Europe particularly during the winter half of the year, Figure 32. The annual average increases more or less linearly between the four 30-year periods shown in the figure. For the different seasons there are exceptions from this linear increase with time. For instance, the change in MSLP during winter over the Atlantic including the North Sea is stronger between 1981-2010 and 2011-2040 compared to between 2011-2040 and 2041-2070 and the change in spring is stronger between 2011-2040 and 2041-2070 compared to between 2041-2070 and 2071-2100. The pattern of change that evolves with time is not fully established already in the first, partly overlapping, 30-year time period. But, the main characteristics, with increasing pressure in the south and decreasing pressure in the north are seen already in this period. The same is true also for the B2 simulation which shows similar changes as in the A2 simulation in all areas and seasons. However, the details of the temporal evolution between the two simulations differ due to the large interannual variability as indicated in Figure 33.

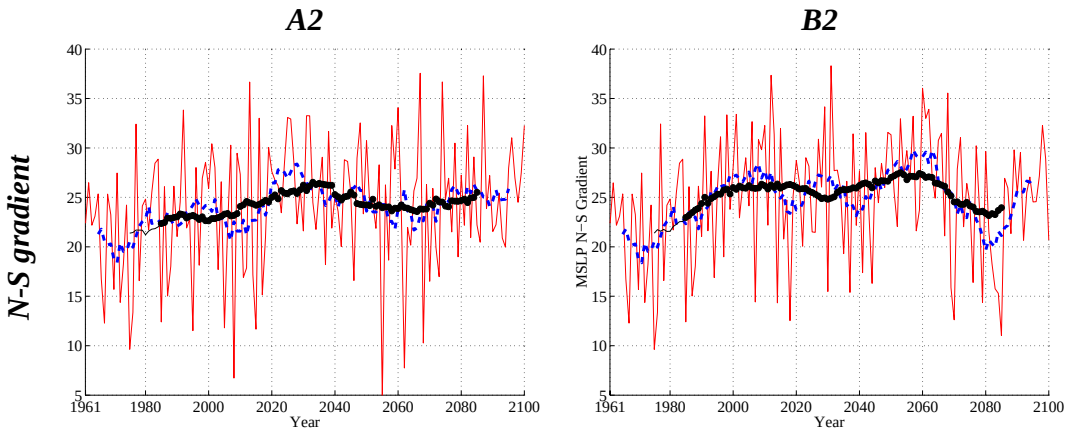

Figure 33. *Evolution of the mean winter (NDJF) north-south pressure-gradient between Portugal and Iceland in RCA3ECHAM4A2 and RCA3ECHAM4B2. The red line shows the gradient in each year, the blue line the 10-year running mean, and the black line the 30-year running mean. In the 30-year running mean periods that are at the 95% level statistically different from the control period are denoted by filled circles. Units are hPa.*

The change in the N-S pressure gradient becomes statistically significant already in the partly overlapping period 1971-2000. After about 2040 there is a reduction in the pressure gradient but it remains well above its present levels throughout the A2 simulation. In the B2 simulation there is an even stronger increase during the first decades after which there is stabilization at the higher level before a “dip” in the last few decades. It can be noted that even though there are statistically significant climate change signals in the indexes there is a large degree of overlap between the distributions of seasonal means. These time series clearly show the very large interannual and interdecadal variability that are characteristic for the European climate.

4.2.2 Surface air temperature

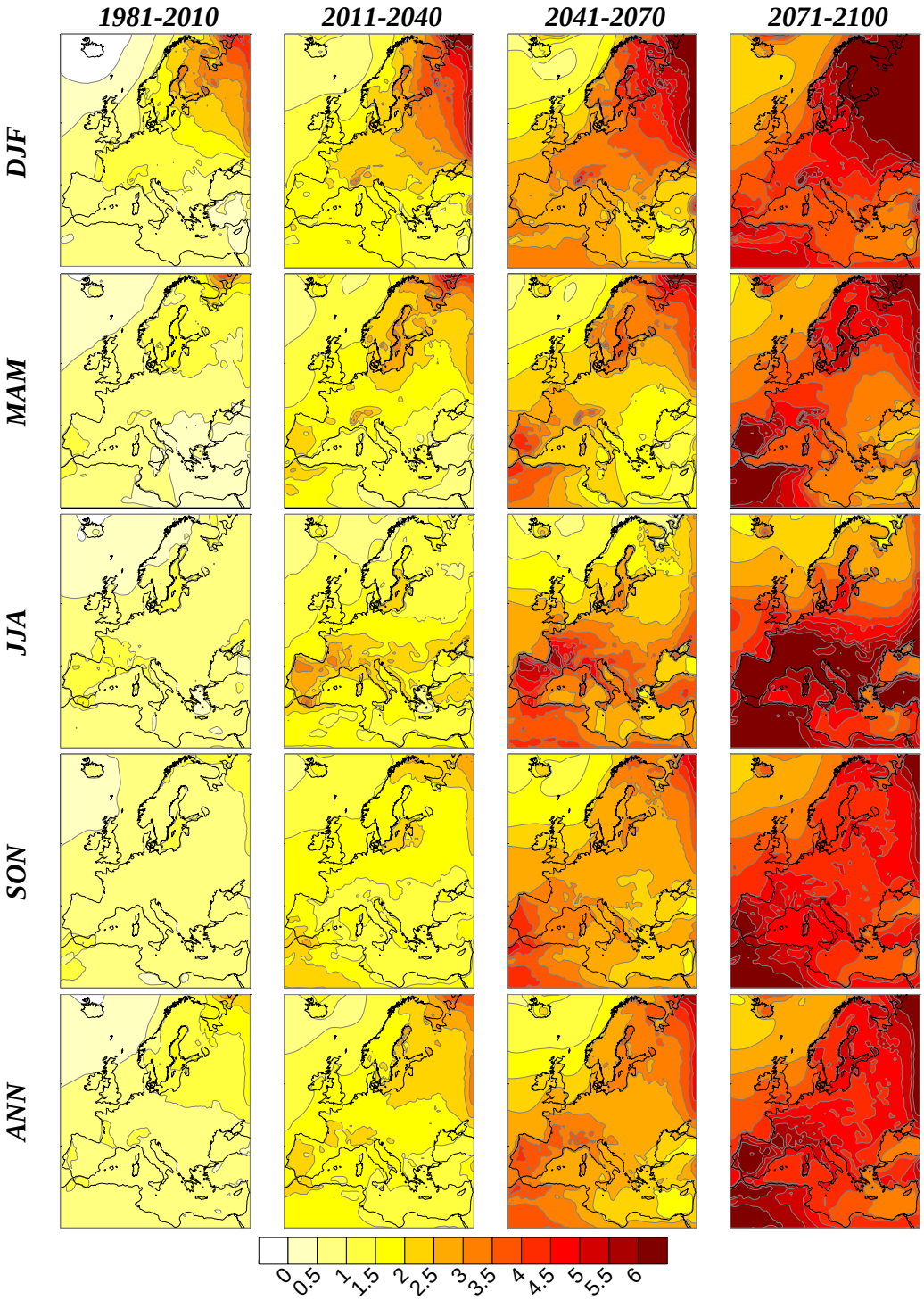

Figure 34. *Changes in seasonal and annual mean surface air temperature (differences from the control period 1961-1990) in RCA3ECHAM4A2. Units are ^{o}C.*

The pattern of temperature increase shows a pronounced land-sea contrast due to the thermal inertia of the oceans that warms more slowly than land areas (Figure 34). In the European continent the clear seasonal cycle, with largest increase in winter in the north-eastern part of the domain and in the southern part of the domain during summer, is seen already in the first 30-year period with mean changes in these areas exceeding 1°C. The large increases in these regions and seasons are due to feedback mechanisms from decreasing snow cover in winter and decreasing soil moisture content during summer as discussed by Räisänen *et al*. (2004) and Kjellström (2004).

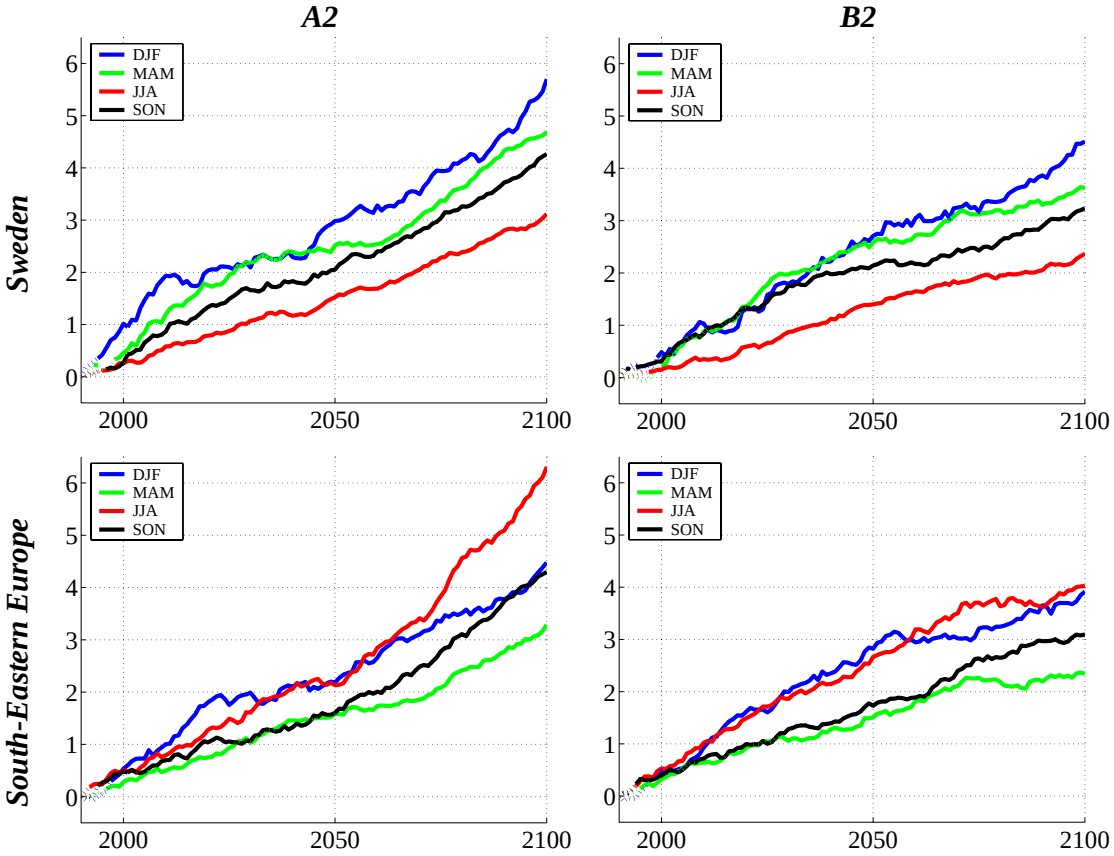

Figure 35. *Change in seasonal and area averaged 2m-temperature in the transient simulations. Periods that are at the 95% level statistically different from the control period are denoted by a full line. Units are °C.*

The temperature increases rapidly in the simulations in all areas and seasons as shown for South-Eastern Europe and Sweden in Figure 35. The simulated climate change signals are statistically significant already after a few years of the simulations. The differences between the A2 and B2 simulations are rather small during the first decades and it is not until the last few decades when differences become clear. In Sweden the changes are largest in winter and spring while in South-East Europe the largest changes are seen in winter and summer. These patterns are seen throughout the simulations although in relative terms the wintertime changes in South-Eastern Europe gets smaller by the end of the A2 simulation when much of the snow has disappeared.

Compared to the simulations with RCAO, as described in Räisänen *et al.* (2003), the present simulations give similar climate change signals for 2071-2100. Despite this fact, there is a tendency that the maximum climate change signals in the last 30-year period are smaller than in the previous simulation with RCAO. This is true both for the maximum increase in winter in the north-eastern part of Europe and for the maximum increase in summer in southern Europe, in both these areas the maximum increase is lower by about 2°C in this simulation. These smaller changes are probably a result of weaker surface feedback mechanisms in RCA3. In winter there is less snow that can vanish in RCA3 than in RCA2 and in summer RCA3 is less sensitive to soil drying than RCA2 due to the new land surface scheme. Therefore, the climate change response gets smaller in both seasons. The temperature change over the Baltic Sea is higher in this experiment as compared to the RCAO simulations. This is a result of the too low SSTs in the ECHAM4/OPYC3 control experiment as discussed above (Section 4.1).

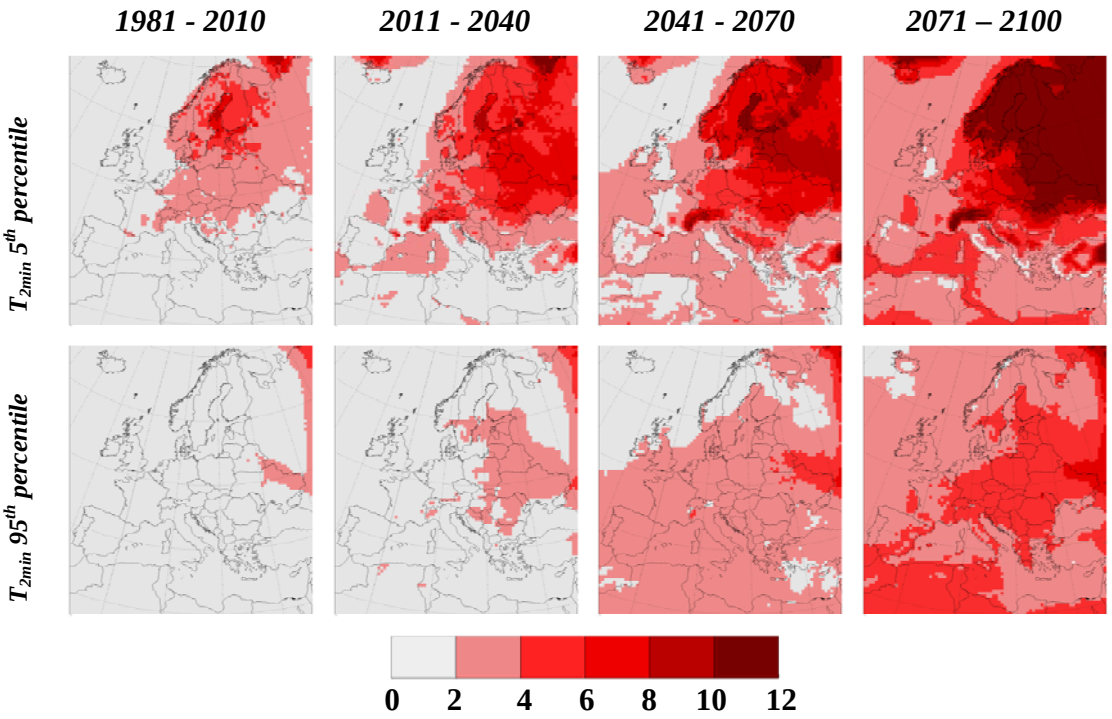

Figure 36. *Change in winter T_{2min} extremes in RCA3ECHAM4A2. Units are ºC.*

Previous studies of the temperature extremes (Kjellström, 2004; Kjellström *et al.*, 2006; Ferro *et al.*, 2005; Beniston, 2004; Schär *et al.*, 2004) indicate that the two tails of the temperature frequency distribution may respond differently to an increasing mean temperature. From Figure 36 it is evident that the winter 5th percentile of T_{2min} shows a stronger climate change signal compared to the 95th percentile. Conversely, during summer the situation is reversed, the 95th percentiles of T_{2max} show a stronger increase compared to the 5th percentile (Figure 37).

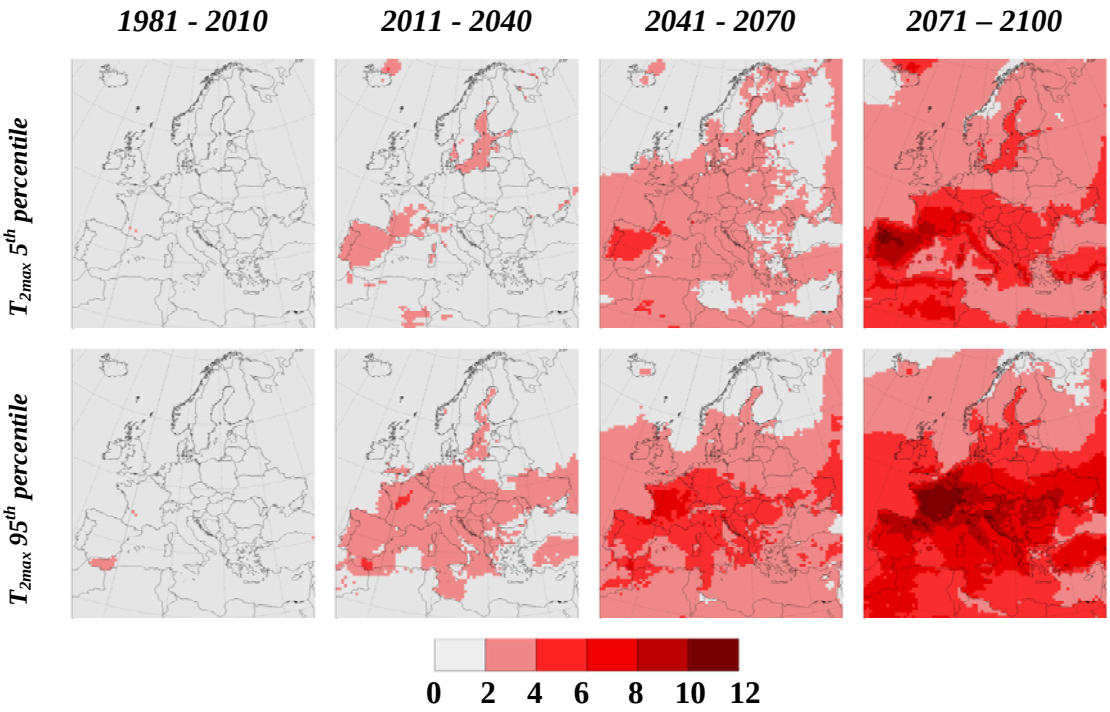

Figure 37. *Change in summer T_{2max} extremes in RCA3ECHAM4A2. Units are ^{o}C.*

The question then arises whether these changes are an effect of the changing mean temperature (*i.e.* a shift of location), or whether there is also a change in the variation or even a more complex change in the shape of the distribution. Ferro *et al*. (2005) suggest a simple non-parametric statistical approach towards analyzing the influence of changes of these three factors (Figure 38).

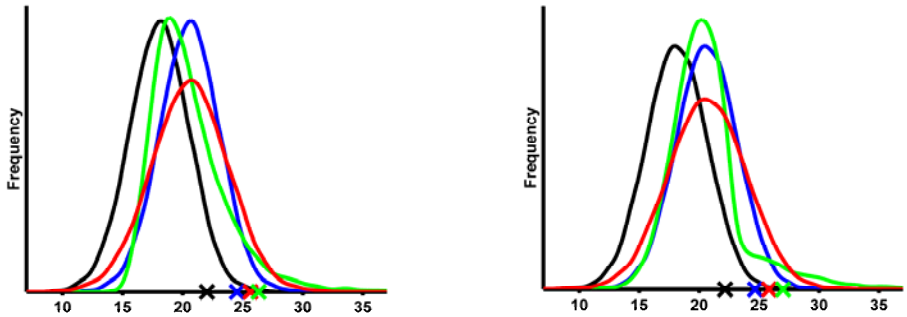

Figure 38. *Different changes to a frequency distribution contribute towards changing a percentile value. In this example, the crosses indicate the position of the 95th percentile. A change in location of a reference distribution (black) only shifts the position of the distribution (blue). If the spread (variation) also increases the percentile value increases more (red). Finally, a more complex shape change of the distribution (green) further influences the percentile. The left graph shows a smooth change of the skewness that, while keeping the same mean and variance as the red curve, places the peak close to the black reference curve. The right graph shows the effect of a change to the extremes only, while keeping the mean and variance the same as for the red curve.*

Following Ferro *et al*. (2005) we denote the p^{th} percentile for the reference period as $\hat{x}_p$ and the corresponding percentile during the future period as $\hat{y}_p$. As a measure of location we use the medians, $m_x = \hat{x}_{50}$ and $m_y = \hat{y}_{50}$. And for scale we use the interquartile range $s_x = \hat{x}_{75} - \hat{x}_{25}$ and $s_y = \hat{y}_{75} - \hat{y}_{25}$. As a measure of shape (asymmetry) we use the Yule-Kendall skewness $a_x = \left(\hat{x}_{75} - 2\hat{x}_{50} + \hat{x}_{25}\right)/ s_x$.

Now, if there is no change to the frequency distribution of temperatures the difference in the p^{th} percentile

$$d = \hat{y}_p - \hat{x}_p$$

is expected to be approximately zero and substantial non-zero values could indicate a shift in the location parameter of the distribution. Such a shift of location could be diagnosed by the location-adjusted percentile difference

$$d_L = \hat{y}_p - \left\{m_y + \left(\hat{x}_p - m_x\right)\right\}.$$

Given a location shift only, this quantity should be approximately zero. If substantial non-zero values remain this could be caused by a change of the scale parameter. Then the location- and scale-adjusted percentile difference

$$d_{LS} = \hat{y}_p - \left\{m_y + s_y\left(\frac{\hat{x}_p - m_x}{s_x}\right)\right\}$$

is expected to be close to zero under the hypothesis of change only of the location and scale parameters. If substantial non-zero values still remain there is a more complex change in the shape of the frequency distribution.

A more precise and quantitative interpretation of what constitutes a substantial change would involve statistical hypothesis testing. For the measures d, d_L and d_{LS} such tests are currently under development (Ferro *et al*., 2005) and here we thus only make a subjective interpretation of map patterns of the three measures. A simple numeric summary of the range of values found in each map is presented in Table 3. If the minimum and maximum values are reasonably close to zero the measure can be subjectively assumed to be insignificant, meaning that the corresponding location-adjustment or location- and scale-adjustment explains the difference in percentile values. This summary does however present the range of values and not the spatial extent or spatial coherence, and thus the subjective significance of the variations in the measures. From Table 3 it is obvious that there is a strong asymmetry towards positive d values in all maps. This is obviously what one could expect when there is an overall increase in average temperature. However, maps of d_L show more complex and varied patterns suggesting that the effect of a change in the scale parameter is more complex. Focussing on wintertime temperature extremes (Figure 39) the strongest effect is found in the north-eastern part of the domain. Further, the d_L measure suggests that in the same region there is a positive change in the 5^{th} percentile and a negative change in the 95^{th} percentile after adjusting for the average temperature increase (location shift). Also, after adjusting both for change in location and in scale there remains a consistent pattern in the 5^{th} percentile and, more weakly, in the 95^{th} percentile. This suggests a more complex climate change signal than just a change in the average conditions. Specific for the region with this consistent pattern in the extreme

temperature percentiles is the strong reduction in snow cover (*cf*. section 4.2.5). The reduced snow cover leads to a strong reduction in albedo and an increase in heat fluxes from the ground. Both these processes lead to higher temperatures influencing particularly the cold end of the probability distribution of temperatures as previously shown by Kjellström (2004). Similar patterns are found in the maps of the spring temperature extremes. For the other seasons, with the possible exception of the autumn, much of the climate change signal in the extreme temperatures depends relatively linearly of the seasonal mean climate change signal.

Table 3. *Minimum and maximum values of the three measures d, d_L and d_{LS} for each variable, season and percentile in RCA3ECHAM4A2. Values in bold indicate that according to a subjective interpretation there were 'substantial' and spatially coherent patterns in the maps.*

Variable and season	Percentile	***Unadjusted change (d)***		***Location adjusted change (d_L)***		***Location and scale adjusted change (d_{LS})***	
		min	max	min	max	min	max
T_{2max}							
DJF	5	**1.9**	**20.4**	**-3.8**	**13.6**	**-5.9**	**10.2**
	95	**0.6**	**9.5**	**-9.3**	**5.0**	-7.0	5.0
MAM	5	**1.7**	**18.0**	**-3.6**	**14.0**	**-4.4**	**27.5**
	95	**0.7**	**10.5**	**-7.2**	**4.9**	**-9.8**	**8.6**
JJA	5	**1.4**	**10.8**	-4.1	4.7	-4.4	1.7
	95	**-1.9**	**12.3**	-3.9	3.4	-2.9	2.0
SON	5	**2.0**	**12.7**	-3.4	6.3	-2.5	3.9
	95	**0.1**	**9.7**	-3.7	5.0	-4.2	4.0
T_{2min}							
DJF	5	**1.4**	**24.3**	**-3.3**	**16.5**	**-6.3**	**9.1**
	95	**1.2**	**11.1**	**-9.4**	**2.4**	-5.9	4.2
MAM	5	**0.6**	**22.0**	**-3.8**	**15.7**	**-8.1**	**10.5**
	95	**1.4**	**8.5**	-6.4	2.5	-2.2	4.9
JJA	5	**1.6**	**9.3**	-4.0	4.8	-4.3	2.1
	95	**-2.0**	**10.9**	-4.1	3.5	-2.6	1.9
SON	5	**1.6**	**13.6**	**-5.2**	**9.2**	-4.2	8.4
	95	**0.1**	**8.9**	-3.8	3.6	-4.2	2.9

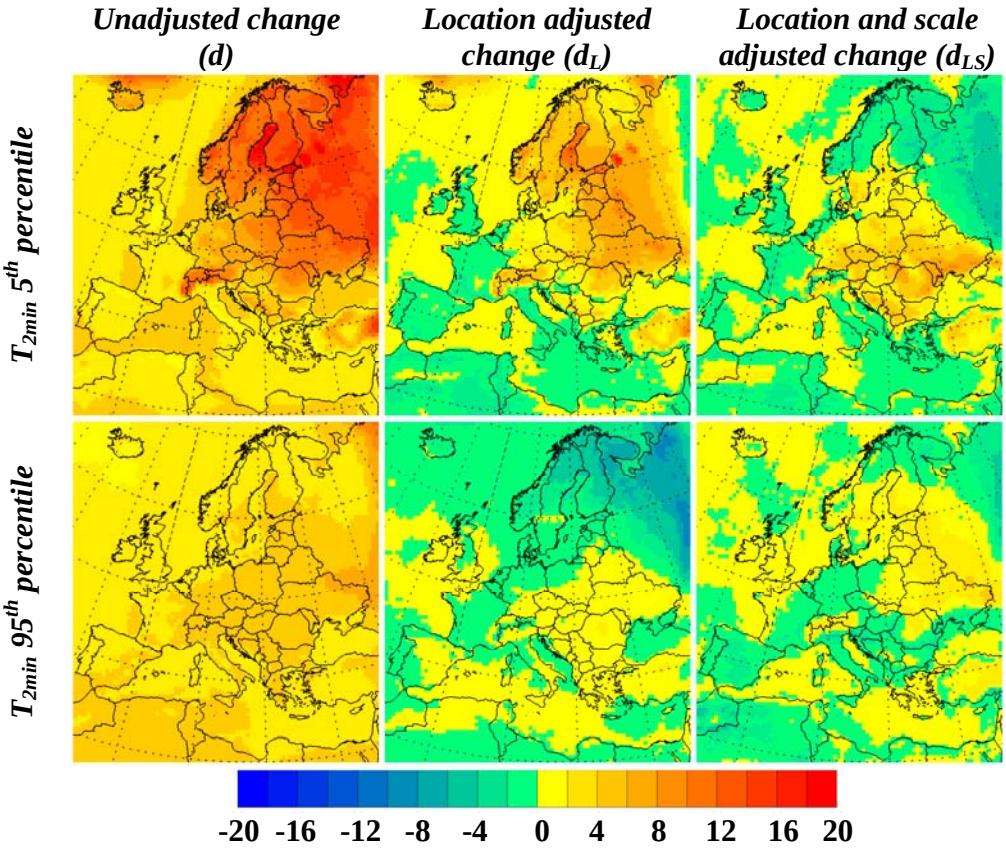

Figure 39. *Decomposition of the climate change signal 2071-2100 minus 1961-1990 for winter temperature extremes in RCA3ECHAM4A2. Units are °C.*

4.2.3 Precipitation

Precipitation increases in the north and decreases in the south in the mean, Figure 40. The border line between increase and decrease moves southwards in winter and northwards in summer. Land areas in the Mediterranean region are projected to get less precipitation in all seasons while the northern parts of Scandinavia are projected to get increases all year round. These projected changes are in line with earlier findings (Christensen and Christensen, 2006; Räisänen *et al.*, 2004; Cubasch *et al.*, 2001). The very large changes in the Mediterranean regions including northern Africa is a result of the very low precipitation in the control climate leading to large relative differences. Again, as for pressure and temperature, the climate change signal generally gets stronger with time. But, in accordance with the pressure changes, the precipitation change for winter in the North Sea region between 1981-2010 and 2011-2040 is larger than the corresponding change between 2011-2040 and 2041-2070 showing the importance of the fast change in the mean westerlies in the first periods compared to the latter ones. Also in spring, the effects of the changes in circulation can be seen, with larger change between 2011-2040 and 2041-2070 as compared to between 2041-2070 and 2071-2100.

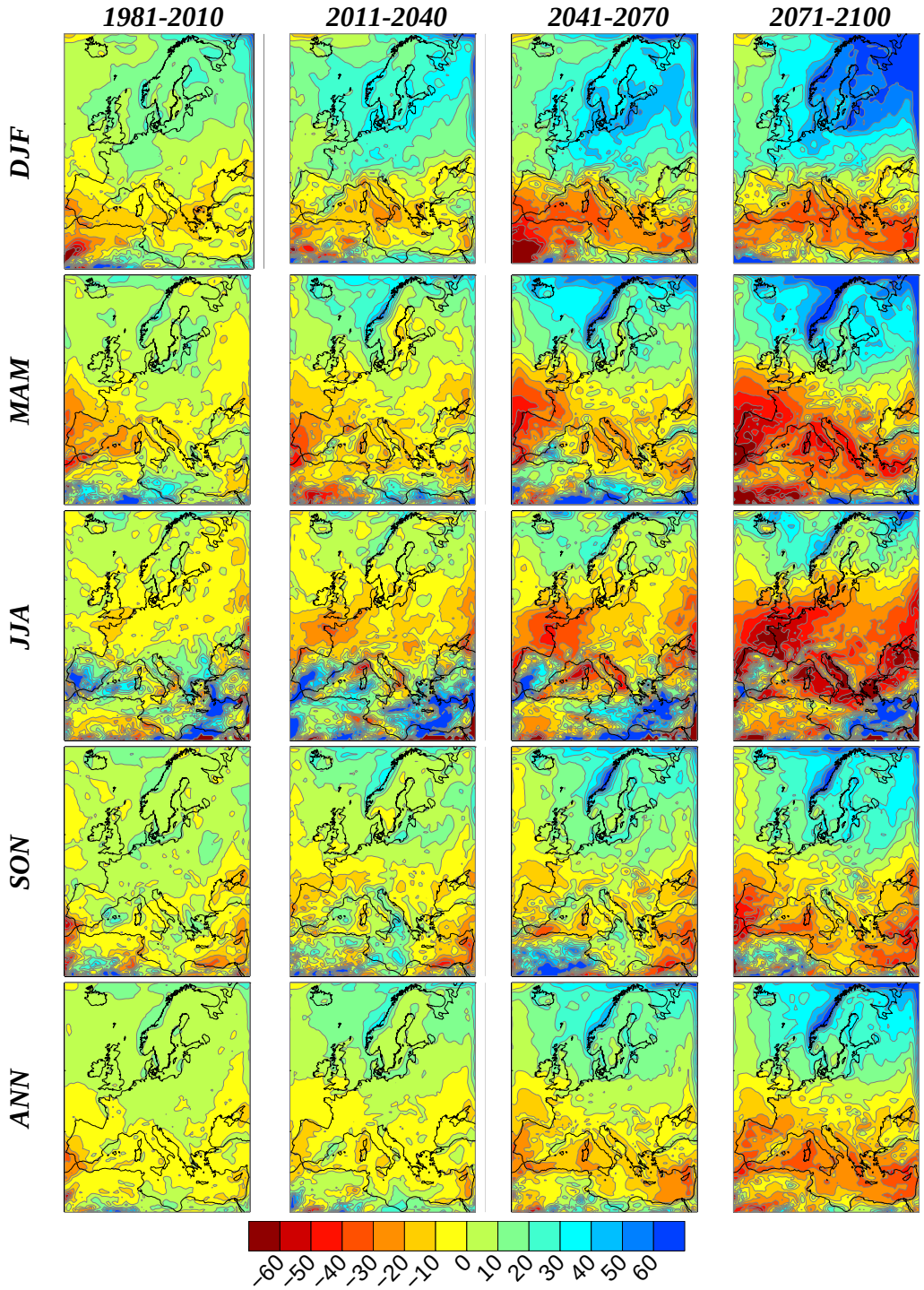

Figure 40. *Changes in seasonal and annual mean precipitation (differences from the control period 1961-1990) in RCA3ECHAM4A2. Units are %.*

Compared to the RCAO simulations the changes are very similar in all regions. There is a tendency for more precipitation over the Baltic Sea, probably a result of the larger increase in SST. Also, since the model domain now includes all of the Mediterranean Sea

the full extent of the large change in the south-eastern part during winter and summer is seen.

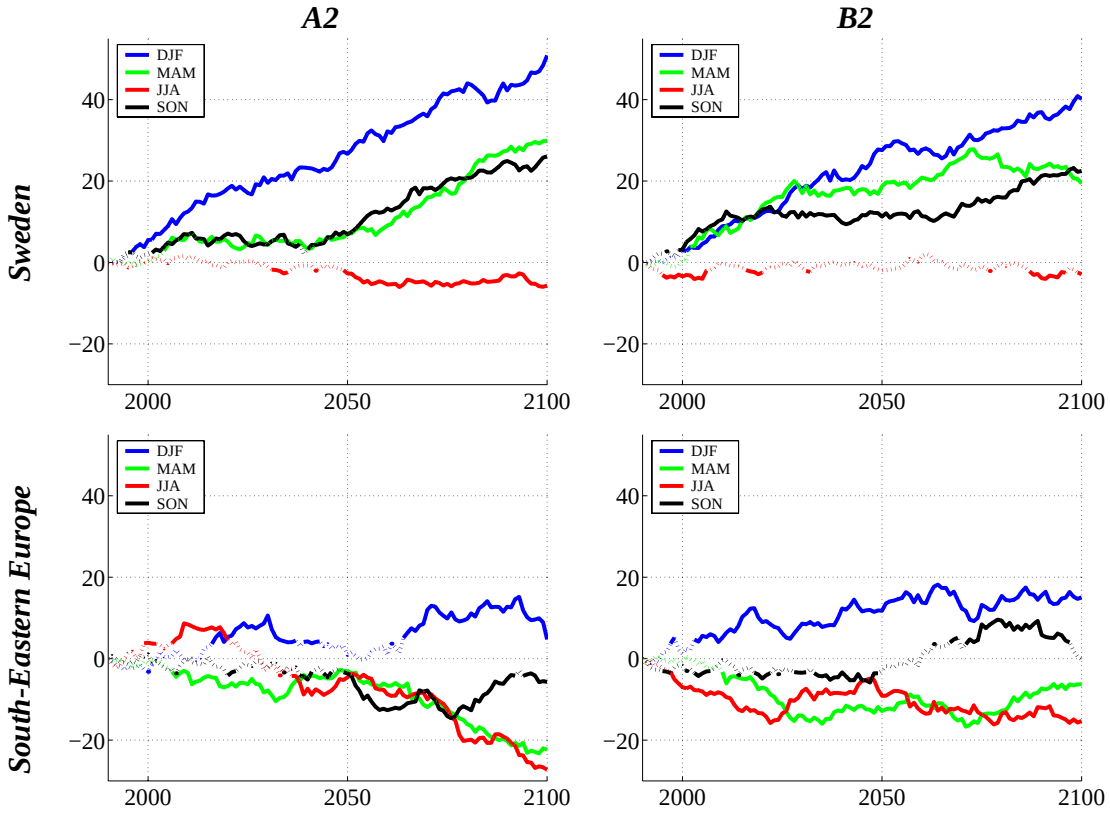

Figure 41. *Change in seasonal and area averaged precipitation in the transient simulations. Periods that are at the 95% level statistically different from the control period are denoted with a full line. Units are %.*

Figure 41 illustrates the decadal variability in the simulated precipitation in two regions. The almost linear trend in winter in Sweden is notable in both simulations while the corresponding trends in spring and fall are very different with a rapid increase in RCA3ECHAM4B2 before it levels off while the reverse is true in RCA3ECHAM4A2. In South-eastern Europe the evolution is even more complex with changes that can be significant in several decades before it gets smaller and sometimes even changes sign. With this kind of evolution it is hard to distinguish between a long-term trend and shorter-term "natural" variability. In this area the strongest trend is the drying in spring and summer which is common to both simulations and to a lesser degree the increasing precipitation during winter.

4.2.4 Surface winds

The increase in the north-south pressures gradient in northern Europe is reflected in the wind speed that increases there during fall, winter and spring, Figures 42 and 43. The changes are particularly strong over the northern parts of the Baltic Sea. The large

increase in SSTs together with a strong reduction in sea ice in that part of the Baltic Sea leads to changes in stability in the lowermost atmosphere which in turns leads to higher wind speed close to the surface (cf. Räisänen *et al.*, 2003 and Meier *et al.*, 2006). The other major change is the decrease in wind speed in central parts of the model domain which can be attributed to the increasing pressure in this area (*cf.* Figure 32).

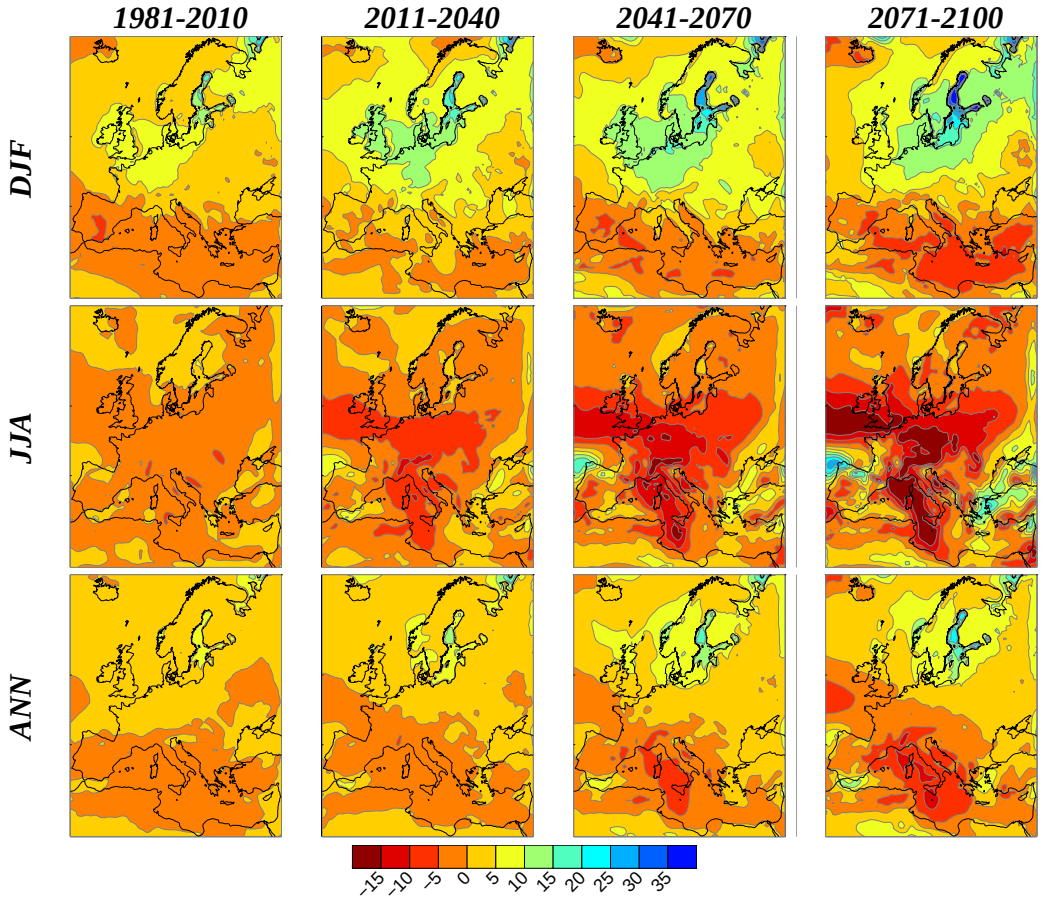

Figure 42. *Changes in seasonal and annual mean wind speed (differences from the control period 1961-1990) in RCA3ECHAM4A2. Units are %.*

It should be emphasized that these changes in wind speed are to a great extent depending on the changes in MSLP as inherited from the GCM. With another GCM the results may become significantly different as previously shown with RCAO (*e.g.* Räisänen *et al.*, 2004; Pryor *et al.*, 2005). While differences between different GCMs clearly has a profound impact on the magnitude (and even the sign) of the changes in the wind climate also "natural" interdecadal variability plays a role. An example of this can be seen in Figure 43 showing the very rapid increase in wind speed, both in the Baltic Sea area and in Ireland, in the first decades of the simulation followed by a stagnation period when changes are small. In the B2 simulation the behaviour is different with a rapid, but steadier trend over the first decades of the simulation.

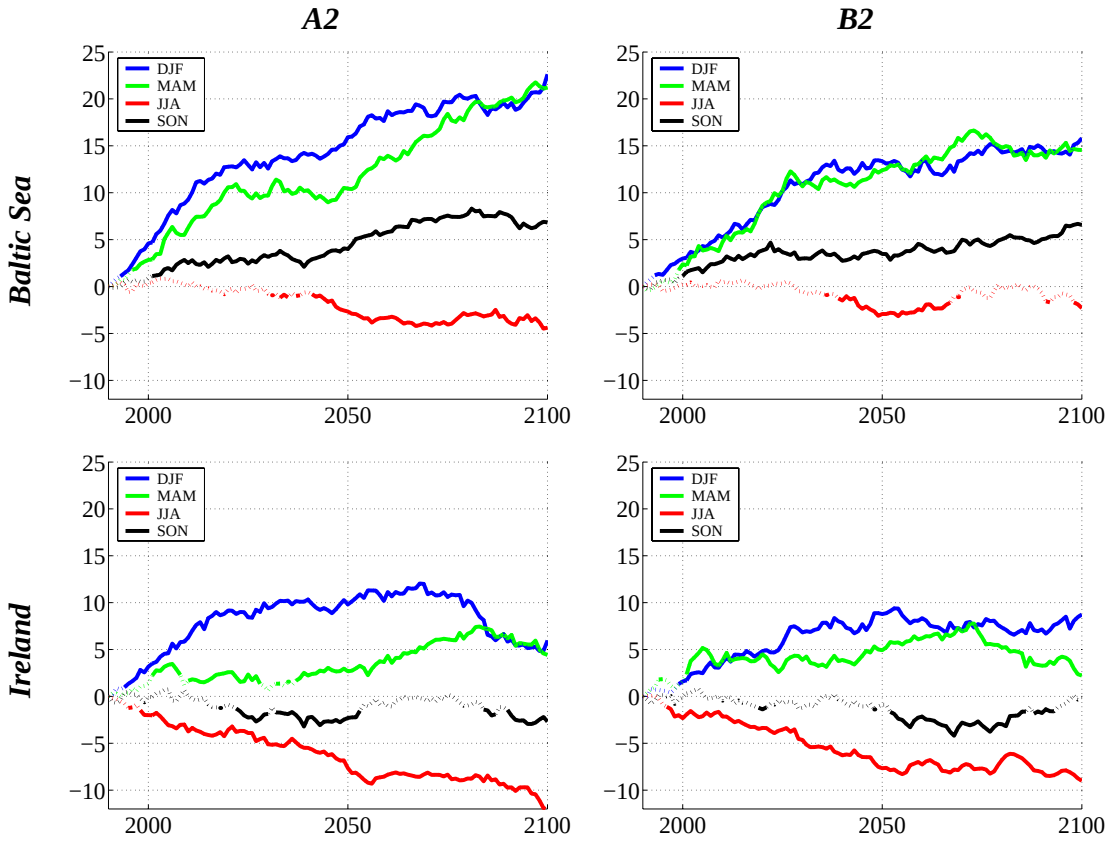

Figure 43. *Change in seasonal and area averaged wind speed in the transient simulations. Periods that are at the 95% level statistically different from the control period are denoted by full lines. Units are %.*

4.2.5 Snow climate

Also the snow cover undergoes dramatic changes during the transient climate simulations. Figure 44 shows the decrease in water content of the snow cover during winter and spring which are the seasons when snow cover large parts of Scandinavia, the Baltic countries and north-western Russia. The largest changes are found in north-eastern Europe in a zone that moves to the northeast with time. This migration is consistent with the migration in the snow fraction. The impact of these changes on extreme temperatures has been discussed in section 4.2.2.

The changes with time are negative in all regions and seasons. It is evident that the effect of increasing temperatures is more important than increasing winter precipitation even as far north as in Northern Sweden and in Finland (Figure 45). The decreases in snow cover are statistically significant in all regions and seasons already at an early stage in the simulations. The relative decrease is quickest in fall and spring in most regions while the decrease in winter is somewhat slower.

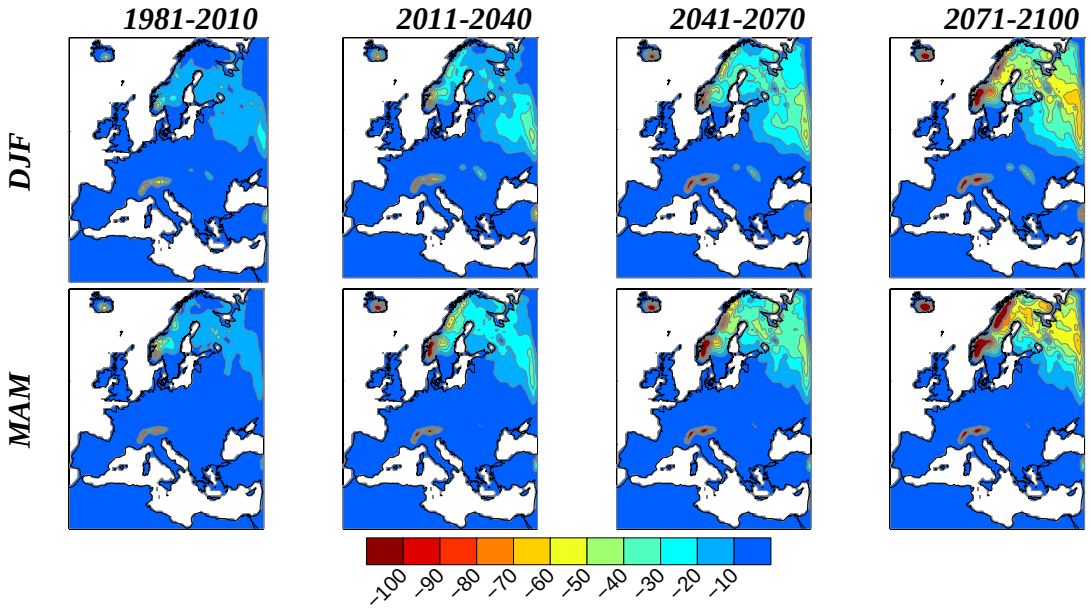

Figure 44. *Changes in the snow water content in winter and spring (differences from the control period 1961-1990) in RCA3ECHAM4A2. Units are %.*

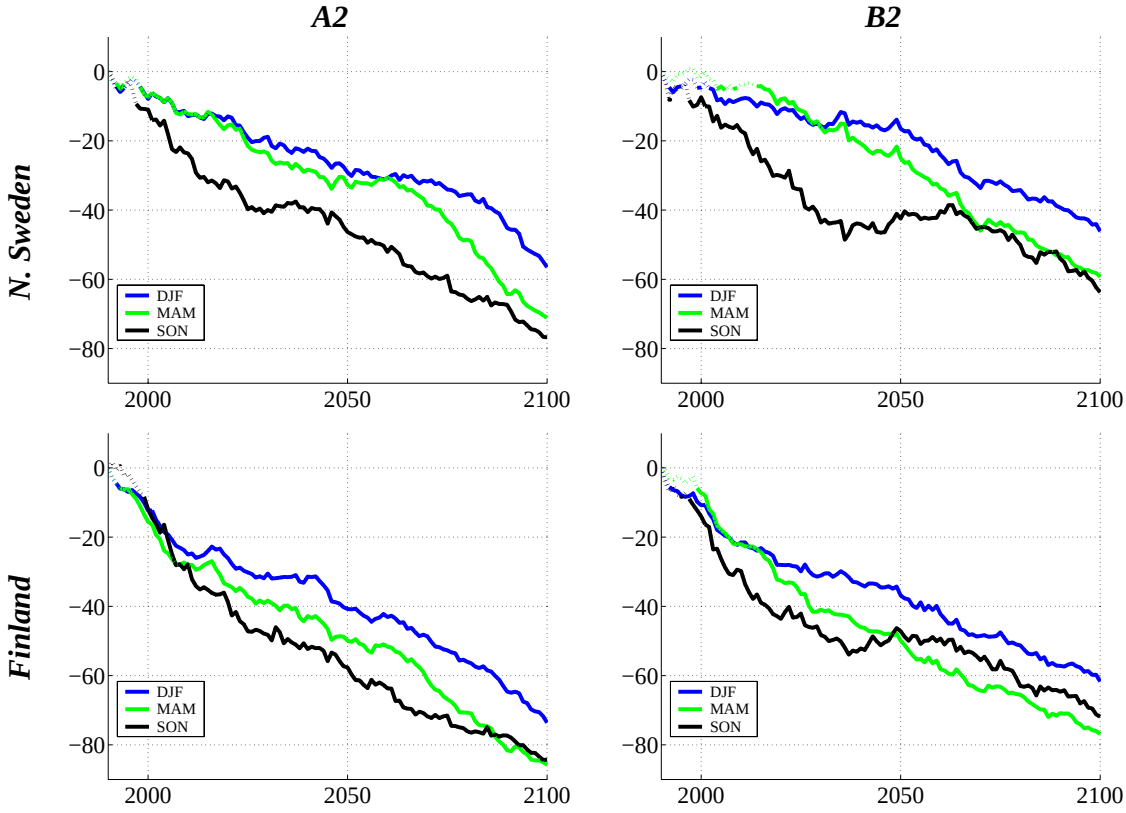

Figure 45. *Change in seasonal and area averaged snow water equivalents in the transient simulations. Periods that are at the 95% level statistically different from the control period are denoted by full lines. Units are %.*

5 Evaluating the method of pattern-scaling in time

The long simulations covering 140 years allow us to evaluate the method of pattern-scaling in time that has been used in previous work (e.g. Christensen *et al.*, 2001 and Rummukainen *et al.*, 2003). The idea of the method is to retrieve information on regional climate change in time periods that have not been dynamically downscaled by use of the global mean temperature increase (ΔT) in combination with the simulated climate change signal for another time period. The climate change signal of a variable (ΔX) in a time period (*e.g.* 2011-2040) w.r.t a reference period (*e.g.* 1961-1990) can be obtained by use of imformation from a period that has been simulated by the RCM (*e.g.* 2071-2100):

$$\Delta X_{2011\text{-}2040} = \Delta X_{2071\text{-}2100} * (\Delta T_{GLOB\ 2011\text{-}2040} / \Delta T_{GLOB\ 2071\text{-}2100})$$

Inherent to this approach is that the the variable X changes linearly in time with respect to the global mean temperature. In Figure 46 we show how the monthly mean temperature and precipitation averaged over Sweden derived with the pattern-scaling method for two different time periods compare with those calculated by the model explicitly. In most months the correspondence between the two methods is good with only small differences. But, particularly for October/November and February/March there are some notable differences for the first 30-year period. Both temperature and precipitation change calculated by the pattern-scaling method are much smaller than that calculated explicitly by the model since these variables increases faster in the early part of the simulation. The reason for these differences is related to the fast changes in circulation as discussed in section 4.2.1. But, since the differences are larger in fall and late winter than in early winter it can be suspected that the reduction of the snow cover over Sweden with its subsequent feedback on temperature also plays a role (*cf.* Section 4.1.5). Later on in the simulation the difference between the pattern-scaling method and the actual temperature change as calculated by the model is much smaller.

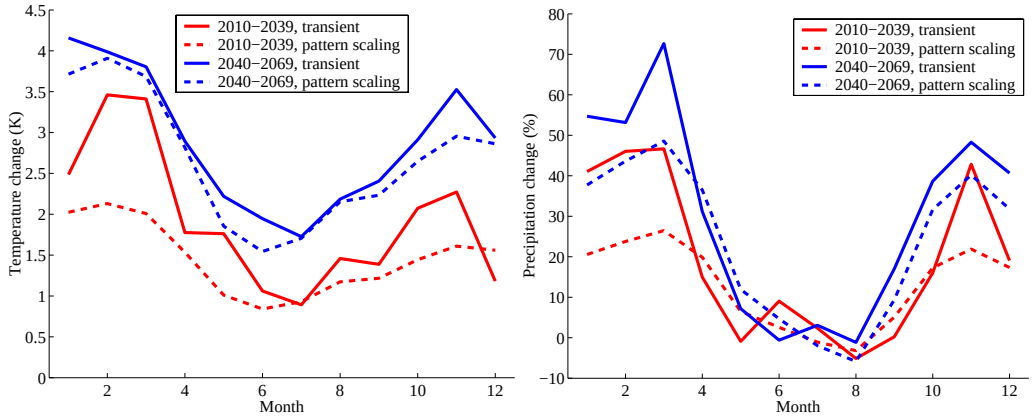

Figure 46. *Seasonal cycle of temperature (left) and precipitation (right) change calculated as area averages over Sweden. The full lines are model output while the dashed lines are results from the pattern-scaling method described in the text. Units are* ^{o}C *and % respectively.*

6 Conclusions

This report documents the most recent version of the Rossby Centre regional climate model, RCA3, including among other changes a new land surface parameterization.

Given so called "perfect boundary conditions" from ERA40, RCA3 is found to reproduce observed seasonal mean features of near surface temperature, precipitation, wind, snow conditions, mean sea level pressure and clouds in today's climate. Seasonal mean temperature errors are generally within $\pm 1^{o}$C except during winter when two major biases are identified; a positive bias in the north-eastern parts of the model domain, and a negative bias in the Mediterranean region. The positive bias is related to too much longwave radiation reaching the surface. The negative bias in the south is related to too little clear-sky shortwave radiation reaching the surface. During most of the year RCA3 simulates excessive amounts of cloud water, particularly in northern Europe. These biases; in cloud water content, downward longwave radiation, and clear-sky downward shortwave radiation all contributes to underestimations in the diurnal temperature range and the annual temperature range in many areas in the model. In many areas precipitation biases are smaller than in the corresponding reanalysis data used as boundary conditions showing the benefit of a higher horizontal resolution. Compared to the observational climatologies RCA3 tends to overestimate precipitation in northern Europe during summer and underestimate it in the south-east. A parameterisation of wind gusts is evaluated against a climatology for Sweden showing encouragingly good results.

In general, RCA3 shows equally good, or better, correspondence to climatologies as compared to the previous model versions. Among other things there are improvements in the representation of the interannual variability in Mean Sea Level Pressure during all seasons. However, there remains a bias in the pressure pattern over the Mediterranean Sea during winter when the MSLP is too high, indicating a problem in cyclone formation in that area. The seasonal mean temperature errors in RCA3 are smaller than in earlier model versions for most areas with the exception of North-Western Russia as mentioned above. The large summertime bias in south-eastern Europe as reported in RCA2 (and other RCMs) has been substantially improved. This is also the area and season where the only notable difference in the precipitation climate compared to RCA2 is found. RCA3 simulates more precipitation in better agreement to observations. Also the snow climate, evaluated against Swedish observations, shows an improvement compared to the previous model version.

The model is then applied in two 140-year transient climate change experiments taking boundary data from the ECHAM4/OPYC3 GCM. These simulations were performed for the time period 1961-2100 with observed forcing conditions until 1990 and following the SRES A2 and B2 emission scenarios after that. The climate change experiments show very similar results for the time period 2071-2100 as to what was simulated with RCAO forced by the same boundary conditions. This includes the large temperature increases in the northeast during winter and in southern Europe during summer. However, there are some differences between the simulations as some of the main surface feedback processes seem weaker in RCA3. This is shown to dampen the maximum temperature increases.

The major improvement in the present experiment setup as compared to previous time slice experiments is the fact that the model is now operated in a transient mode covering also the period between the control period and the previous time slices. This allows us to investigate the evolution of climate change. From these experiments we conclude that many of the changes appear to be rather linear with time. This applies particularly for annual averages and averages over larger areas. On the contrary, some changes do not follow a linear trend with time. Examples of this include rapid changes in snow cover in the transition seasons and changes in precipitation that changes sign with time. While many of the changes are statistically significant compared to the interannual variability in the control climate it is not always easy to judge whether it is indeed a trend or if it is the matter of natural variability.

As an example we show how the results from the transient climate change experiments can be used to evaluate an often used method for pattern-scaling in time in which scaling is done with respect to the change in global mean temperature. As expected, we show that the method works well in many aspects but fails when it comes to the changes that are non-linear and occurs at a different rate compared the change in global mean temperature.

Acknowledgements

This work has been supported through the ENSEMBLES project, funded by the EC through contract GOCE-CT-2003-505539 and the Climate and Energy (CE) project funded by Nordic Energy Research and the Nordic energy sector. Many of the model simulations were performed on the climate computing resource Tornado funded with a grant from the Knut and Alice Wallenberg foundation. The ECHAM4/OPYC3 global simulations were kindly provided by the Max Planck Institute for Meteorology in Hamburg, Germany, and the Danish Meteorological Institute in Copenhagen.

References

Adler, R.F., G.J. Huffman, A. Chang, R. Ferraro, P. Xie, J. Janowiak, B. Rudolf, U. Schneider, S. Curtis, D. Bolvin, A. Gruber, J. Susskind, and P. Arkin, 2003. The Version 2 Global Precipitation Climatology Project (GPCP) Monthly Precipitation Analysis (1979-Present). *J. Hydrometeor*., **4**, 1147-1167.

Albrecht, B.A., 1981. Parameterization of trade-cumulus cloud amounts. *J. Atmos. Sci*., **38**. 97-105.

Beniston, M., 2004. The 2003 heat wave in Europe: A shape of things to come?, *Geophys. Res. Lett*., **31**, L02202, doi:10.1029/2003GL018857.

Brasseur, O., 2001. Development and Application of a Physical Approach to Estimating Wind Gusts, *Monthly Weather Review*, **129**, 5-25.

Bringfelt B., Räisänen J., Gollvik S., Lindström G., Graham L. P. and Ullerstig A., 2001. The land surface treatment for the Rossby Centre Regional Atmospheric Climate Model – version 2 (RCA2). *Reports Meteorology and Climatology No. 98,* SMHI, SE-60176 Norrköping, Sweden, 40 pp.

Christensen, J. H., B. Machenhauer, R.G. Jones, C. Schär, P.M. Ruti, M. Castro, and G. Visconti, 1997. Validation of present-day regional climate simulations over Europe: LAM simulations with observed boundary conditions. *Clim. Dyn*., **13**, 489-506.

Christensen, J.H., Räsiänen, J., Iversen, T., Bjørge, D., Christensen, O.B., and Rummukainen, M., 2001. A synthesis of regional climate change simulations. A Scandinavian perspective. *Geophys. Res. Lett.*, **28**, 1003-1006.

Christensen, J.H. and Christensen, O.B., 2006. The PRUDENCE simulations: Model validation and climate change' *Clim. Change*, submitted.

Cubasch, U., Meehl, G.A., Boer, G.J., Stouffer, R.J., Dix, M., Noda, A., Senior, C.A., Raper, S. and Yap, K.S.,2001. Projections of future climate change. In: *Climate Change 2001: The Scientific Basis. Contribution of Working Group I to the Third Assessment Report of the Intergovernmental Panel on Climate Change*. Houghton, J.T., Ding, Y., Griggs, D.J., Noguer, M., van der Linden, P.J., Dai, K., Maskell, K. and Johnson, C.A. (eds). Cambridge University Press, Cambridge, U.K., 881 pp.

Cuxart, J., Bougeault, Ph. and Redelsperger, J-L., 2000. A turbulences scheme allowing for mesoscale and large eddy simulations. *Q. J. R. Meteorol. Soc.,* **126**, 1-30.

Ferro C.A.T., Hannachi A., Stephenson D.B., 2005. Simple non-parametric techniques for exploring changing probability distributions of weather. *J. Clim.,* **18**, 4344-4354.

Giorgi, F. and Mearns, L. O.,1999. Introduction to special section: Regional climate modelling revisited. *J. Geophys. Res*., **104**:D6, 6335-6352.

Hagemann, S., Arpe, K., and Bengtsson, L., 2005. Validation of the hydrological cycle of ERA-40. In *ECMWF ERA-40 Project Report Series, No. 24*. European Centre for Medium-Range Weather Forecasts, Shinfield, Reading, UK (available from www.ecmwf.int/publications).

Häggmark, L., Ivarsson, K.-I., Gollvik, S. and Olofsson, P.-O., 2000. Mesan, an operational mesoscale analysis system. *Tellus*, **52**A, 2-20.

IPCC, 2001. *Climate Change 2001: The Scientific Basis.* Contribution of Working Group I to the Third Assessment Report of the Intergovernmental Panel on Climate Change. Houghton, J.T., Ding, Y., Griggs, D.J., Noguer, M., van der Linden, P.J., Dai, K., Maskell, K. and Johnson, C.A. (eds). Cambridge University Press, Cambridge, U.K., 881 pp.

Jones C.G. and Sanchez, E., 2002. The representation of shallow cumulus convection and associated cloud fields in the Rossby Centre Atmospheric Model. *HIRLAM Newsletter 41*, Available on request from SMHI, S-60176 Norrköping, Sweden.

Jones, C.G., Ullerstig, A., Willén, U. and Hansson, U., 2004. The Rossby Centre regional atmospheric climate model (RCA). Part I: Model climatology and performance characteristics for present climate over Europe. *Ambio*, **33**, 199-210.

Kain, J.S. and J.M. Fritsch, 1993. Convective parameterizations for MEsoscale Models: The KAin-Fritsch scheme. In: The representation of cumulus convection in numerical models, Eds: K.A. Emanuel and D.J. Raymond. *AMS Monograph*, **46**, 246 pp.

Kjellström, E., 2004. Recent and future signatures of climate change in Europe, *Ambio* **33**, 193-298.

Kjellström, E., Bärring, L., Jacob, D., Jones, R., Lenderink, G and Schär, C., 2006. Modelling daily temperature extremes: Recent climate and future changes over Europe. *Clim. Change*. Submitted.

Klein Tank, A.M.G., Wijngaard, J.B., Können, G. P., Böhm, R., Demarée, G., Gocheva, A., Mileta, M., Pashiardis, S., Hejkrlik, L., Kern-Hansen, C., Heino, R., Bessemoulin, P., Müller-Westermeier, G., Tzanakou, M., Szalai, S., Pálsdóttir, T., Fitzgerlad, D., Rubin, S., Capaldo, M., Maugeri, M., Leitass, A., Bukantis, A., Aberfeld, R., van Engelen, A.F.V., Førland, E., Mietus, M., Coelho, F., Mares, C., Razuvaev, V., Nieplova, E., Cegnar, T., Antonio López, J., Dahlström, B., Moberg, A., Kirchhofer, W., Ceylan, A. Pachaliuk, O., Alexander, L.V. and Petrovic, P., 2002. Daily dataset of 20th-century surface air temperature and precipitation series for the European Climate Assessment, *Int. J. Climatology*, **22**, 1441-1453.

Lenderink, G., and de Rooy, W., 2000. A robust mixing length formulation for a TKE-1 turbulence scheme, *Hirlam Newsletter*, **36**, 25-29.

Lenderink, G., and Holtslag, A. A. M., 2004. An updated length-scale formulation for turbulent mixing in clear and cloudy boundary layers, *Quart. J. Roy. Meteor. Soc.*, **130**, 3405-3427.

Ljungemyr P., Gustafsson N. and Omstedt A., 1996. Parameterization of lake thermodynamics in a high resolution weather forecasting model. *Tellus*, **48A**, 608–621.

Meier, H.E.M., Broman, B., Kallio, H., and Kjellström, E., 2006. Projections of future surface winds, sea levels, and wind waves in the late 21st century and their application for impact studies of flood prone areas in the Baltic Sea region. of the Baltic Sea Region. In *Sea Level Change Affecting the Spatial Development*. Edited by Philipp Schmidt-Thom. Geological Survey of Finland, Special Paper 41, 23-44, 2006.

Mitchell, T.D. and Jones, P.D., 2005. An improved method of constructing a database of monthly climate observations and associated high-resolution grids. *Int. J. Climatol.*, **25**, 693-712.

Nakićenović, N., Alcamo, J., Davis, G., de Vries, B., Fenhann, J., Gaffin, S., Gregory, K., Grübler, A., et al., 2000. *Emission scenarios.* A Special Report of Working Group III of the Intergovernmental Panel on Climate Change. Cambridge University Press, 599 pp.

Nordström, M., 2005. *Estimation of gusty winds in RCA.* Master thesis at the Dept. of Earth Sciences, Uppsala Unisversity. ISSN 1650-6553 Nr 101. 42 pp.

Pryor, S.C., Barthelmie, R.J., and Kjellström, E., 2005. Potential climate change impact on wind energy resources in northern Europe: analyses using a regional climate model. *Clim. Dyn.*, **25**, 815-835.

Raab B. and Vedin H. (Special Editors), 1995. *Climate, Lakes and Rivers. National Atlas of Sweden, vol. 14.* SNA Publishing, Box 45029 S-10430 Stockholm, Sweden, 176 pp.

Räisänen, P., Rummukainen, M., and Räisänen, J., 2000. Modification of the HIRLAM radiation scheme for use in the Rossby Centre regional atmospheric climate model. *Report No. 49,* Department of Meteorology, University of Helsinki, 71 pp.

Räisänen, J., Hansson, U., Ullerstig, A., Döscher, R., Graham, L.P., Jones, C., Meier, M., Samuelsson, P. and Willén, U. 2003. GCM driven simulations of recent and future climate with the Rossby Centre coupled atmosphere – Baltic Sea regional climate model RCAO. *Reports Meteorology and Climatology 101*, SMHI, SE 60176 Norrköping, Sweden, 61 pp.

Räisänen, J., U. Hansson, A. Ullerstig, R. Döscher, L.P. Graham, C. Jones, H.E.M. Meier, P. Samuelsson, U. Willén, 2004. European climate in the late 21st century: regional simulations with two driving global models and two forcing scenarios. *Clim. Dyn.,* **22**, 13-31.

Rasch, P.J. and Kristjansson, J.E., 1998. A comparison of the CCM3 model climate using diagnosed and predicted condensate parameterisations, *J. Climate,* **11**, 1587-1614.

Roeckner, E., Bengtsson, L., Feicther, J., Lelieveld, J. and Rodhe, H., 1999. Transient climate change simulations with a coupled atmosphere-ocean GCM including the tropospheric sulfur cycle. *J. Climate*, **12**, 3004-3032.

Rossow, W.B., and Schiffer, R.A., 1999. Advances in Understanding Clouds from ISCCP. *Bull. Amer. Meteor. Soc.*, **80**, 2261-2288.

Rubel, F., and Hantel, M., 2001. BALTEX 1/5-degree daily precipitation climatology 1996-1998. *Meteorol. Atmos. Phys.,* **77**, 155-166.

Rummukainen, M., Räisänen, J., Ullerstig, A., Bringfelt, B., Hansson, U., Graham, P. and Willén, U., 1998. RCA – Rossby Centre regional Atmospheric climate model: model description and results from the first multi-year simulation. *Reports Meteorology and Climatology 83,*SMHI, SE-601 76 Norrköping, Sweden, 76 pp.

Rummukainen, M., Räisänen, J., Bringfelt, B., Ullerstig, A., Omstedt, A., Willén, U., Hansson, U. and Jones, C., 2001. A regional climate model for northern Europe: model description and results from the downscaling of two GCM control simulations. *Clim. Dyn.*, **17**, 339-359.

Rummukainen, M., Räisänen, J., Bjørge, D., Christensen, J.H., Christensen, O.B., Iversen, T., Jylhä, K., Ólafsson, H., and Tuomenvirta, H., 2003. Regional climate scenarios for use in Nordic water resources studies. *Nordic Hydrology*, **34(5)**, 399-412.

Rummukainen, M., Bergström, S., Persson, G., Rodhe, J. and Tjernström, M., 2004. The Swedish regional climate modeling programme, SWECLIM: A review. *Ambio*, **33**, 176-182.

Samuelsson, P., Gollvik, S. and Ullerstig, A., 2006. The land-surface scheme of the Rossby Centre regional atmospheric climate model (RCA3). *Report in Meteorology 122*, SMHI. SE-601 76 Norrköping, Sweden.

Sass, B. and Christensen, J. H., 1995. A simple framework for testing the quality of atmospheric limited-area models. *Mon. Wea. Rev*., **123**, 444-459.

Sass B.H., Rontu L., Savijärvi H., Räisänen P., 1994. HIRLAM-2 Radiation scheme: Documentation and tests. *Hirlam technical report No 16.,* SMHI. SE-601 76 Norrköping, Sweden, 43 pp.

Savijärvi H., 1990. A fast radiation scheme for mesoscale model and short-range forecast models. *J. Appl. Met*., **29**, 437-447.

Schär, C., Vidale, P.L., Lüthi, D., Frei, C., Häberli, C., Liniger, M.A. and Appenzeller, C., 2004. The role of increasing temperature variability for European summer heat waves, *Nature*, **427**, 332-336.

Smith, T.M., and R.W. Reynolds, 2004. Improved Extended Reconstruction of SST (1854-1997). *J. Climate*, **17**, 2466-2477.

Taylor, K. E., 2001. Summarizing multiple aspects of model performance in single diagram}, *J. Geophys. Res.*, **106**, D7, 7183—7192.

Undén P., Rontu L., Järvinen H., Lynch P., Calvo J., Cats G., Cuxart J., Eerola K., Fortelius K., Garcia-Moya J. A., Jones C., Lenderlink G., McDonald A., McGrath R., Navascues B., Nielsen N. W., Ødegaard V., Rodrigues E., Rummukainen M., Rõõm R., Sattler K., Sass B. H., Savijärvi H., Schreuer. B. W., Sigg R., The H., Tijm A., 2002. HIRLAM-5 Scientific Documentation. *HIRLAM Report*, SMHI, SE-601 76 Norrköping, Sweden, 144 pp.

Uppala, S. M., P.W. Kållberg, A.J. Simmons, U. Andrae, V. da Costa Bechtold, M. Fiorino, J.K Gibson, J. Haseler, A. Hernandez, G.A. Kelly, X. Li, K. Onogi, S. Saarinen, N. Sokka, R.P. Allan, E. Andersson, K. Arpe, M.A. Balmaseda, A.C.M. Beljaars, L. van de Berg, J. Bidlot, N. Bormann, S. Caires, F. Chevallier, A. Dethof, M. Dragosavac, M. Fisher, M. Fuentes, S. Hagemann, E. Holm, B.J. Hoskins, L. Isaksen, P.A.E.M. Janssen, R. Jenne, A.P. McNally, J.-F. Mahfouf, J.-J. Morcrette, N.A Rayner, R.W. Saunders, P. Simon, A. Sterl, K.E. Trenberth, A. Untch, D. Vasiljevic, P. Viterbo and J. Woollen, 2005. The ERA-40 Re-analysis, *Q. J. Roy. Meteorol. Soc*., **131**, 2961-3012.

von Storch, H., 2005. Conceptual basis and applications of Regional Climate Modeling. In Bärring and Laprise (Eds.), Extended abstracts of a WMO/WCRP-sponsored Regional-Scale Climate Modelling Workshop. *Lund eRep. Phys. Geogr., No 5*, May 2005. Department of Physical Geography & Ecosystem Analysis, Lund University, Sweden (ISSN: 1402-9006), 26-37.

Willmott, C. J. and K. Matsuura, 1995. Smart Interpolation of Annually Averaged Air Temperature in the United States. *J. Appl. Met.*, **34**, 2577-2586.

Wyser, K., L. Rontu and H. Savijärvi, 1999. Introducing the effective radius into a fast radiation scheme of a mesoscale model. *Contr. Atm. Phys.*, **72**, 205-218.

Zwiers F. W. and von Storch H., 1995. Taking serial correlation into account in tests of the mean. *J. Clim.*, **8**, 336-351.

SMHI Publications

SMHI publishes six report series. Three of these, the R-series, are intended for international readers and are in most cases written in English. For the others the Swedish language is used.

Names of the Series	Published since
RMK (Report Meteorology and Climatology)	1974
RH (Report Hydrology)	1990
RO (Report Oceanography)	1986
METEOROLOGI	1985
HYDROLOGI	1985
OCEANOGRAFI	1985

Earlier issues published in serie RMK

1 Thompson, T., Udin, I. and Omstedt, A. (1974)
Sea surface temperatures in waters surrounding Sweden.

2 Bodin, S. (1974)
Development on an unsteady atmospheric boundary layer model.

3 Moen, L. (1975)
A multi-level quasi-geostrophic model for short range weather predictions.

4 Holmström, I. (1976)
Optimization of atmospheric models.

5 Collins, W.G. (1976)
A parameterization model for calculation of vertical fluxes of momentum due to terrain induced gravity waves.

6 Nyberg, A. (1976)
On transport of sulphur over the North Atlantic.

7 Lundqvist, J.-E. and Udin, I. (1977)
Ice accretion on ships with special emphasis on Baltic conditions.

8 Eriksson, B. (1977)
Den dagliga och årliga variationen av temperatur, fuktighet och vindhastighet vid några orter i Sverige.

9 Holmström, I., and Stokes, J. (1978)
Statistical forecasting of sea level changes in the Baltic.

10 Omstedt, A. and Sahlberg, J. (1978)
Some results from a joint Swedish-Finnish sea ice experiment, March, 1977.

11 Haag, T. (1978)
Byggnadsindustrins väderberoende, seminarieuppsats i företagsekonomi, B-nivå.

12 Eriksson, B. (1978)
Vegetationsperioden i Sverige beräknad från temperaturobservationer.

13 Bodin, S. (1979)
En numerisk prognosmodell för det atmosfäriska gränsskiktet, grundad på den turbulenta energiekvationen.

14 Eriksson, B. (1979)
Temperaturfluktuationer under senaste 100 åren.

15 Udin, I. och Mattisson, I. (1979)
Havsis- och snöinformation ur datorbearbetade satellitdata - en modellstudie.

16 Eriksson, B. (1979)
Statistisk analys av nederbördsdata. Del I. Arealnederbörd.

17 Eriksson, B. (1980)
Statistisk analys av nederbördsdata. Del II. Frekvensanalys av månadsnederbörd.

18 Eriksson, B. (1980)
Årsmedelvärden (1931-60) av nederbörd, avdunstning och avrinning.

19 Omstedt, A. (1980)
A sensitivity analysis of steady, free floating ice.

20 Persson, C. och Omstedt, G. (1980)
En modell för beräkning av luftföroreningars spridning och deposition på mesoskala.

21 Jansson, D. (1980)
Studier av temperaturinversioner och vertikal vindskjuvning vid Sundsvall-Härnösands flygplats.

22 Sahlberg, J. and Törnevik, H. (1980)
A study of large scale cooling in the Bay of Bothnia.

23 Ericson, K. and Hårsmar, P.-O. (1980)
Boundary layer measurements at Klock-rike. Oct. 1977.

24 Bringfelt, B. (1980)
A comparison of forest evapotranspiration determined by some independent methods.

25 Bodin, S. and Fredriksson, U. (1980)
Uncertainty in wind forecasting for wind power networks.

26 Eriksson, B. (1980)
Graddagsstatistik för Sverige.

27 Eriksson, B.(1981)
Statistisk analys av nederbördsdata. Del III. 200-åriga nederbördsserier.

28 Eriksson, B. (1981)
Den "potentiella" evapotranspirationen i Sverige.

29 Pershagen, H. (1981)
Maximisnödjup i Sverige (perioden 1905-70).

30 Lönnqvist, O. (1981)
Nederbördsstatistik med praktiska tillämpningar.
(Precipitation statistics with practical applications.)

31 Melgarejo, J.W. (1981)
Similarity theory and resistance laws for the atmospheric boundary layer.

32 Liljas, E. (1981)
Analys av moln och nederbörd genom automatisk klassning av AVHRR-data.

33 Ericson, K. (1982)
Atmospheric boundary layer field experiment in Sweden 1980, GOTEX II, part I.

34 Schoeffler, P. (1982)
Dissipation, dispersion and stability of numerical schemes for advection and diffusion.

35 Undén, P. (1982)
The Swedish Limited Area Model. Part A. Formulation.

36 Bringfelt, B. (1982)
A forest evapotranspiration model using synoptic data.

37 Omstedt, G. (1982)
Spridning av luftförorening från skorsten i konvektiva gränsskikt.

38 Törnevik, H. (1982)
An aerobiological model for operational forecasts of pollen concentration in the air.

39 Eriksson, B. (1982)
Data rörande Sveriges temperaturklimat.

40 Omstedt, G. (1984)
An operational air pollution model using routine meteorological data.

41 Persson, C. and Funkquist, L. (1984)
Local scale plume model for nitrogen oxides. Model description.

42 Gollvik, S. (1984)
Estimation of orographic precipitation by dynamical interpretation of synoptic model data.

43 Lönnqvist, O. (1984)
Congression - A fast regression technique with a great number of functions of all predictors.

44 Laurin, S. (1984)
Population exposure to SO and NO_x from different sources in Stockholm.

45 Svensson, J. (1985)
Remote sensing of atmospheric tempera-ture profiles by TIROS Operational Vertical Sounder.

46 Eriksson, B. (1986)
Nederbörds- och humiditetsklimat i Sverige under vegetationsperioden.

47 Taesler, R. (1986)
Köldperioden av olika längd och förekomst.

48 Wu Zengmao (1986)
Numerical study of lake-land breeze over Lake Vättern, Sweden.

49 Wu Zengmao (1986)
Numerical analysis of initialization procedure in a two-dimensional lake breeze model.

50 Persson, C. (1986)
Local scale plume model for nitrogen oxides. Verification.

51 Melgarejo, J.W. (1986)
An analytical model of the boundary layer above sloping terrain with an application to observations in Antarctica.

52 Bringfelt, B. (1986)
Test of a forest evapotranspiration model.

53 Josefsson, W. (1986)
Solar ultraviolet radiation in Sweden.

54 Dahlström, B. (1986)
Determination of areal precipitation for the Baltic Sea.

55 Persson, C., Rodhe, H. and De Geer, L.-E. (1986)
The Chernobyl accident - A meteorological analysis of how radionucleides reached Sweden.

56 Persson, C., Robertson, L., Grennfelt, P., Kindbom, K., Lövblad, G. och Svanberg, P.-A. (1987)
Luftföroreningsepisoden över södra Sverige 2 - 4 februari 1987.

57 Omstedt, G. (1988)
An operational air pollution model.

58 Alexandersson, H. and Eriksson, B. (1989)
Climate fluctuations in Sweden 1860 - 1987.

59 Eriksson, B. (1989)
Snödjupsförhållanden i Sverige - Säsongerna 1950/51 - 1979/80.

60 Omstedt, G. and Szegö, J. (1990)
Människors exponering för luftföroreningar.

61 Mueller, L., Robertson, L., Andersson, E. and Gustafsson, N. (1990)
Meso-γ scale objective analysis of near surface temperature, humidity and wind, and its application in air pollution modelling.

62 Andersson, T. and Mattisson, I. (1991)
A field test of thermometer screens.

63 Alexandersson, H., Gollvik, S. and Meuller, L. (1991)
An energy balance model for prediction of surface temperatures.

64 Alexandersson, H. and Dahlström, B. (1992)
Future climate in the Nordic region - survey and synthesis for the next century.

65 Persson, C., Langner, J. and Robertson, L. (1994)
Regional spridningsmodell för Göteborgs och Bohus, Hallands och Älvsborgs län. (A mesoscale air pollution dispersion model for the Swedish west-coast region. In Swedish with captions also in English.)

66 Karlsson, K.-G. (1994)
Satellite-estimated cloudiness from NOAA AVHRR data in the Nordic area during 1993.

67 Karlsson, K-G. (1996)
Cloud classifications with the SCANDIA model.

68 Persson, C. and Ullerstig, A. (1996)
Model calculations of dispersion of lindane over Europe. Pilot study with comparisons to easurements around the Baltic Sea and the Kattegat.

69 Langner, J., Persson, C., Robertson, L. and Ullerstig, A. (1996)
Air pollution Assessment Study Using the MATCH Modelling System. Application to sulfur and nitrogen compounds over Sweden 1994.

70 Robertson, L., Langner, J. and Engardt, M. (1996)
MATCH - Meso-scale Atmosperic Transport and Chemistry modelling system.

71 Josefsson, W. (1996)
Five years of solar UV-radiation monitoring in Sweden.

72 Persson, C., Ullerstig, A., Robertson, L., Kindbom, K. and Sjöberg, K. (1996)
The Swedish Precipitation Chemistry Network. Studies in network design using the MATCH modelling system and statistical methods.

73 Robertson, L. (1996)
Modelling of anthropogenic sulfur deposition to the African and South American continents.

74 Josefsson, W. (1996)
Solar UV-radiation monitoring 1996.

75 Häggmark, L. Ivarsson, K.-I. and Olofsson, P.-O. (1997)
MESAN - Mesoskalig analys.

76 Bringfelt, B., Backström, H., Kindell, S., Omstedt, G., Persson, C. and Ullerstig, A. (1997)
Calculations of PM-10 concentrations in Swedish cities- Modelling of inhalable particles

77 Gollvik, S. (1997)
The Teleflood project, estimation of precipitation over drainage basins.

78 Persson, C. and Ullerstig, A. (1997)
Regional luftmiljöanalys för Västmanlands län baserad på MATCH modell-beräkningar och mätdata - Analys av 1994 års data

79 Josefsson, W. and Karlsson, J.-E. (1997)
Measurements of total ozone 1994-1996.

80 Rummukainen, M. (1997)
Methods for statistical downscaling of GCM simulations.

81 Persson, T. (1997)
Solar irradiance modelling using satellite retrieved cloudiness - A pilot study

82 Langner, J., Bergström, R. and Pleijel, K. (1998)
European scale modelling of sulfur, oxidized nitrogen and photochemical oxidants. Model development and evaluation for the 1994 growing season.

83 Rummukainen, M., Räisänen, J., Ullerstig, A., Bringfelt, B., Hansson, U., Graham, P. and Willén, U. (1998)
RCA - Rossby Centre regional Atmospheric climate model: model description and results from the first multi-year simulation.

84 Räisänen, J. and Döscher, R. (1998)
Simulation of present-day climate in Northen Europé in the HadCM2 OAGCM.

85 Räisänen, J., Rummukainen, M., Ullerstig, A., Bringfelt, B., Hansson, U. and Willén, U. (1999)
The First Rossby Centre Regional Climate Scenario - Dynamical Downscaling of CO_2-induced Climate Change in the HadCM2 GCM.

86 Rummukainen, M. (1999)
On the Climate Change debate

87 Räisänen, J. (2000)
CO_2-induced climate change in northern Europé: comparison of 12 CMIP2 experiments.

88 Engardt, M. (2000)
Sulphur simulations for East Asia using the MATCH model with meteorological data from ECMWF.

89 Persson, T. (2000)
Measurements of Solar Radiation in Sweden 1983-1998

90 Michelson, D. B., Andersson, T., Koistinen, J., Collier, C. G., Riedl, J., Szturc, J., Gjertsen, U., Nielsen, A. and Overgaard, S., (2000)
BALTEX Radar Data Centre Products and their Methodologies

91 Josefsson, W. (2000)
Measurements of total ozone 1997 – 1999

92 Andersson, T. (2000)
Boundary clear air echos in southern Sweden

93 Andersson, T. (2000)
Using the Sun to check some weather radar parameters

94 Rummukainen, M., Bergström, S., Källén, E., Moen, L., Rodhe, J. and Tjernström, M. (2000)
SWECLIM – The First Three Years

95 Meier, H. E. M. (2001)
The first Rossby Centre regional climate scenario for the Baltic Sea using a 3D coupled ice-ocean model

96 Landelius, T., Josefsson, W. and Persson, T. (2001)
A system for modelling solar radiation parameters with mesoscale spatial resolution

97 Karlsson, K.-G. (2001)
A NOAA AVHRR cloud climatology over Scandinavia covering the period 1991-2000

98 Bringfelt, B., Räisänen, J., Gollvik, S., Lindström, G., Graham, P. and Ullerstig, A., (2001)
The land surface treatment for the Rossby Centre Regional Atmospheric Climate Model - version 2 (RCA2)

99 Kauker, F. and Meier, H. E. M., (2002)
Reconstructing atmospheric surface data for the period 1902-1998 to force a coupled ocean-sea ice model of the Baltic Sea.

100 Klein, T., Bergström, R. and Persson, C. (2002)
Parameterization of dry deposition in MATCH

101 Räisänen, J., Hansson, U., Ullerstig A., Döscher, R., Graham, L. P., Jones, C., Meier, M., Samuelsson, P.and Willén, U. (2003)
GCM driven simulations of recent and future climate with the Rossby Centre coupled atmosphere - Baltic Sea regional climate model RCAO

102 Tjernström, M., Rummukainen, M., Bergström, S., Rodhe, J. och Persson, G., (2003)
Klimatmodellering och klimatscenarier ur SWECLIMs perspektiv.

103 Segersson, D. (2003)
Numerical Quantification of Driving Rain on Buildings

104 Rummukainen, M. and the SWECLIM participants (2003)
The Swedish regional climate modeling program 1996-2003. Final report.

105 Robertson, L. (2004)
Extended back-trajectories by means of adjoint equations

106 Rummukainen, M., Bergström S., Persson G., Ressner, E (2005)
Anpassningar till klimatförändringar

107 Taesler, R., Andersson, C., Nord, M (2005)
Optimizing Energy Efficiency and Indoor climate by Forecast Control of Heating Systems and Energy Management in Buildings

Swedish Meteorological and Hydrological Institute
SE-601 76 Norrköping · Sweden
Tel +46 11 495 80 00 · Fax +46 11 495 80 01

ISSN 0347-2116